Development of Dual Enzyme and Oxidation-responsive Drug Delivery Systems

Sung Hwa Hong

A Thesis

in

The Department

of

Chemistry and Biochemistry

Presented in Partial Fulfillment of the Requirements

for the Degree of Master of Science (Chemistry) at

Concordia University

Montreal, Quebec, Canada

April 2018

© Sung Hwa Hong, 2018

CONCORDIA UNIVERSITY

School of Graduate Studies

This is to certify that the thesis prepared

By: Sung Hwa Hong

Entitled: **Development of Dual Enzyme and Oxidation-responsive Drug Delivery Systems**

and submitted in partial fulfillment of the requirements for the degree of

Master of Science (Chemistry)

complies with the regulations of the University and meets the accepted standards with respect to

originality and quality.

Signed by the final examining committee:

_____Chair
Dr. Ashlee J. Howarth

_____Examiner
Dr. Louis Cuccia

_____Examiner
Dr. Christine DeWolf

_____Supervisor
Dr. John Oh

Approved by _____Chair of Department or Graduate Program Director

and _____ Dean of Faculty.

April/12/2018

Abstract

Development of Dual Enzyme and Oxidation-responsive Drug Delivery Systems

Sung Hwa Hong

Conventional chemotherapy using small molecular weight anticancer drugs presents many side effects due to poor specificities and aqueous solubility. To overcome the limitations, polymer-based drug delivery systems (PDDS) have been emerged for targeted delivery of therapeutic agents. Upon introduction of stimuli-responsive platform, the drugs can be released in controlled manner at the targeted tumor site providing enhanced drug efficacy and reduced toxicity. Stimuli-responsive degradation platform involves incorporation of covalent linkages that can be cleaved in response to external stimuli. The external stimuli can be found in altered microenvironment in pathophysiological tissues. For example, elevated levels of esterase and reactive oxygen species (ROS) are found in cancer tumor cells. As esters can be cleaved by the esterase and sulfides can be oxidized by the ROS, esters and sulfides can be incorporated to polymer to exhibit esterase and oxidation-responsive properties.

Size is an important consideration for the design of drug delivery systems. Ideally, the size should be ranged from 50 to 150 nm for optimal biodistributions and targeting ability. Microfluidic process provides high degree of control over the size of NPs. Chapter 2 examines size tunability of the dual enzyme- and oxidation-responsive polyester-based nanoparticulates (DPE-NPs) using a microfluidic instrument for cancer therapy. The DPE-NPs can be fabricated by using the polyester and polymeric stabilizer. The size of NPs can be influenced by changing the variables such as microfluidic parameters (total flow rate and organic/aqueous flow rate ratio) and formulation parameters (molecular weight of polyesters, concentration of nanoparticles, and nature and amount of stabilizers). In addition to size of NPs, it turns out that these parameters have an effect on colloidal stability. The results obtained from dual stimuli-responsive degradation and *in vitro* experiments with an enhanced cellular uptake demonstrate that the DPE-NPs can offer a versatile platform for the development of drug delivery systems.

Chapter 3 describes biological assessment of DPE-NPs as effective tumor-targeting intracellular nanocarriers. Doxorubicin (Dox), a clinically used anticancer drug, was incorporated into DPE-NPs stabilized with PEG and Brij S20. They exhibited excellent colloidal stability and as well as in pseudo-physiological conditions without any aggregation. They were destabilized in response to esterase that cleaved ester linkages and to hydrogen peroxide that oxidized sulfides. Such disruption led to an enhanced release of encapsulated therapeutics. For biological perspectives, the DPE-NPs were assessed *in vitro* using HeLa cervical cancer cells as a model. The results from MTT assay, epifluorescence microscope, flow cytometry, and cellular entry assay suggest that the dual responses triggered the intracellular release of the Dox to prohibit the cell proliferation followed by a rapid internalization through caveolae-mediated endocytosis. Further evaluation on 3D HeLa multicellular tumor spheroid (MCTS) indicated that the penetration ability of Dox was significantly enhanced when encapsulated in DPE NPs, suggesting that such deep penetration could be effective *in vivo*.

Acknowledgments

Publications in this thesis

1. **<u>S. H. Hong</u>**, K. Larocque, D. Jaunky, A. Piekny, J. K. Oh* Dual disassembly and biological evaluation of enzyme/oxidation-responsive polymer-based nanoparticulates for targeted delivery of anticancer therapeutics. (under review)

2. F. Yang, J. Xu, A. Skripka, A. Benayas, X. Dong, **<u>S. H. Hong</u>**, F. Ren, Z. Yang, F. Vetrone, J. K. Oh, X. Liu, D. Ma* An integrated multifunctional nanoplatform for deep-tissue dual-mode imaging, *Advanced Functional Materials* **2018**, 1706235.

3. **<u>S. H. Hong</u>**, P. Twinkal, S. Ip, S. Garg, J. K. Oh* Microfluidic assembly to synthesize dual enzyme/oxidation-responsive polyester-based nanoparticulates with controlled sizes for drug delivery, *Langmuir* **2018**, 34, 3316-3325.

4. S. Jung, J. T. Liu, **<u>S. H. Hong</u>**, D. Arunbabu, S. M. Noh, J. K. Oh* A new reactive Polymethacrylate bearing pendant furfuryl groups: synthesis, thermoreversible reactions, and self-healing, *Polymer* **2017**, 107, 58-65.

5. S. Y. An, **<u>S. H. Hong</u>**, C. Tang, J. K. Oh* Rosin-based block copolymer intracellular delivery nanocarriers with reduction-responsive sheddable coronas for cancer therapy, *Polymer Chemistry* **2016**, *7*, 4751-4760.

Contribution of Authors

A majority of research results presented in this thesis was conducted independently by the author under the supervision of Prof. John Oh at Concordia University. The chapters 2 and 3 are reproduced in part from the original articles.

Chapter 2 was done in collaboration with Precision NanoSystems located in Vancouver. The company provided a benchtop NanoAssemblr, a microfluidic instrument and feedbacks for the results of microfluidic preparation of nanoparticulates in the regular meetings. Provided the recipe and experimental design by the author, Twinkal Patel, an undergraduate student, worked under my supervision to prepare nanoparticles and carried out degradation experiments.

The work in chapter 3 was done in collaboration with Prof. Alisa Piekny's group at Concordia University in the Department of Biology. More specifically, Kevin Larocque conducted 3D tumor spheroids experiment and Dilan Jaunky determined endocytic mechanism.

Table of Contents

List of Figures

List of Schemes

List of Abbreviations

DLS	Dynamic light scattering
DMF	Dimethylformamide
Dox	Doxorubicin
DPE	Dual enzyme and oxidation-responsive polyester
FDA	Food and drug administration
FRR	Flow rate ratio
GSH	Glutathione
HDPE	High molecular weight dual enzyme and oxidation-responsive polyester
HPLC	High performance liquid chromatography
LDPE	Low molecular weight dual enzyme and oxidation-responsive polyester
LiBr	Lithium bromide
MMP	Matrix metalloproteinase
Mn	Number average molecular weight
Mw	Weight average molecular weight
NMR	Nuclear magnetic resonance
NP_L, NP_D	Nanoparticles with peptides in L-configuration and D-configuration
PCL	Poly (ε-caprolactone)
PDDS	Polymer-based drug delivery system
PDI	Polydispersity index
PEG	Poly(ethylene glycol)
PENP	Polyester-based nanoparticles
PES	Polyethersulfone
PGA	Penicillin G amidase

PLA	Polylactide
PLE	Porcine liver esterase
PLGA	Poly(lactide-co-glycolic acid)
PMMA	Poly(methyl methacrylate)
PMTC	Poly(trimethylene carbonate)
PS	Polystyrene
PTFE	Polytetrafluoroethylene
RAFT	Reversible addition fragmentation chain transfer
ROS	Reactive oxygen species
SRD	Stimuli-responsive degradation
TFR	Total flow rate
THF	Tetrahydrofuran
UV/Vis	Ultraviolet-visible

Chapter 1
Introduction

1.1 Overview of research and goals

My Master's research aims to fabricate polyester-based (DPE) nanocarriers and to explore dual enzyme and oxidation-responsive degradation. The DPE designed to have both ester and sulfide linkages in the backbone, was synthesized by a click-type thiol-ene Michael addition reaction. Due to its hydrophobicity, the polyester formed colloidally-stable nanoparticles with an aid of stabilizers. The resulting nanoparticulates underwent polarity change or main chain degradation upon dual responses, leading to enhanced release of encapsulated anticancer drugs in targeted cells. Further, they were evaluated *in vitro* as intracellular nanocarriers for cancer therapy exhibiting an enhanced release of anti-cancer drugs (Doxorubicin).

1.2 Polymer-based drug delivery systems

As a counter-measure to cancer, chemotherapy has long been used as a means of treatment due to its ability not only to kill cancer cells, but also, to prevent the spread of cancer throughout the body. However, conventional chemotherapy presents several issues.[1-3] One issue involves the poor solubility of drugs in aqueous environment. The poorly-soluble molecules are subjected to be removed by reticuloendothelial systems, resulting in a limited circulation time in the body.[4, 5] To achieve therapeutic effect, an increase in the dose of drug is required. The other issue is the rapid clearance from the body which limits drug efficacy. Drugs with small molecular weights (diameter < 5 nm or molecular weight < 45 kDa) are subjected to be removed by kidney filtration.[6] Another issue involves cytotoxicity that is not only limited to cancer cells, but also, normal healthy cells.[3]

To overcome the limitations of small molecular weight therapeutics, polymer-based drug delivery systems (PDDS) have been emerged as promising candidates for advanced cancer therapy. Small molecular weight drugs can be incorporated in nanocarriers to be carried to cancer tissues. Nanocarriers' targeting ability is due to the rapid growth of cancer tissues compared to normal tissues. Maeda *et al.* claimed that cancer tumors have leaky vasculatures where macromolecules can be extravasated due to tight lymphatic capillaries allowing for the accumulation of nanocarriers

(Scheme 1.1).[7] On the other hand, nanocarriers could not be infiltrated into normal tissues due to tight endothelial cell lines and functional lymphatic drainage systems. This phenomenon is so-called the enhanced permeability and retention (EPR) effect facilitates the development of passive targeted drug delivery systems. In addition, PDDS enable the enhancement of pharmacokinetics and biodistributions of the small molecule drugs thereby increasing the therapeutic efficacy and minimizing the side effects.[3] Further, nanocarriers have been designed to provide a stealth effect (bypassing biological barriers), thus reducing side effects common to small drugs and enhancing circulation half-life.[8-11]

The performance of the nanocarriers to exhibit these features are dependent on the size of the nanocarriers. Small nanocarriers below 10 nm are subjected to be removed by glomerulus filtration whereas large nanocarriers, in micrometer range, lack the ability to accumulate in the tumor.[12] For cancer targeting drug delivery system, nanocarriers with hydrodynamic radius of 50 nm to 200 nm are considered optimal to avoid clearance by the body and to effectively extravasated and accumulated in tumor sites.[4, 5, 13] Moreover, the size affects other features of nanocarriers such as the release kinetics of the encapsulated drug; larger particles tend to have smaller initial burst release and sustained release.[14]
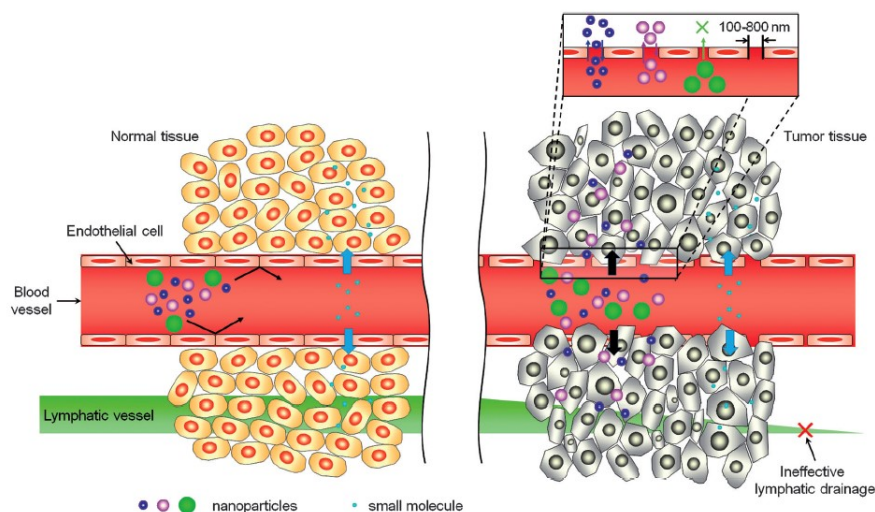
Scheme 1. 1. Schematic illustration of the enhanced permeability and retention (EPR) effect and passive targeting.[3]

1.3 Polyesters in DDS

The use of polymers had a dramatic impact in the landscape of oncology. The most widely explored polymers are polyesters, typically poly(ε-caprolactone) (PCL), polylactide (PLA), poly(lactide-coglycolide) (PLGA) and poly(trimethylene carbonate) (PTMC). Their popularity can be attributed to three of their properties: biocompatibility, biodegradability and tunability.

First, biocompatibility is one of the most important criteria to evaluate biomaterials.[15] The aforementioned polyesters are ideal biomaterials because they are determined to be non-toxic, non-immunogenic and provoke no other diseases. Furthermore, the polyesters do not react with the most of encapsulated drugs. For instance, PLA has been widely used for clinics followed by the FDA approval, demonstrating the safety of the PLA for biomedical applications.[16] Second, biodegradability is an important consideration. Biodegradable polyesters retain their structures until they complete their role and degrade to smaller molecules that can be readily removed from the body. For example, PLGA is degraded chemically by hydrolytic cleavage of ester linkages in the backbone producing lactic acid and glycolic acid. These products are water soluble and non-toxic. They can be removed by the body through renal clearance or metabolized to carbon dioxide and water through the tricarboxylic acid cycle.[17, 18] Third, polyesters can be modified to affect certain features of nanoparticles. For instance, a PEG-PCL diblock copolymer was synthesized via ring opening polymerization for breast cancer treatment.[19] In this system, the PCL component of the micelle enables the encapsulation of Dox (Doxorubicin) while the PEG component provides stealth effect to avoid immune response and long circulating half-life in the body.

1.4 Stimuli-responsive degradation (SRD) systems

Conventional drug delivery systems show slow and uncontrolled release kinetics of encapsulated drugs. Stimuli-responsive degradation (SRD) systems (so-called smart or intelligent drug delivery systems) have been emerged as a promising platform for drug delivery to overcome the limitations of sustained and uncontrolled release of drug from drug delivery systems.[20-22] SRD involves the introduction of dynamic covalent linkages into the design of polymers. To integrate SRD platforms for PDDS, a fundamental understanding of physiological and pathophysiological environments are necessary; the differences can be utilized to design more specific drug delivery systems towards cancer tumor tissues.

As illustrated in Figure 1.1, external stimuli include endogenous stimuli such as pH,[23] glutathione (GSH),[24] reactive oxygen species (ROS),[25] and enzymes[26] and exogenous stimuli such as light,[27] temperature,[28] and magnetic field.[29] The major advantage of SRD polymers is to enable the release of cargoes only when specific trigger is present. Therefore, the timing and the duration of drug release can be adjusted.
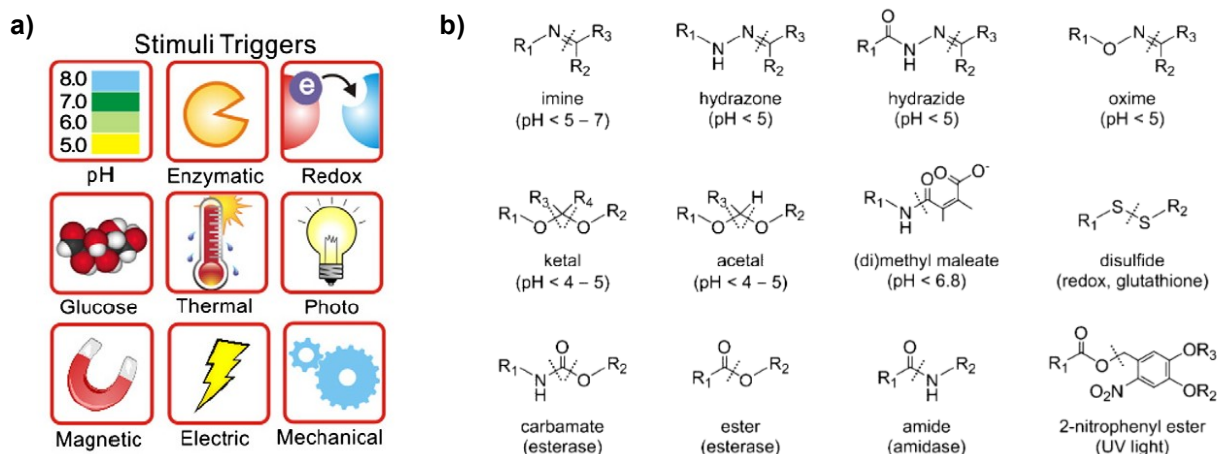
Figure 1. 1. Illustration of variety of stimuli triggers[30] (a) and cleavable linkers that have been used for stimuli-responsive drug delivery systems[31] (b).

1.4.1 Enzyme-responsive DDS

Enzymes play important roles as biological catalysts in the body. They can act on specific substrates, functional groups, or specific molecules in physiological and metabolic processes. The enzymatic activities are necessary for physiological homeostasis and therefore dysregulation of enzyme expressions are often associated with many diseases including cancer.[32-36] Such overexpressed enzymes serve as particularly promising biomarkers.

Given the promise of enzymes, various types of enzyme-responsive PDDS have been developed for controlled release of drugs. Most systems contain covalent linkages that are susceptible to be cleaved by enzymes. Upon cleavages, polymeric nanoparticles can degrade or disassemble to release the encapsulated therapeutics.[37, 38] Two main strategies have been developed. One strategy involves introduction of enzymatically labile linkages to polymer backbone. The other strategy involves incorporation of peptide linkages that can be recognized

and react with specific enzymes. This section highlights the advances in enzyme-responsive polymeric nanoparticles using two strategies.

1.4.1.1 Hydrolase-responsive polymers

In this strategy, polymers are rendered enzyme-sensitive as they have labile moieties in the backbone or side chain that can be cleaved by enzymes. Proteases, glycosidases, and esterases are classified as the subclass of hydrolases and they have been utilized as biomarkers due to their abundance in diseases.[39] A several polymeric nanoparticles have been synthesized targeting different enzymes such as acid phosphatase (APase), penicillin G admidase (PGA) and porcine liver esterase (PLE). The design of the APase, PGA, and PLE-responsive polymers involves incorporation of phosphate group, amide group and ester group, respectively.

For example, APase-responsive double hydrophilic diblock copolymer have been synthesized *via* nitroxide-mediated polymerization.[40] The diblock copolymer contains PEG block and phosphorylated poly(4-vinylphenol) block, yielding water soluble polymer due to the hydrophilicity of PEG and phosphate group. Upon the cleavage of the phosphate group in the presence of APase, the polymer turns to an amphiphilic block copolymer because of the hydrophobicity of the resulting poly(4-vinylphenol) block. Subsequently, this amphiphilic block copolymer spontaneously form spherical micelles with an average diameter of 90 nm by transmission emission microscopy (TEM) (Figure 1.2a). The analysis by ^{31}P NMR indicates that the enzymatic dephosphorylation was slow and some amount of phosphate remained unreacted even after 11 days of incubation with APase at 0.13 mg/mL. Such slow reaction is attributed to the formation of micelles before the cleavage of all the phosphate groups. This work shows great potential of polymeric assemblies as drug delivery systems since their physical and chemical characteristics can be modulated enzyme reactions.

In another study, hydrophobic dendrons have been functionalized with PGA-cleavable phenyl acetamide groups on the end groups stabilized and attached to PEG (Figure 1.2b).[41] The cleavage of the acetamide groups produces amines that are protonated in a physiological pH. The decrease in amphiphilicity triggered the disassembly of micelles, resulting in the release of encapsulated cargoes. On the other hand, they were stable in the presence of PLE (that cleaves the ester bonds) demonstrating their specificities. These results were supported by the decrease in

fluorescence intensity of the Nile red encapsulated in the micelles and by the disappearance of the peaks corresponding to amphiphilic hybrids in the HPLC. These results suggest the accumulation of partially degraded micelles. The fully degraded tetra-amine hybrid was not observed at the relatively low enzyme concentration (0.14 µM) or high enzyme concentration (1.4 µM) over time.
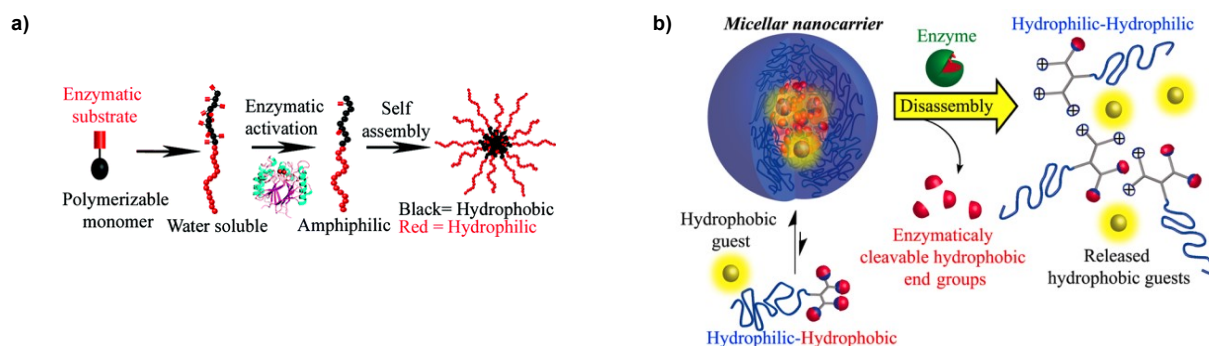
Figure 1. 2. Schematics of enzymatic activation of water soluble diblock copolymer to produce amphiphilic diblock copolymer that can self-assemble[40] (a) and enzyme-responsive release of hydrophobic guests (drugs) from the micellar nanocarriers[41] (b).

The same group has reported esterase-responsive PEG-dendrons consisting of hydrophobic PLE-responsive esters attached to PEG groups.[42] They studied the drug release kinetics by physically encapsulating the coumarin (hybrid 1) or by covalently attaching the coumarin (hybrid 2). The hybrid 1 displayed complete degradation within 2.5 h in the presence of 2.3 µM of PLE whereas the hybrid 2 achieved it after 160 h. All the ester groups were cleaved in the presence of PLE. This type of system could be advantageous since the enzyme-sensitive groups in the mainchain of the polymeric micelles can be degraded into small molecules that can be easily removed by the body followed by the delivery of the encapsulated drug.

1.4.1.2 Polymers labeled with enzyme-responsive peptides

Peptides have been incorporated in various ways to target different disease-associated enzymes such as matrix metalloproteinases (MMP), cathepsin B and elastase. One of the enzymes that are overexpressed in cancer tissues is MMP-2, a type of MMPs.[43-46] MMP-2 is a class of endopeptidases that can recognize and cleave specific peptide bonds. Therefore, substrate peptides of the MMPs can be utilized as enzyme-sensitive moieties in the synthesis of polymeric nanoparticles. Recently, PLA-b-Polypeptide-b-PLA polymer was synthesized by ring opening

polymerization of L-lactide initiated with a peptide containing MMP-2-responsive site (Pro-Leu-Gly-Leu-Ala-Gly sequence).[47] Its nanoparticles with chemotherapeutic agent (5-Fluoruracil), show enhanced cytotoxicity with C2C12 cells expressing MMP-2.[48] Selectivity of the MMP was demonstrated by synthesizing the same polymer with a different peptide sequence. This control experiment did not indicate any cleavage in the peptide linkages. Another group has targeted MMP-2 using synthesized diblock copolymer nanoparticles.[49] The nanoparticles consist of Paclitaxel, an anticancer drug, conjugated to the hydrophobic block and peptide, containing MMP-2 responsive sequence in L-configuration, to the hydrophilic block (Figure 1.3a). The nanoparticles with peptide in L configuration (NP$_L$) proved significant enhancement of therapeutic efficacy *in vivo*. Contrarily, their control experiment with peptide sequence in D-configuration (NP$_D$) demonstrated accumulation of micelles in the targeted tissues but without any recognizable therapeutic effect (Figure 1.3c). Compared to paclitaxel, NP$_L$ exhibited similar degree of tumor growth inhibition with an improved biocompatibility in healthy mice (Figure 1.3b).
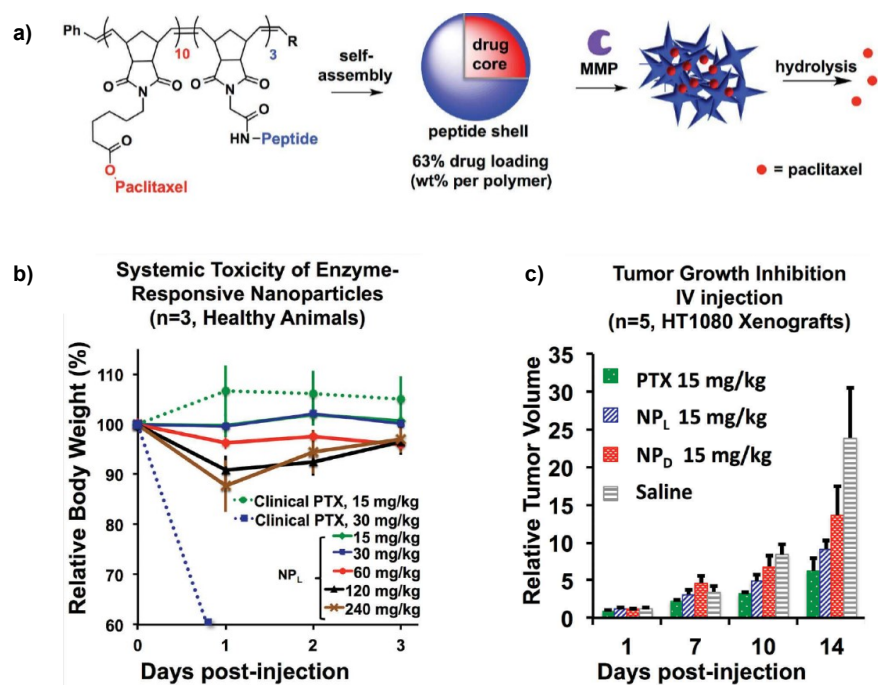
Figure 1. 3. Preparation of MMP-responsive nanoparticles (a). Toxicity of paclitaxel-loaded nanoparticles in healthy mice at the maximum tolerated dose (b) and effective inhibition of tumor growth post IV injection of NP$_L$.[49]

Cathepsin B has been selected as a biological cue for drug delivery systems. Cathepsin B is a lysosomal cysteine protease that is abundant in the intracellular compartment of cancer cells.[50-52] The substrate peptide (Gly-Phe-Leu-Gly, GFLG), has been used for the development of cathepsin B-responsive materials. For example, peptide dendrimer drug conjugate (PEGylated dendron-GFLG-Dox) was synthesized by a copper catalyzed alkyne-azide two-step click reaction.[53] Drug release of conventional polymer-drug conjugate has been reported to be slow mechanism due to high steric hindrance.[54-56] To increase the rate of drug release, Dox was attached to GFLG where this peptide can be cleaved to activate Dox. The resulting nanocarriers show an enhanced Dox release, which is cleaved from peptide. The performance of the formulation was significantly increased in terms of antitumor activity compared to the free Dox *in vivo* at an equal dose.

Another enzyme that is excessively secreted in the diseased site is elastase.[57, 58] Elastase is known to break down peptide bonds of the small amino acids such as Ala-Ala bond.[59] Elastase-sensitive polymer-peptide diblock copolymer was synthesized by a combination of N-carboxyanhydride ring-opening polymerization and nitroxide-mediated radical polymerization.[60] Polystyrene or poly(*n*-butyl acrylate) was used as hydrophobic block. The polypeptide consists of L-glutamic acid and of various quantities of L-alanine. The resulting polymer self-assembles to form micelles which were destabilized in response to the elastase. The rate of disassembly was controlled with the amount L-alanine content in the polypeptide. The results demonstrate the tunability and selectivity of enzyme-sensitive systems to achieve both spatial and temporal control of the drug release.

1.4.2 Oxidation-responsive DDS

ROS, chemically reactive species, are produced in the body. Typical examples of ROS include superoxide (O_2^-), hydrogen peroxide (H_2O_2), hydroxyl radical ($\cdot OH$), hypochlorite ion (OCl^-). These ROS play an important role in cellular signaling pathways.[61] Under healthy physiological condition, ROS levels are controlled through the generation of ROS scavenging species, such as GSH.[62, 63] Upregulated ROS could cause cell deaths or cellular damages. On the other hand, high level of ROS could be found in pathological conditions. In the case of cancer cells, they can survive at the higher concentration of ROS and their ROS level is 10 to 100-fold higher than that in normal cells.[69, 70] The distinct concentration can be an attractive trigger for the

development of drug delivery systems. [64, 65 64, 6564-66,71,72] Consequently, ROS-responsive materials, or oxidation-responsive materials, have been synthesized oxidizable groups such as sulfides and boronic esters. These materials can be categorized based on two mechanisms: solubility switch mechanism and degradation mechanism.

1.4.2.1 Solubility switch mechanism

Sulfide (or thioether) containing polymeric biomaterials are an example of ROS-responsive materials by solubility switch mechanism. Under oxidative environment, hydrophobic sulfide groups can be converted to hydrophilic sulfoxide and to sulfone group.[66] For example, Gupta et al. synthesized and characterized diblock copolymer of propylene sulfide and N,N-dimethylacrylamide (poly(PS-b-DMA)) through the reversible addition-fragmentation chain transfer (RAFT) polymerization.[67] Poly(PS-b-DMA) micelles were formed by solvent evaporation method and the diameter was determined to be 99 nm by DLS. After 24 hrs of incubation with H_2O_2 (3.3 vol %), the size of micelles decreased to 5 nm in diameter. To further evaluate oxidation-triggered release, they incorporated fluorescent dye, Nile Red, into the micelles (Figure 1.4). They exhibit more rapid release at the relatively high concentration of H_2O_2 and slower release at the lower concentration. In another study, a sulfide-containing diblock copolymer consisting of PEG block and 2-(methylthio)ethyl glycidyl ether block has been synthesized by anionic ring opening polymerization.[68] As shown in Figure 1.4, both DLS and ^{1}H-NMR results show the disassembly of micelles as a consequence of oxidation of sulfide to sulfoxide and to sulfone in the presence of H_2O_2 (1% by weight) or sodium hypochlorite (1% by weight).
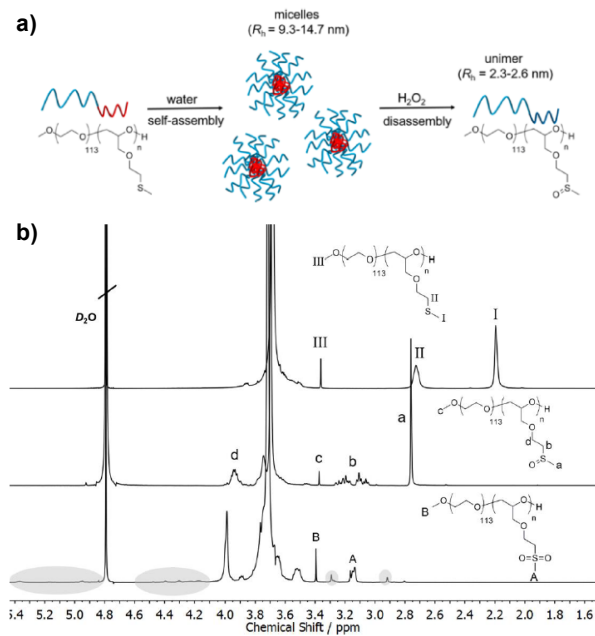
Figure 1. 4. Illustration of micelle formation of PEG-b-PMTEGE and the disassembly upon treatment with H_2O_2 (a) and the ^{1}H NMR spectra before (top) and after oxidation with H_2O_2 (middle) and NAOCl (bottom) (b).[68]

1.4.2.2 Degradation mechanism

Boronic ester groups are an example of degradable ROS-responsive materials. Aryl boronic ester group can be oxidized to initiate the quinone methide rearrangement leading to the polymer degradation (Figure 1.5b).[69-72] For example, new oxidation-responsive polymer bearing aryl boronic ester and adipic acid was synthesized through step growth polymerization.[72] To vary the release rate, two different polymers were synthesized where the aryl boronic ester is either directly linked to the polymer backbone or linked to an ether group (Figure 1.5a). Then, Nile red was encapsulated in the polymeric micelles through an oil-in-water emulsion technique. Upon exposure to H_2O_2, the release rate of the polymer **2** (with ether linkage) was determined to be an order of magnitude more rapid than that of polymer **1** (Figure 1.5c) because H_2O_2 is more accessible to the reactive site. For biological assessment in vitro, activated neutrophil was used to create high levels of ROS. The release of the model drug from polymer 2 micelles was twice as fast as polymer 1 micelles. In this study, sensitivity of the polymeric assemblies has been significantly improved by introducing a linker, showing versatility of polymeric systems.
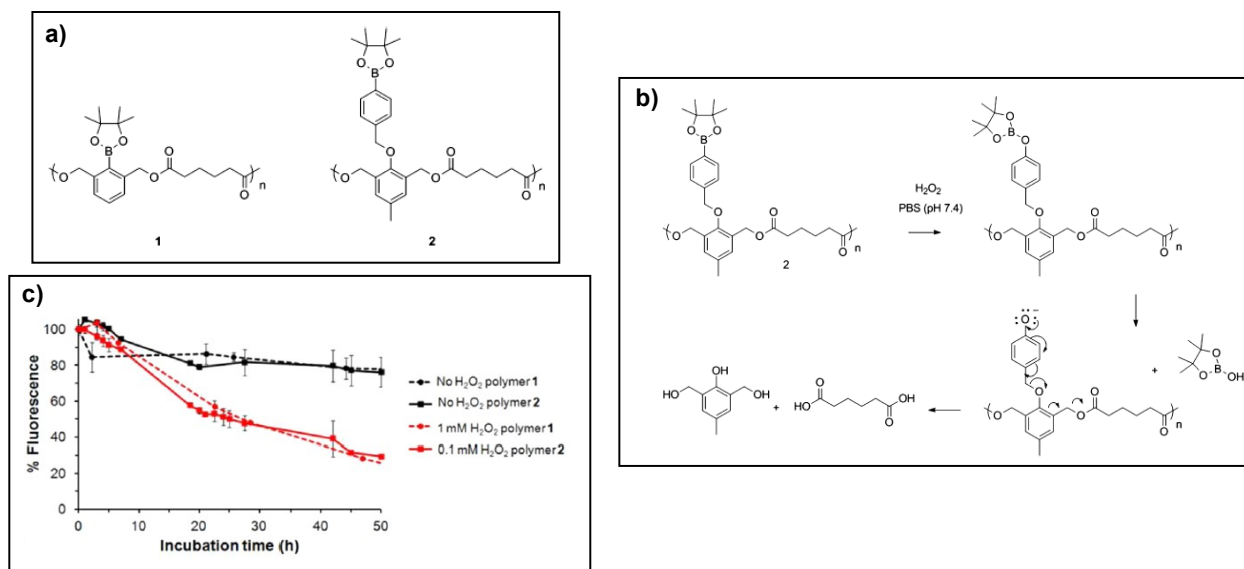
Figure 1. 5. Chemical structures of polymer 1 and 2 (a). Mechanism of polymer 2 degradation upon oxidation by H_2O_2 (b). Fluorescence of Nile Red upon exposure to H_2O_2 (c).[72]

1.5 Scope of this thesis

My master thesis describes the synthesis and biological assessment of dual ROS and esterase-responsive drug delivery systems based on polyesters for cancer therapy. Stimuli-responsive polyester was synthesized via the facile thiol-ene Michael addition reaction. This polyester was used throughout studies in chapter 2 and chapter 3.

Chapter 2 describes synthesis and size optimization of dual enzyme and oxidation-responsive polyester-based nanoparticulates (DPE-NPs) formulations. The hydrophobic polyester can form nanoparticulates with the aid of biocompatible stabilizers. The sizes of the nanoparticulates were tuned by employing different fabrication methods such as solvent evaporation emulsion method and microfluidics method. For each method, the effects of different parameters were studied: formulation parameters (molecular weight of DPE, concentration of NPs, nature and amount of stabilizers) and microfluidic parameters (flow rate ratio and total flow rate). The enzyme and oxidation-responsive degradations were examined and the cytotoxicity of the DPE-NPs were assessed *in vitro*.

In chapter 3, a promising formulation of DPE-NPs was assessed in depth as nanocarriers for cancer therapy. The enhanced and controlled drug release was examined in the presence of H_2O_2 and esterase. H_2O_2 can change the hydrophobic/hydrophilic balance of the nanoparticulates that can trigger release of encapsulated drugs. In the presence of the esterase, the cleavage of ester linkages causes the degradation of polymeric integrity. Two mechanisms lead to the enhanced release of encapsulated cargoes. The potential of DPE-NPs as intracellular nanocarriers was evaluated *in vitro* experiments using 2D and 3D cell culture.
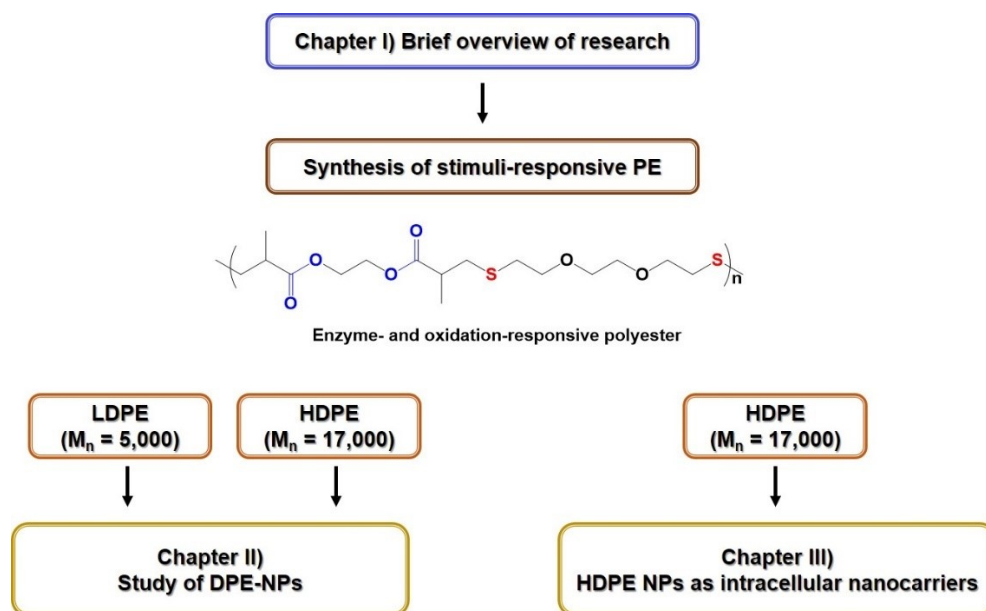
Figure 1. 6. Summary of overall projects of esterase and oxidation-responsive polyester-based materials. (LDPE and HDPE = low molecular weight and high molecular weight dual enzyme and oxidation-responsive polyester).

Chapter 2
Microfluidic assembly to synthesize dual enzyme/oxidation-responsive polyester-based nanoparticulates with controlled sizes for drug delivery

This chapter reproduced the article published in *Langmuir*, **2018**, 34, 3316-3325 with the permission from the publisher.

2.1 Introduction

Polymer-based drug delivery systems (PDDS) that can deliver therapeutics to disease sites have been considered as a promising nanoplatform in pharmaceutical science and biomedical research.[73-75] Well-designed PDDS can improve the biodistribution of small molecular weight drugs in the body, thus enhancing drug efficacy and minimizing side effects. Given the promise of PDDS, polymer-drug conjugates (prodrugs),[76-78] dendrimers,[79] crosslinked nanogels,[80-84] and block copolymer-based nanoassemblies,[85-88] and nanoparticulates[89, 90] are the typical examples of extensively studied as promising candidates.

Particularly, nanoparticulates are composed of hydrophobic cores enabling the encapsulation of hydrophobic drugs. A conventional method for the fabrication of aqueous nanoparticulates is the batch process where a mixture of aqueous solution of stabilizers with organic solution of polyesters is subjected to sonication, dialysis, or emulsification. However, conventional batch process could be limited in affording control of NP sizes. Indeed, the optimal size of nanoparticulates (NPs) for effective drug delivery to biological systems is reportedly 50–200 nm in order to reduce undesired side effects while maintaining antitumor activity via the so-called enhanced permeability and retention effect.[91-94] Microfluidic process utilizing continuous mixing of the aqueous and organic solutions in micro-channels of miniature chips has been explored as a promising means to the fabrication of various polymer-based nanostructures for drug delivery.[95-97] Microfluidic process enables the fabrication of NPs with their tunable sizes as well as to produce well-defined NPs smaller than those by conventional methods achieving their size limit.[98, 99] Given such features, numerous reports describe self-assembled nanoassemblies,[100-103] liposomes,[104-107] microcapsules,[36, 108-112] and microgels.[113] However, only few reports describe the exploration of

microfluidics to fabricate hydrophobic nanoparticulates dispersed with external stabilizers in aqueous solutions.

Polyesters typically hydroxyalkanoic acid-based aliphatic polyesters such as polylactide and its copolymers have been mostly used as hydrophobic core-forming polymers for the fabrication of polyester-based nanoparticulates (PENPs).[114, 115] However, a critical challenge of conventionally-designed aqueous PENP colloids is the slow and uncontrolled release of encapsulated drugs in targeted sites. Such slow release is attributed to delayed diffusion of hydrophobic drugs through nanopores in hydrophobic cores.[116] Stimuli-responsive degradation (SRD) is a promising platform that involves the incorporation of stimuli-responsive linkages into the design of PDDS. In response to external stimuli, preferably cellular components, these linkages can be cleaved or be involved in a change of polarity.[3, 117-123] This process causes the disintegration or the destabilization of PDDS, thus leading to controlled/enhanced release of encapsulated therapeutics. In particular, enzymatic and oxidative reactions are among cellular stimuli that have recently received an increasing attention. Enzymes such as esterase to cleave ester linkages[124-126] and oxidants such as hydrogen peroxide as a typical reactive oxygen species[127] can be found in cellular environments. However, these stimuli have been explored mostly on amphiphilic block copolymers in the synthesis of self-assembled nanoassemblies with single response.[128-130] To our understanding, no reports describe aqueous stabilizer-aided DPE colloids exhibiting dual enzyme and oxidation response.

In this work, we have investigated the microfluidic process for the fabrication of aqueous dual stimuli-responsive nanoparticulate colloids with diameters ranging at 50-150 nm. The colloids are composed of dual enzyme and oxidation-responsive polyester (DPE) labeled with ester (enzyme response) and sulfide (oxidation response) linkages on the backbones that were synthesized by polyaddition through a click-type thiol-ene reactions. With a selection of polymeric stabilizers including poly(ethylene glycol) and a Pluronic surfactant, microfluidic parameters (total flow rate (TFR) and organic/aqueous flow rate ratio (FRR)) as well as formulation parameters (molecular weight of DPE, concentration of NPs, nature and amount of stabilizers) were investigated to map the tunability of NP sizes. The formed colloids were further characterized for dual stimuli-responsive degradation as well as in vitro cell cultures with cytotoxicity and cellular uptake.

2.2 Experimental

2.2.1 Instrumentation

^{1}H-NMR spectra were recorded using a 500 MHz Varian spectrometer. The CDCl$_3$ singlet at 7.26 ppm was selected as the reference standard. Molecular weight and molecular weight distribution of DPEs were determined by gel permeation chromatography (GPC). An Agilent GPC was equipped with a 1260 Infinity Isocratic Pump and a RI detector. Two Agilent PLgel mixed-C and mixed-D columns were used with DMF containing 0.1 mol% LiBr at 50 °C at a flow rate of 1.0 mL/min. Linear poly(methyl methacrylate) standards from Fluka were used for calibration. Aliquots of the polymer samples were dissolved in DMF/LiBr. The clear solutions were filtered using a 0.45 μm PTFE filter to remove any solvent-insoluble species. A drop of anisole was added as a flow rate marker. The size of DPE-NPs in hydrodynamic diameter (by intensity) was measured by dynamic light scattering (DLS) at a fixed scattering angle of 175° at 25 °C with a Malvern Instruments Nano S ZEN1600 equipped with a 633 nm He-Ne gas laser. Transmission Electron Microscopy (TEM) images were obtained using a Philips Tecnai12 TEM, operated at 80kV and equipped with a thermionic LaB6 filament. An AMT V601 DVC camera with point to point resolution and line resolution of 0.34 nm and 0.20 nm respectively was used to capture images at 2048 by 2048 pixels. To prepare specimens, the NP dispersions were dropped onto copper TEM grids (400 mesh, carbon coated), blotted and allowed to air dry at room temperature. Subsequently, uranyl acetate (1%) was applied on the TEM grids and then dried again at room temperature. Fluorescence spectra on a Varian Cary Eclipse Fluorescence spectrometer were recorded using a 1 cm wide quartz cuvette.

2.2.2 Materials

2,2'-(ethylenedioxy)diethanethiol (DSH, 95%), ethylene glycol dimethacrylate (EGDMA, 98%), triethylamine (Et$_3$N, ≥99%), poly(ethylene glycol) (PEG, MW = 6,000 g/mol), Pluronic L-64 (PL02, MW = 2,900 g/mol), esterase from porcine liver (18 U/mg; one unit will hydrolyze 1 μmol of ethyl butyrate to butyric acid and ethanol per minute at pH 8.0 at 25 ºC), Nile Red (NR), and hydrogen peroxide (H$_2$O$_2$, 30% w/w) from Aldrich, dialysis tubing from Spectrum Labs, Dulbecco's modified eagle medium (DMEM) and fetal bovine serum (FBS) from Wisent, phenol-red free DMEM from Thermo-Fisher Scientific, and 3-(4,5-dimethylthiazol-2-yl)-2,5-diphenyltetrazolium bromide (MTT) from Promega were purchased and used as received.

2.2.3 Synthesis of DPE

For the synthesis of HDPE, DSH (3.7 g, 20.2 mmol) was added to a solution consisting of EGDMA (4.0 g, 20.2 mmol) and Et$_3$N (565 μL, 4.0 mmol) dissolved in DMSO (13.5 mL) to start polymerization. For the synthesis of LDPE, DSH (2.0 g, 10.1 mmol) was added to a solution consisting of EGDMA (2.11 g, 11.6 mmol) and Et$_3$N (565 μL, 4.0 mmol) dissolved in DMSO (7 mL). The reaction mixture for HDPE was stirred at room temperature for 2 days and the reaction mixture for LDPE was stirred for 24 hrs. The as-synthesized solutions were precipitated from cold methanol to remove excess Et$_3$N and unreacted monomers. The precipitates were isolated by a vacuum filtration and dried in a vacuum oven at room temperature for 12 hrs, prior to analysis by ^{1}H NMR in CDCl$_3$ and GPC.

2.2.4 Microfluidic preparation of stabilizer-aided NP colloids by nanoprecipitation

Scheme 2.1a illustrates the fabrication of DPE-NPs using NanoAssemblr Benchtop equipped with disposable cartridges (Precision Nanosystems Inc, Vancouver, Canada). Total volume was set to 2 mL where the first 0.25 mL was discarded and 1.75 mL of resulting solution was collected and analyzed. For fabrication, stock solutions of DPE in acetone at varying concentrations (2- 50 mg/mL) as well as PL02 and PEG in water at varying concentrations (0.004-5 mg/mL) were prepared. As an example to fabricate aqueous HDPE-NP colloids under the microfluidic conditions of NP (HDPE+PL02) = 3.8 mg/mL, TFR = 12 mL/min, and FRR = 3/1 (aqueous/organic), an organic HDPE solution (14 mg/mL, 0.5 mL) and an aqueous PL02 solution (0.47 mg/mL, 1.5 mL) were injected into each inlet, to attain total volume of the resulting dispersion = 2 mL. The resultant HDPE-NP dispersions were subjected to dialysis using a dialysis tubing with MWCO = 12 kDa against water (1 L) for 4 hrs to remove acetone. To study the effect of TFR and FRR, the concentrations and injected volumes of aqueous and organic stock solutions were varied as the input parameters for *in-suite* software of NanoAssemblr Benchtop microfluidic mixer. The size and diameter of syringes were fixed. Further experiments were performed with a single sample. The reproducibility for microfluidic preparation was examined with the freshly-prepared triplicates from a formulation as a typical example shown in Figure A.4.

Similar procedure was used to fabricate NR-loaded HDPE-NPs with the use of NR (0.4 mg) dissolved in acetone with HDPE (2 mg/mL, 1 mL) and PEG (2 mg/mL, 1 mL) under the conditions of NP =2 mg/mL, HDPE/PEG = 1.0 wt/wt, FRR = 1/1, and TFR = 12 mL/min. Followed by the

removal of acetone by dialysis against water, resulting NR-loaded dispersion was filtered by using 0.45 μm PES filter to remove free NR, yielding aqueous NR-loaded NPs.

2.2.5 Batch preparation of stabilizer-aided NPs with solvent evaporation method

Generally, a mixture of aqueous stabilizer solution and organic HDPE solution was sonicated for 5 min (amplitude = 15 %, 10 sec on, 2.5 sec off) using a digital sonifier (Branson). The resulting mixture was kept stirred for 24 hrs at room temperature to remove residual THF, yielding aqueous NP dispersion at 2.0 mg/mL.

2.2.6 Oxidative/enzymatic degradation of NPs

For oxidation-responsive degradation of NPs in the presence of hydrogen peroxide, aliquots of aqueous NP dispersion (0.4 mg/mL, 2.3 mL) were incubated with 1% v/v hydrogen peroxide under stirring at room temperature. For enzymatic degradation in the presence of esterase, aliquots of aqueous NP dispersion (0.4 mg/mL, 1.7 mL) were incubated with esterase, attaining 10 U. For both oxidation/enzymatic degradation, aliquots of NP dispersion (0.4 mg/mL, 1.7 mL) were incubated with 1% v/v hydrogen peroxide and esterase, attaining to 10 U. DLS was used to follow any changes in size distribution over incubation time.

2.2.7 Cell culture

HeLa cervical cancer cells were cultured in DMEM (Dulbecco's modified Eagle's medium) containing 10% FBS (fetal bovine serum) and 1% antibiotics (50 units/mL penicillin and 50 units/mL streptomycin) at 37 °C in a humidified atmosphere containing 5% CO_2.

2.2.8 Cell viability using MTT assay

HeLa cells were plated at 5×10^5 cells per well into a 96-well plate and incubated for 24 h in DMEM (100 μL) containing 10 % FBS and 1 % antibiotics. Then, they were incubated with various concentrations of NPs for 48 h. Blank controls without nanoparticulates (cells only) were run simultaneously as control. Cell viability was measured using CellTiter 96 Non-Radioactive Cell Proliferation Assay kit (MTT, Promega) according to the manufacturer's protocol. Briefly, a MTT solutions (15 μL) was added into each well. After 4 h incubation, the medium containing unreacted MTT was carefully removed. DMSO (100 μL) was added into each well in order to dissolve the formed formazan purple crystals, and then the absorbance at $\lambda = 570$ nm was recorded

using Powerwave HT Microplate Reader (Bio-Tek). Each concentration was 6-replicated. Cell viability was calculated as the percent ratio of the absorbance of mixtures with nanoparticulates to control (cells only).

2.2.9 Live cell imaging

Stable HeLa cancer cells were plated at 1×10^5 cells/well in 35-mm glass-bottom dishes. HeLa cells were then washed with PBS three times and phenol red free DMEM medium (0.5 mL) was added to the cells. Cells were treated with aqueous NR-loaded NPs or NR solution in acetone to make NR = 1 µg/mL and incubated for 4 h at 37 ºC. Live-cells were visualized on a Nikon Eclipse Ti, inverted epifluorescence-Lambda XL Microscope equipped with LED Heliophor at 488 nm with a Photometrics Evolve EMCCD camera and a 40x/0.95NA objective. Images were acquired with NISElements Version 4.0. Images were viewed and analyzed on Image J.
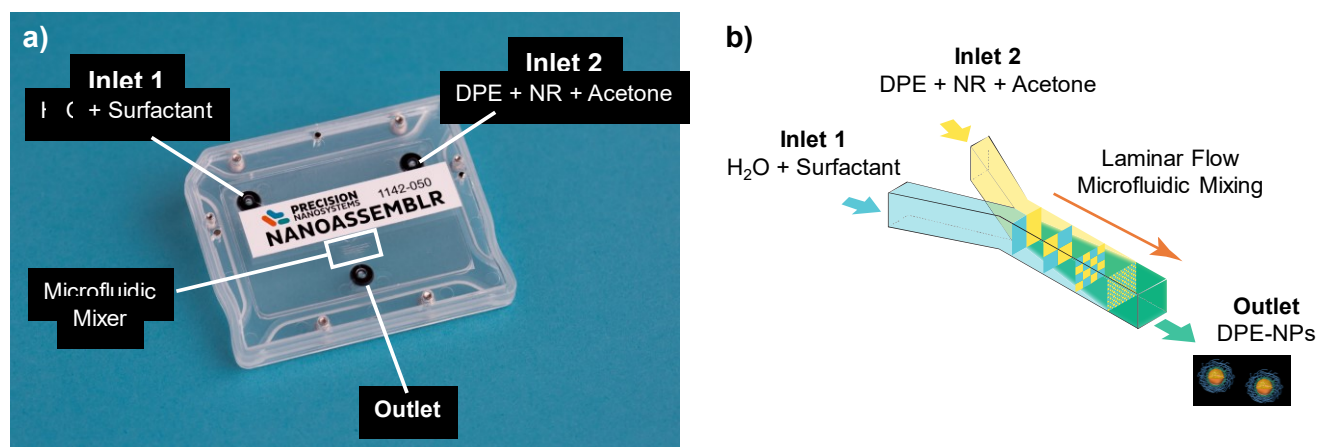
Scheme 2. 1. Digital image of microfluidic cartridge (a) and illustration of microfluidic preparation of DPE-NPs using the NanoAssemblr Benchtop (b).

2.3 Results and discussion

2.3.1 Synthesis of DPEs

Figure 2.1a illustrates our approach utilizing a base-catalyzed thiol-ene addition to synthesize dual enzyme/oxidation-responsive DPE labeled with ester and sulfide linkages on their backbones. In the presence of Et_3N as a base, the mole ratio of DSH to EGDMA (i.e. thiol and methacrylate groups) was varied to synthesize well-defined PEs with two different molecular weights at room temperature. The number average molecular weight (M_n) was 5 kg/mol with $M_w/M_n = 1.7$ (M_w:

the weight average molecular weight) for LDPE and 17 kg/mol with $M_w/M_n = 1.5$ for HDPE, determined by GPC with PMMA standards. ^{1}H-NMR spectrum in Figure 2.1b confirms the structure of the purified PEs.
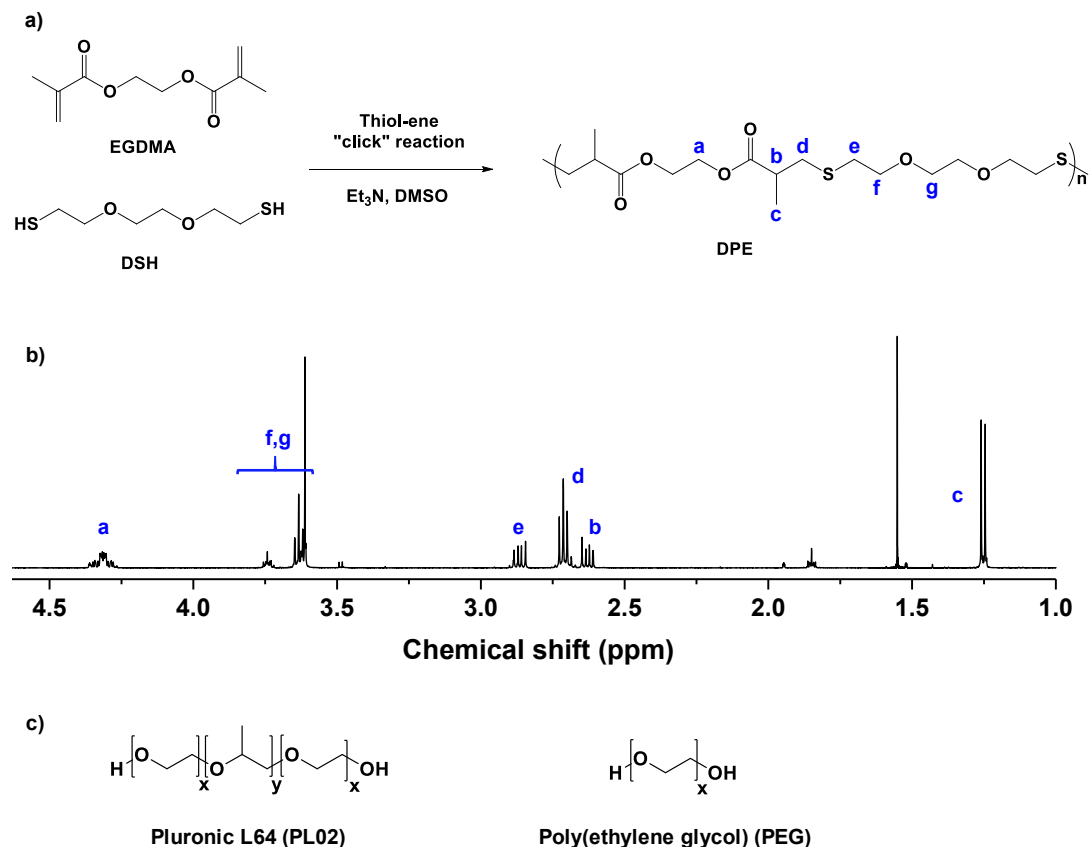
Figure 2. 1. Synthetic scheme through a base-catalyzed thiol-ene reaction to polyesters labeled with sulfide and enzyme linkages on the backbones, (a) ^{1}H-NMR spectrum of HDPE in CDCl$_3$ (b) and chemical structure of Pluronic and PEG (c).

2.3.2 Design of microfluidic preparation

The procedure in our experiments includes the preparation of an organic stock solution of DPE in acetone and an aqueous stock solution of stabilizers at given concentrations. As illustrated in Scheme 2.1b, they were injected to be mixed in the microfluidic channels to form nanoaggregates in a mixture of organic solvent and water. In our experiments, acetone (boiling point = 56 °C) was used as an organic solvent to dissolve DPE. The removal of acetone allows for the preparation of colloidally-stable DPE-NPs stabilized with stabilizers in aqueous solution. Two methods to

remove acetone were examined: a dialysis method with dialysis tubing with MWCO = 12 kDa over water and a solvent evaporation method to open air in fume hood. HDPE was examined with PL02 stabilizer under microfluidic conditions including TFR (total flow rate) = 12 mL/min, and FRR (aqueous/organic flow rate ratio) = 3/1. The final concentration of NP (DPE and PL02) was designed to be 3.7 mg/mL.

As compared in DLS diagrams of Figure 2.2, aqueous NPs prepared by two methods had monomodal and narrow size distribution as PDI < 0.13. Although a small portion of large aggregates is present at less than 4% by intensity in both DLS diagrams, they are negligible by volume analysis (<0.1% population). Nevertheless, aqueous NPs prepared by dialysis method had diameter = 89 nm, which appeared to be smaller than that (102 nm) for NPs prepared by solvent evaporation method by intensity. Further, the dialysis method could remove not only acetone but also more importantly excess stabilizers from aqueous dispersion. Consequently, the dialysis method was used for our further experiments.
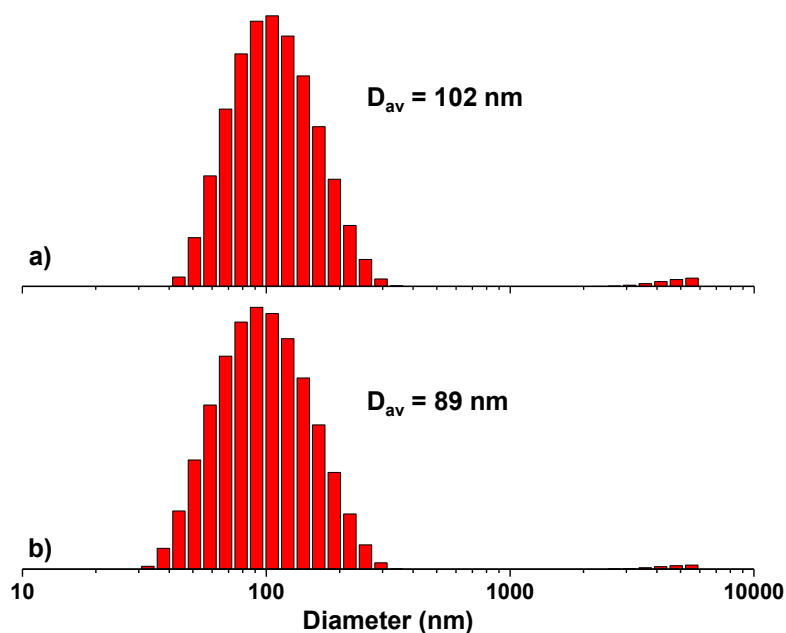
Figure 2. 2. DLS diagrams (by intensity) of HDPE-NPs stabilized with PL02 in aqueous solution purified by solvent evaporation method (a) and dialysis (b). Microfluidic conditions: PL02/HDPE = 0.1/1 wt/wt, NP = 3.7 mg/mL, TFR = 12 mL/min, and FRR = 3/1.

2.3.3 Investigation of microfluidic parameters

The microfluidic device enables control over two additional parameters compared to conventional solvent evaporation method. TFR depicts the total volume of fluids that are pumped into the two inlets at a given time frame. FRR describes volume ratio of the aqueous and organic phases. Both TFR and FRR are the important microfluidic parameters that significantly influence the mixing rate of organic and aqueous phases in the microchannel, thus the size and size distribution of NPs in aqueous solutions.[100] Here, the two parameters were examined with both HDPE and LDPE in the presence of PL02 stabilizer as the ratio PL02/DPE = 0.1/1 wt/wt.

TFR was first varied from 2 to 12 mL/min with a fixed FRR = 3/1. Figure 2.3 shows the size results. For HDPE NPs, the diameter was 104 nm with TFR = 4 mL/min. It decreased to 94 nm when TFR increased to 6 mL/min. Upon the further increase in TFR to 12 mL/min, the diameter appeared to be unchanged. For LDPE NPs, the diameter was 137 nm with TFR = 4 mL/min and continuously decreased to 118 nm by 20 nm upon further increase of TRP to 12 mL/min. Furthermore, the diameters of all HDPE-NPs were smaller than those of all LDPE-NPs at the given TFR. For example with TRF = 12 mL/min, the diameter was 96 nm for HDPE-NPs comparable to 118 nm for LDPE-NPs. Promisingly, all the formed NPs were monomodal with narrow size distribution as PDI < 0.1.
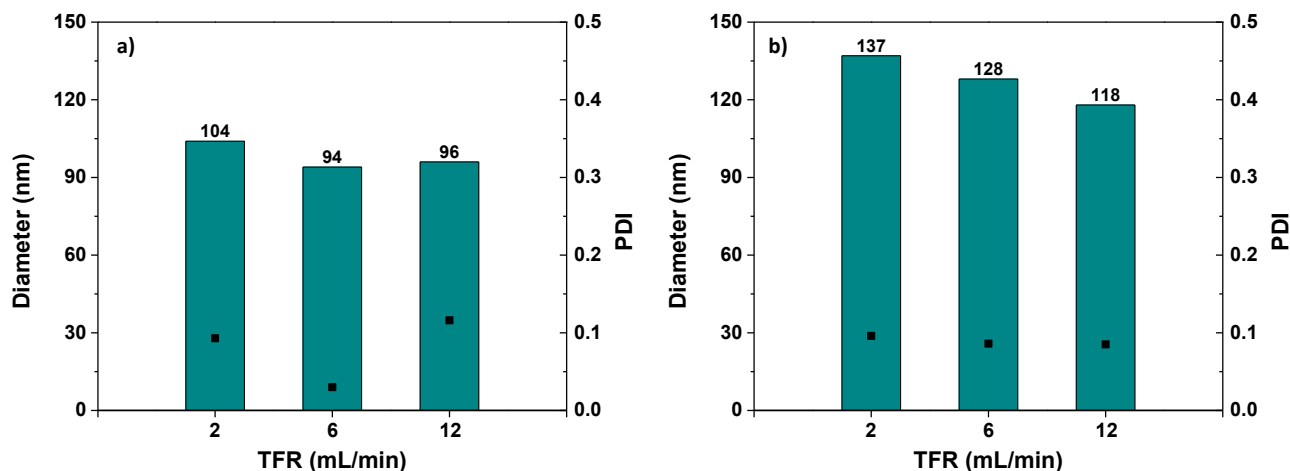
Figure 2. 3. Sizes and size distributions of aqueous NPs of HDPE (a) and LDPE (b) prepared with varying TFRs. Microfluidic conditions: FRR = 3/1, PL02/HDPE = 0.1/1 wt/wt, and NP = 3.7 mg/mL. Note the number on each bar denotes the average diameter.

In another set of the experiments, FRR (here, PL02/DPE ratio) was examined with the fixed TFR = 12 mL/min. As seen in Figure 2.4, the diameter increased with an increasing FRR from 1 to 9. Specifically, the diameter increased largely from 60 to 119 nm by 59 nm for HDPE-NPs, while it increased from 111 to 136 nm by 25 nm for LDPE-NPs. An interesting observation was that the trend of increasing size with FRR is different from a lipid nanoparticle system based on 1-palmitoryl-2-oleyl phosphatidylcholine (POPC), which shows the limit size nanoparticle with FRR >2.[99] Such opposite trend is presumably attributed to different stabilization mechanisms: oil-in-water emulsion-type polyester nanoparticles stabilized with external stabilizers for our system vs self-assembled nanoparticles of lipid amphiphiles. Similar to TFR results, HDPE-NPs had smaller diameters than LDPE-NPs prepared under similar conditions. Promisingly, PDI values for both HDPE and LDPE-NPs were as low as ≈0.2, although they appeared to increase with an increasing FRR.
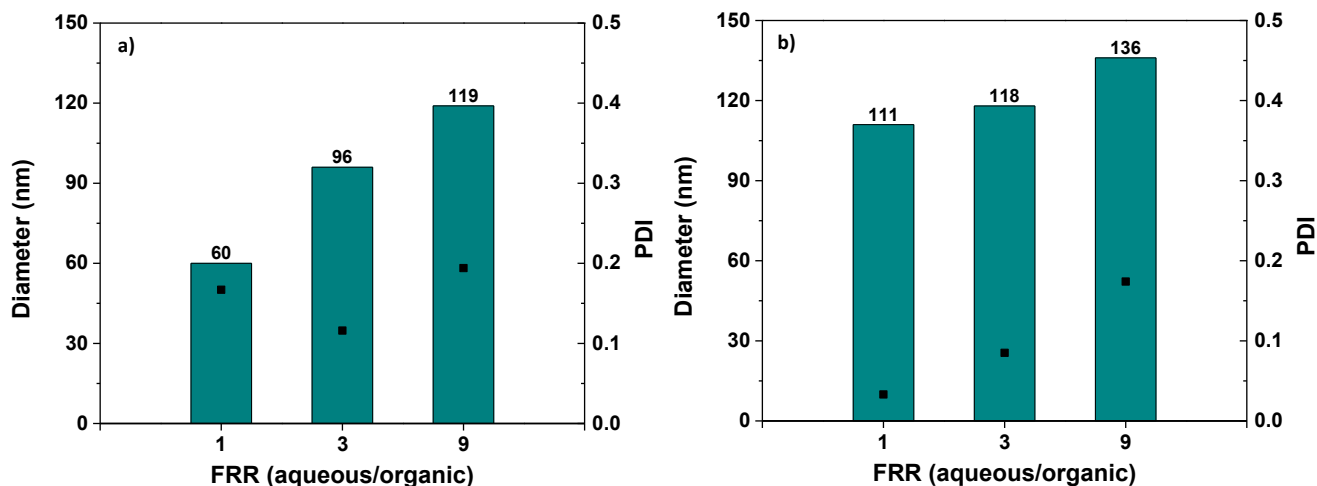
Figure 2. 4. Sizes and size distributions of aqueous NPs of HDPE (a) and LDPE (b) prepared with varying FRR. Microfluidic conditions: TFR = 12 mL/min, PL02/DPE = 0.1/1 wt/wt, and NP = 3.7 mg/mL. Note the number on each bar denotes the average diameter.

2.3.4 Investigation of formulation parameters

Given the results obtained from our investigation on microfluidic parameters, three formulation parameters were examined with HDPE: concentration of NPs, nature and amount of stabilizers. Figure 2.5 summarizes the size and size distributions of HDPE-NPs prepared with PL02 and PEG

with varying concentrations of NPs (HDPE + stabilizer) under the microfluidic conditions including TFR = 12 mL/min and aqueous/organic FRR = 3/1. Overall the diameter increased with an increasing concentration of NPs in aqueous solution. Interestingly, it increased step-wise in the three ranges of NP concentrations: as low as 1 mg/mL, 4-7 mg/mL, and as high as 14 mg/mL. For example, the diameter of HDPE-NPs with PEG stabilizer was 54 nm at 1 mg/mL, 86-93 nm at 4-7 mg/mL, and 181 nm at 14 mg/mL (Figure 2.5b). The formed HDPE-NPs were monomodal at up to 7 mg/mL, but bimodal at 14 mg/mL by intensity (see Figure A.1). The NPs prepared at 1 and 4 mg/mL concentrations exhibit excellent colloidal stability on shelf with no evidence of precipitation over 2 months. However, the NPs prepared at 7 and 14 mg/mL concentrations were precipitated after 2 months. No significant effect of stabilizers (PEG and PL02) was observed on size and size distribution.
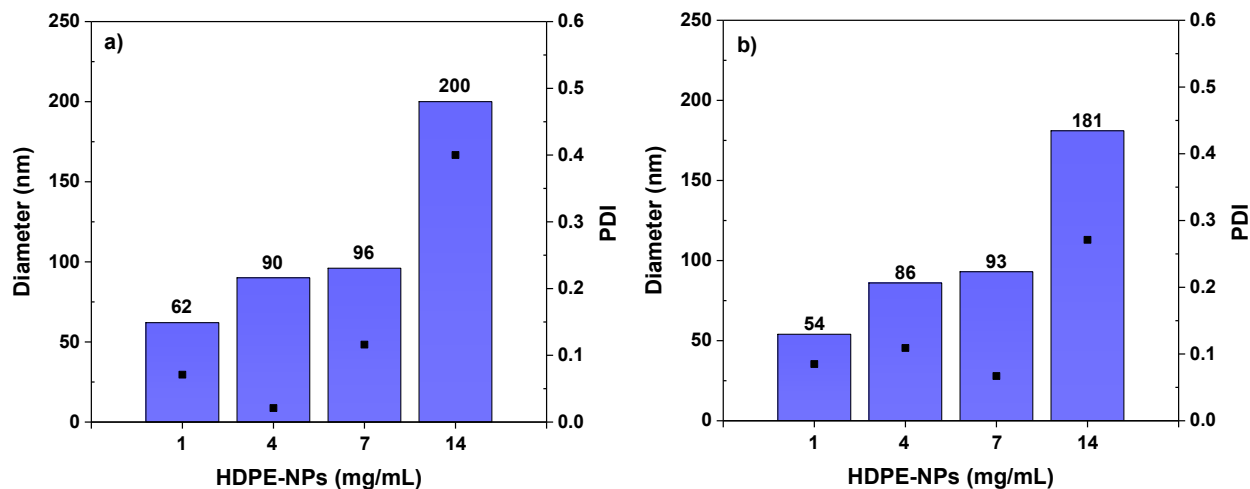
Figure 2. 5. Sizes and size distributions of aqueous HDPE-NPs prepared in the presence of PL02 (a) and PEG (b) at various NP concentrations. Microfluidic conditions: TFR = 12 mL/min, FRR = 3/1, and stabilizer/HDPE = 0.1/1 wt/wt.

Figure 2.6 shows the effect of the amount of stabilizers (PL02 and PEG) as the weight ratio of stabilizer/HDPE on size and size distribution. When the stabilizer was added up to stabilizer/HDPE = 0.5/1 (33 wt%), the diameter decreased to 96 nm with PL02 and 93 nm with PEG. Upon further addition of stabilizer as stabilizer/HDPE = 5/1 (83 wt%), the diameter significantly decreased to 47 nm with PL02 and 67 nm with PEG. Interestingly, HDPE enabled formation of aqueous NPs whose diameter = 102 nm with monomodal and narrow size distribution (PDI = 0.03) in the

absence of stabilizers. This result suggests the formation of aqueous HDPE-NPs with no aids of stabilizers through microfluidic process (Figure A.2). The plausible reason is due to the presence of two ethylene oxide units in repeating units of polyester backbones, which could retain the hydrophilicity of the formed NPs. However, the stability was lower with precipitation within 1 week.
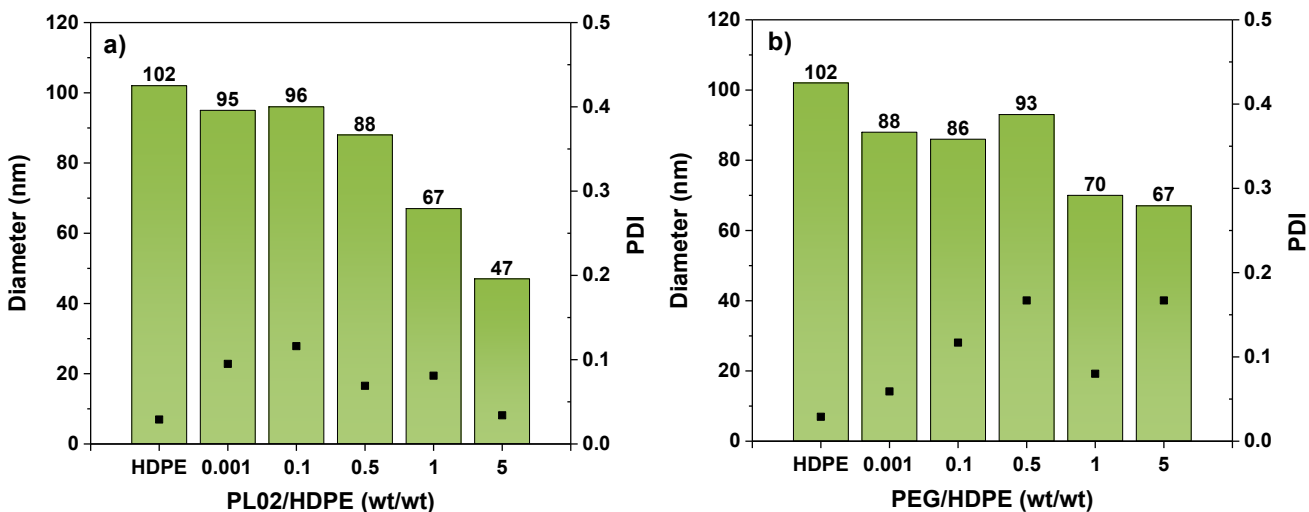
Figure 2. 6. Sizes and size distributions of aqueous NPs of HDPE prepared in the presence of PL02 (a) and PEG (b) at various NP concentrations. Microfluidic conditions: TFR = 12 mL/min, FRR = 3/1, and NP concentration = 3.4 g/mL.

2.3.5 TEM for morphology analysis

TEM was used to get an insight into the morphology of NPs in dried state on carbon grid. Figure 2.7 shows the typical TEM image of aqueous HDPE-NPs prepared with PEG/HDPE = 5/1 wt/wt. Their morphologies appeared to be spherical, with an average diameter to be 60 ± 18 nm, which is similar to the results obtained by DLS (67 ± 2 nm by intensity).
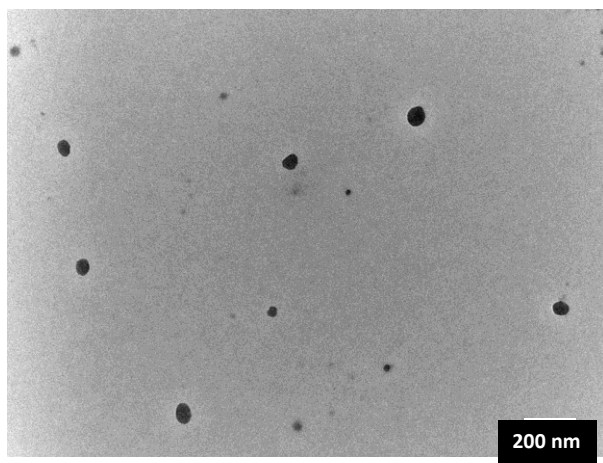
Figure 2. 7. TEM image of aqueous HDPE-NPs prepared with PEG/HDPE = 5/1 wt/wt. (n = 20)

2.3.6 Comparison with batch process for nanoparticulate preparation

A batch process involving mixing organic HDPE solution with aqueous stabilizer solution by sonication was examined to synthesize a series of HDPE-NPs in the presence of PL02 or PEG stabilizers. Figure 2.8 compares the diameter of aqueous HDPE-NPs prepared by microfluidic process with batch process at NP = 4 mg/mL as a function of stabilizer/HDPE ratio. Note that microfluidic conditions include TFR = 12 mL/min and FRR = 3/1. The result shows that HDPE-NPs prepared by microfluidic process were smaller than those by batch process under similar conditions. As suggested in literature, the smaller size by microfluidic process is attributed to rapid mixing of aqueous and organic phases in micro-channels. Similar results were reported on an amphiphilic block copolymer consisting of PEG and poly(lactide-co-glycolide) blocks.[100]
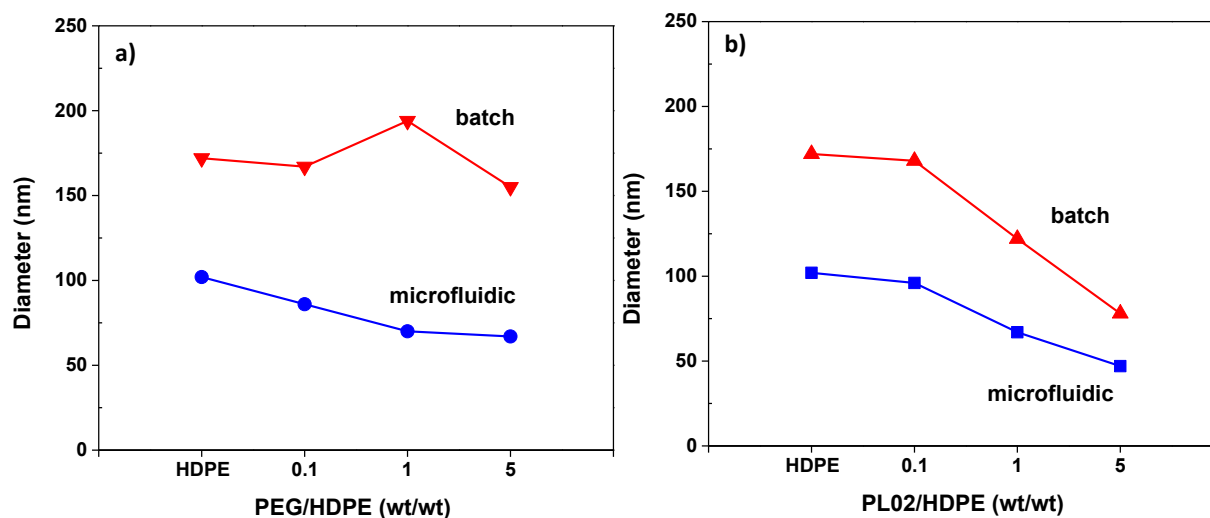
Figure 2. 8. Comparison of the size of aqueous HDPE-NPs prepared by microfluidic process with batch process in the presence of varying amounts of PEG (a) and PL02 (b) at NP = 2 mg/mL.

2.3.7 Dual enzyme/oxidation-responsive disassembly

The formed DPE-NPs contain sulfide and ester linkages in the hydrophobic cores. Their responses to enzyme and oxidation were examined using the DLS technique to follow any changes in not only size distribution (based on volume) but also Z-ave diameter (based on intensity) (Figure 2.9). Together with esterase that can cleave ester groups, hydrogen peroxide was selected as a typical reactive oxygen species (ROS) along with superoxide, hydroxyl radical, and hypochlorite that are found in the body. In the absece of those stimuli, aqueous HDPE-NPs were colloidally stable with no change in size distribution. When they were incubated with either 10 U esterase or 1% hydrogen peroxide individually, they were disintegrated with the occurrence of large aggregates over the time. Furthermore, the disintegration of the NPs appeared to be accerelated in the presence of both stimuli. As reported, ester bonds can be cleaved in response to esterase,[125] while sulfide bonds can be oxidized to the coresponding more hydrophilic sulfoxides and further sulfones by hydrogen peroxide.[68, 131] Consequenty, such responses can change the hydrophobic/hydrophophilic balance of polyesters, causing the loss of colloidal stability and thus destabilization of DPE-NP colloids, resulting in the occurence of large aggregates. These results are promising in that such destabilization of the NPs can result in the enhanced release of encapsualted biomolecules in the presence of enzymes, under oxidation condition, or both.
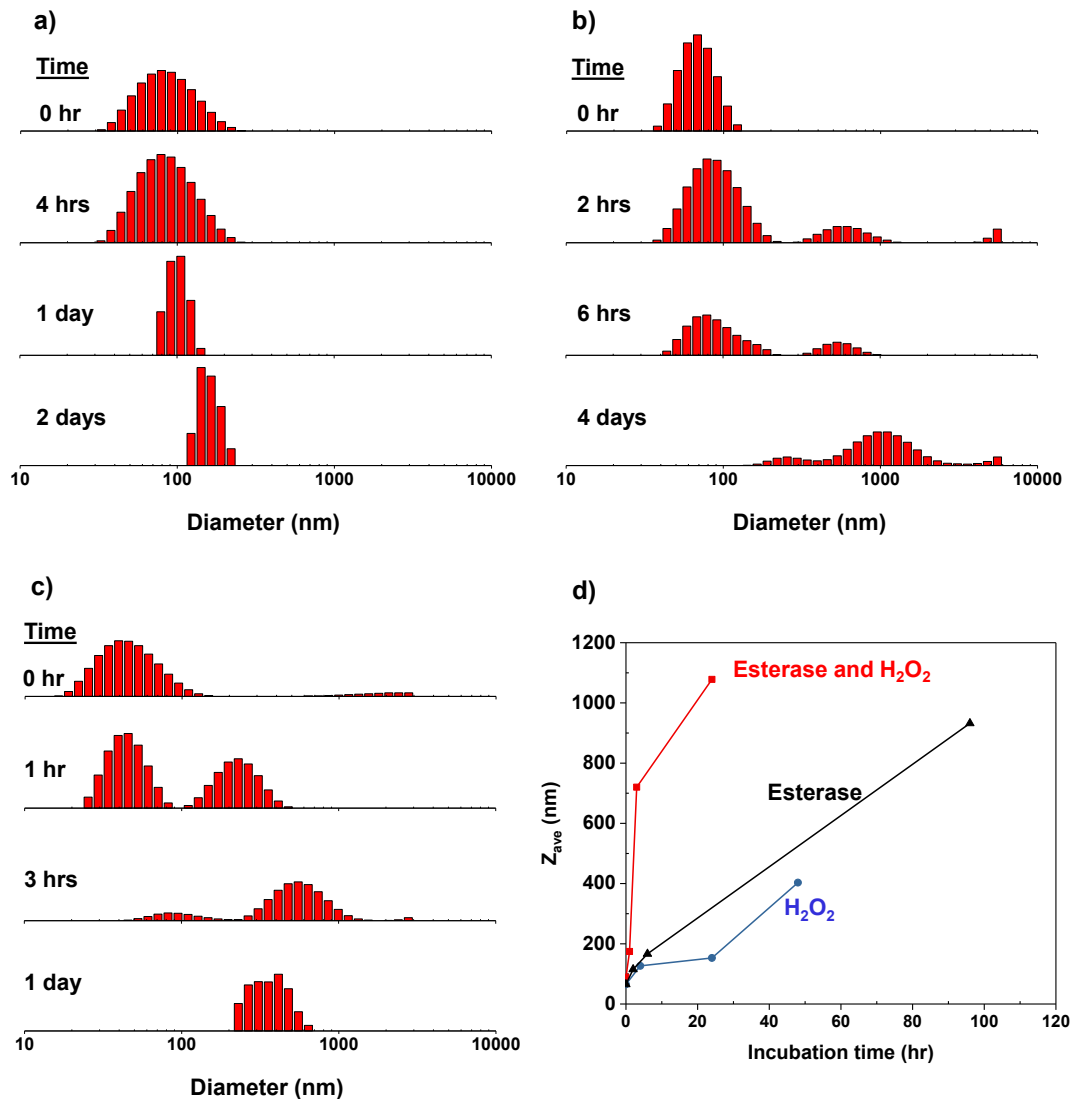
Figure 2. 9. Evolution of DLS diagrams (volume %) of aqueous HDPE-NPs in the presence of 1% hydrogen peroxide (H_2O_2) (a), 10 U esterase (b), and both stimuli (c), as well as evolution of Z-ave diameter (by light scattering intensity) at 0.4 mg/mL and pH = 7.2.

2.3.8 Preliminary biological assessment: in vitro cytotoxicity and cellular uptake

To preliminarily assess the formed aqueous HDPE-NP colloids toward biomedical applications, *in vitro* cytotoxicity with HeLa cells was first examined using a MTT colorimetric assay in the presence of NPs prepared with different amounts of PEG and PL02. HeLa cells were cultured and incubated with different concentrations of NPs for 48 hrs. Their viability was determined by the absorbance ratio of formazan generated with living cells in the presence to absence of NPs (i.e.

44

cells only as controls). As seen in Figure 2.10, NPs prepared without stabilizers had the HeLa viability ranging at 40-70% at 100 – 500 µg/mL. Promisingly, the viability was enhanced with an increasing amount of PEG stabilizer as the increasing ratio of PEG/HDPE wt/wt (Figure 2.10a). For HDPE NPs prepared with PEG/HDPE = 5/1 wt/wt, the viability was >80% up to 500 µg/mL. However, no significant enhancement of the HeLa viability was observed in the presence of PL02 coatings (Figure 2.10b).
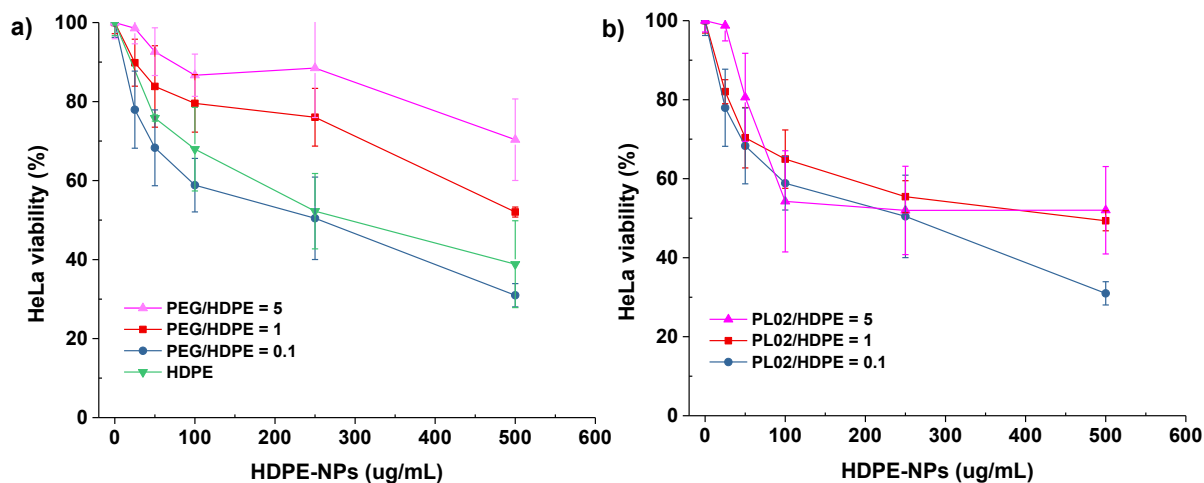
Figure 2. 10. Viability of HeLa cancer cells incubated with various amounts of aqueous HDPE-NPs prepared with different amounts of PEG (a) and PL02 (b) for 48 hrs, determined by a MTT assay.

To explore cellular uptake of HDPE-NPs to HeLa cells, Nile Red (NR), a hydrophobic fluorophore, was incorporated into NPs. For microfluidic preparation, an organic solution consisting of NR and HDPE dissolved in acetone was mixed with an aqueous PEG solution in microchannel. The mixture was subjected to dialysis to remove solvent and free (not encapsulated) NR that is dissolved in aqueous solution. Most of free NR were precipitated in dialysis tubing due to its low solubility in water (<1 µg/ml).[132] Those precipitates were removed by filtration with a PES filter. Thus, free NR could be completely removed from the mixture by a combined purification of dialysis and filtration. The formed NR-loaded NPs had the diameter to be 51 nm by DLS (Figure A.3a) and exhibit the strong fluorescence at 622 nm (Figure A.3b). Then, the formed

NR-loaded NPs were incubated with HeLa cells and live-cell imaging based on fluorescence was conducted to study the internalization of NPs into cells. Figure 2.11 shows the fluorescent images of HeLa cells incubated with and without NR-loaded HDPE-NPs, along with free NR as a control, for 4 hrs. HeLa cells incubated with NR-loaded NPs and free NR showed strong NR fluorescence in their nuclei although the signal was more intense for HeLa cells treated with the NR-loaded NPs, compared with free NR. In addition, fluorescence intensity in arbitrary unit was calculated to be 1202 ± 190 for NR-loaded NPs, which is greater than that 464 ± 144 for free NR. This result suggests the rapid internalization of NR-loaded NPs, compared to free NR.
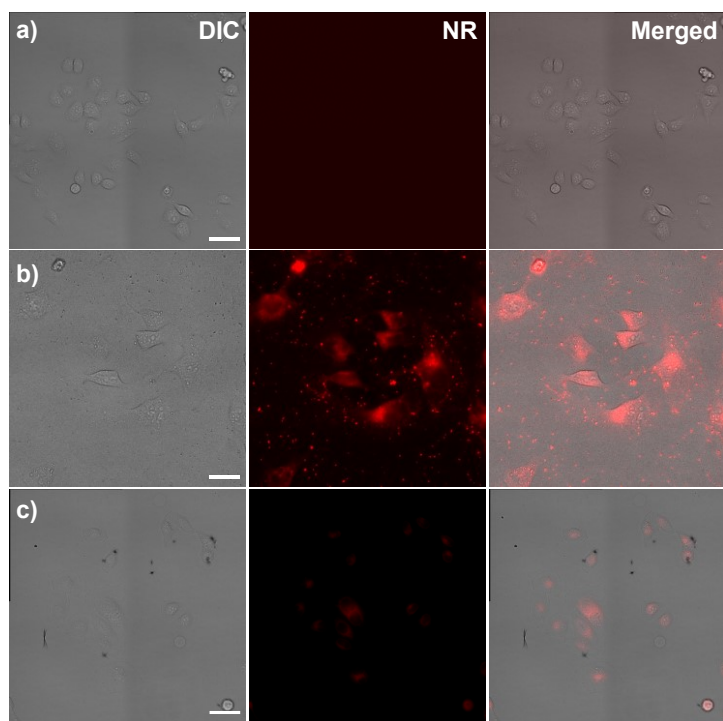
Figure 2. 11. Viability of HeLa cancer cells incubated with various amounts of aqueous HDPE-NPs prepared with different amounts of PEG (a) and PL02 (b) for 48 hrs, determined by a MTT assay.

2.4 Conclusion

Colloidally-stable NPs based on dual stimuli-responsive polyesters having enzyme-responsive ester bonds and oxidation-responsive sulfide linkages were fabricated by microfluidic method

mixing organic DPE solution with aqueous stabilizer solution in micro-channels. The resulting NPs had their sizes ranging 50-150 nm in diameter with monomodal and narrow distribution (PDI <0.1), confirmed by DLS and TEM measurements. Overall, sizes of DPE-NPs were varied by controlling the microfluidic parameters (TFR and FRR) and as well as formulation parameters. They were smaller for aqueous HDPE-NPs, compared with LDPE-NPs. With an increasing amount of PEG and PL02 polymeric stabilizers, the sizes of NPs decreased; however, no difference in sizes was observed with two stabilizers. In comparison with batch process, the microfluidic NPs were not only smaller in diameter but also more colloidally-stable (no occurrence of precipitation) as high as 4 mg/mL. The formed NPs by microfluidic process degraded in the presence of enzyme (ester linkages) and/or hydrogen peroxide as an oxidizing agent (sulfide bonds), confirmed by DLS with the occurrence of large aggregates. As biomedical assessment, the results from cell viability experiments with NPs prepared by microfluidic process relied on the nature and amount of surface coatings (stabilizers). The use of PEG had enhanced the viability as high as >80% up to 500 μg/mL of NPs, while the presence of PL-02 had no effect, suggesting that aqueous HDPE-NPs stabilized with PEG exhibit less toxicity to HeLa cells. Further, fluorescence imaging results indicate the greater endocytosis of NR-loaded NPs inside cells, compared with free NR.

Chapter 3
Dual disassembly and biological evaluation of enzyme/oxidation-responsive polyester-based nanoparticulates for tumor-targeting drug delivery

3.1 Introduction

Cancer is one of the leading causes of death worldwide, and tremendous resources have been devoted to developing anticancer therapies over the past few decades. While small molecule anticancer drugs are effective chemotherapeutics, they typically are not selective to cancer cells and cause severe side effects. Further, high doses of drugs must be administered to overcome issues with solubility, metabolic reactivity, and/or poor efficacy due to their elimination by kidney filtration (or renal clearance) during blood circulation.[1-3] Recent efforts have shifted toward developing methods for the controlled delivery and release of small molecule anticancer drugs to improve their efficacy. Polymer-based drug delivery systems (PDDS),[133-136] particularly hydrophobic nanoparticulates,[89, 90, 137] possess a number of desirable properties such as biodegradability, biocompatibility, ability to encapsulate therapeutic agents and deliver them to tumor tissues. Upon intravenous injection, well-designed PDDS with excellent colloidal stability have prolonged blood circulation; thus offering improved pharmacokinetics and biodistribution to tumors *via* enhanced permeability and retention (EPR),[138-140] Followed by their endocytosis into cancer cells, drug-loaded PDDS release encapsulated drugs rapidly at predetermined rate, thus minimizing side effects and maximizing therapeutic efficacy common to small molecule anticancer drugs.

Stimuli-responsive degradation (SRD) has been explored as a promising platform in the design of smart PDDS. SRD involves the incorporation of dynamic covalent linkages into the design of PDDS; when needed, response of these linkages to external stimuli changes their chemical and physical properties. In such, SRD-exhibiting PDDS which are stable under physiological conditions can be dissociated in a controlled fashion as cellular components are provided appropriate stimuli thus enabling biodegradation.[20, 117, 118, 123, 141] Examples of endogenous stimuli include acidic pH, glutathione, reactive oxygen species (ROS), and changes in enzymatic activities, while light and temperature are exogenous stimuli.[142, 143] Thus, the use of single, dual or multiple

stimuli has led to more precise control over the disassembly of smart PDDS.[144-146] Among them, enzyme-responsive systems are especially promising in that enzymes are great catalysts with high selectivity towards specific substrates. Overexpressed disease-associated enzymes including esterase act as an effective cellular trigger.[33, 147] With growing interest in enzyme-responsive platforms, numerous PDDS have been designed with specific peptide linkages that can be cleaved in response to enzymes.[148-153] However, there are few reports of systems designed to respond to esterase.[125, 126, 128, 129, 154] In addition to esterase, ROS is found at elevated concentrations in cancer cells compared to healthy cells.[64, 65] ROS-responsive systems have been developed where ROS-responsive linkages are cleaved, or hydrophobic/hydrophilic balance is changed upon oxidation.[127, 155-157] Although smart PDDS responding to esterase or ROS are promising, dual stimuli enzyme/oxidative-responsive PDDS have not been reported yet to our best knowledge.

In this work, we developed dual enzyme/oxidation-responsive polyester-based nanoparticlulates (DPE-NPs) exhibiting enhanced/controlled release for the tumor-targeting intracellular delivery of anticancer drugs. As illustrated in Scheme 3.1, a facile oil-in-water emulsion process using hydrophobic polyester (DPE) labeled with both ester and sulfide linkages formed aqueous core/shell-type NPs loaded with drugs with an aid of external polymeric stabilizers. While the shell provides stealth effect, minimizing immune response and maximizing colloidal stability in the blood, the DPE cores are designed to have esterase-responsive ester bonds and oxidation-responsive sulfide linkages. Porcine liver esterase and hydrogen peroxide were examined here to model the response of DPE-NPs to esterase and ROS. Dual response DPE-NPs to these stimuli resulted in main chain degradation or altered polarity, leading to the enhanced release of encapsulated doxorubicin (Dox) or hydrophobic model drug (Nile Red). Further, aqueous DPE-NPs were assessed as intracellular nanocarriers *in vitro* in two-dimensional (2D) monolayer cell culture and three-dimensional (3D) multicellular tumor spheroids (MCTS).
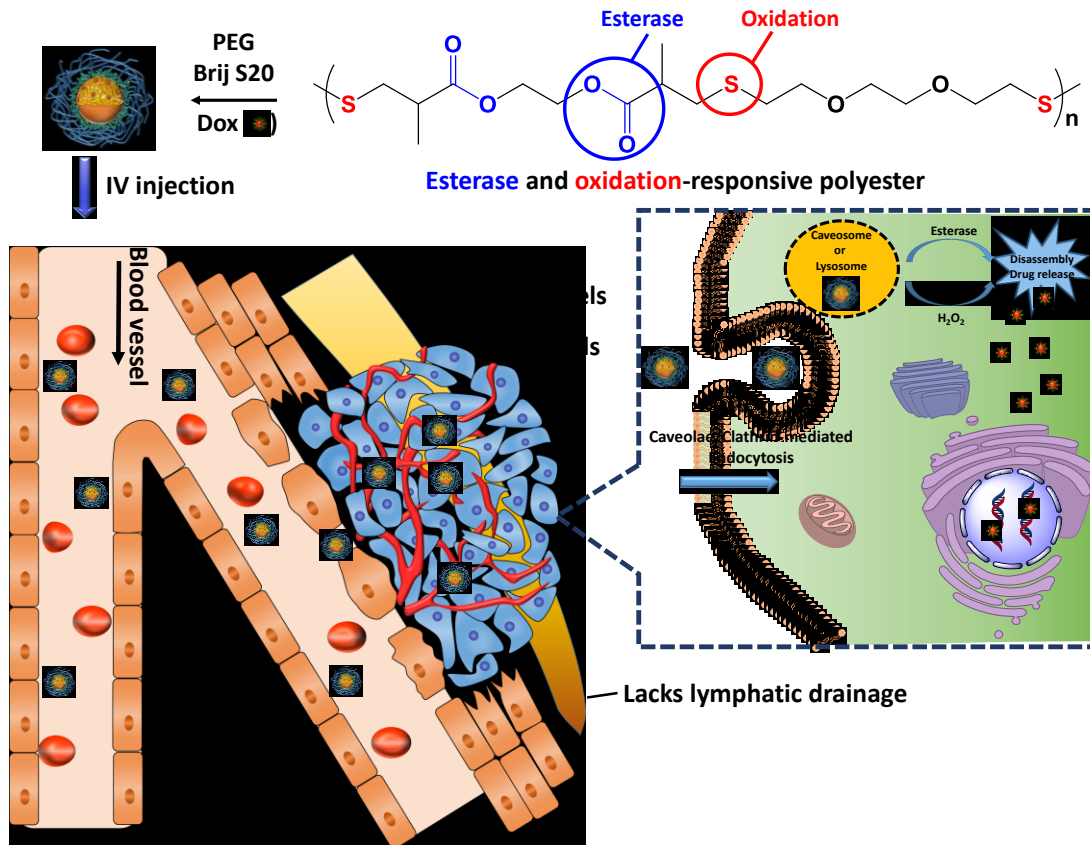
Scheme 3. 1. Schematic illustration of intracellular drug delivery of DPE-based core/shell NPs loaded with Dox.

3.2 Experimental

The detailed instrumentations, TEM analysis, cell viability using MTT assay and polyester synthesis are described in the previous chapter. Note that DPE in this chapter indicates HDPE.

3.2.1 Microscope Imaging

Two types of microscopes were used. First, HeLa cells and multi-cellular tumor spheroid (HeLa and A549) were visualized with Nikon TI-E microscope equipped with LED Heliophors with a Photometrics Evolve EMCCD camera. Secondly, endocytosis mechanism of Dox-NPs was determined by using inverted Nikon Ti-E Livescan confocal microscope (CLSM) equipped with laser source (405 nm and 488 nm), a piezo Z stage (Mad City Labs), iXON897 EMCCD camera

(Andor). NIS Elements acquisition software was used for both the microscopes. All the images were analyzed using Image J (NIH).

3.2.2 Materials.

Brij® S20 (B20), poly(ethylene glycol) (PEG, MW = 6,000 g/mol), esterase from porcine liver (18 U/mg; one unit will hydrolyze 1 µmol of ethyl butyrate to butyric acid and ethanol per minute at pH 8.0 at 25 ºC), Nile Red (NR), doxorubicin hydrochloride (Dox, $-NH_3^+Cl^-$ forms, >98%), hydrogen peroxide (30% w/w), Bovine Serum Albumin (BSA), and Immunoglobulin G (IgG) from human serum (≥95%) from Aldrich, Pierce BCA protein assay kit from Bio-Rad, dialysis tubing from Spectrum Labs were purchased and used as received. Dulbecco's modified eagle medium (DMEM), F12K medium, and fetal bovine serum (FBS) from Wisent, phenol-red free DMEM from Thermo Fisher Scientific and 3-(4,5-dimethylthiazol-2-yl)-2,5-diphenyltetrazolium bromide (MTT) from Promega, and Hoescht 33342 from Invitrogen were purchased and used for biological assessment *in vitro*.

3.2.3 Stabilizer-assisted NP formation by solvent evaporation method

An organic solution of the purified and dried DPE (10.8 mg) dissolved in THF (2.3 mL) was mixed with an aqueous solution of PEG (10.7 mg) and B20 (0.1 mg) in water (13.6 mL). The resulting dispersion was homogenized using sonifier (Branson) for 5 min (amplitude = 15 %, 10 sec on, 2.5 sec off) and then kept stirred for 24 hrs at room temperature to remove residual THF. A stable NP dispersion was formed at 2.0 mg/mL. The resulting mixtures, after being sonified, were purified by dialysis with MWCO = 12,000.

3.2.4 Enzyme/oxidative degradation of NPs

For oxidation-responsive degradation of NPs in the presence of hydrogen peroxide, aliquots of aqueous NP dispersion (2.0 mg/mL, 2.3 mL) were incubated with 1% v/v hydrogen peroxide under stirring at room temperature. For enzymatic degradation in the presence of esterase, aliquots of aqueous NP dispersion (2.0 mg/mL, 1.8 mL) were incubated with esterase (1 mg), attaining 10 U. Alternatively, the dispersion was incubated with esterase (2 mg) to attain 20 U. DLS was used to follow any changes in size distribution.

3.2.5 Preparation of Dox-loaded NPs (Dox-NPs)

An organic solution containing DPE (12 mg), Dox (1 mg), and Et$_3$N (3.5 µL) dissolved in THF (2.8 mL) was mixed with an aqueous solution of B20 (0.6 mg) and PEG (11.5 mg) in water (11.7 mL). The resulting mixtures were homogenized using a sonifer (Branson) for 5 min (amplitude = 15 %, 10 sec on, 2.5 sec off) and stirred for 24 hrs to remove THF. They were then dialyzed over water (1 L) for 6 hrs to remove excess (free) Dox and Et$_3$N, yielding aqueous Dox-NPs at 2.0 mg/mL. First, the extinction coefficient of Dox was determined in a mixture of water/THF (1/4 v/v) using a UV/vis spectroscopy along with Beer-Lambert equation. Then, the loading level and loading efficiency of Dox were determined with mixtures consisting of aliquots of Dox-NPs (1 mL) mixed with THF (4 mL). The UV/vis spectra were recorded to obtain the absorbance at 498 nm.

3.2.6 Colloidal stability in the presence of proteins

Aqueous DPE NP dispersion (1 mL, 2 mg/mL) was divided into two aliquots and was mixed with BSA (1 mL, 80 mg/mL) and IgG (1 mL, 16 mg/mL) in PBS. As controls, BSA and IgG solutions were prepared at the same concentrations. The mixtures were incubated at 37 °C for 48 hrs. Aliquots from each mixture were withdrawn and subjected to centrifugation (10,000 rpm x 15 min) to precipitate undesirably-formed aggregates. The supernatants were quantitatively analyzed using BCA assays according to the Pierce® BCA assay kit instructions. Briefly, supernatant (25 µL) was transferred to a 96-well plate and BCA reagent (200 µL) was added to each well. The plate was then placed at 37 °C for 30 min and the absorbance was measured at $\lambda = 562$ nm using Powerwave HT Microplate Reader (Bio-Tek). Percentage of free protein was calculated by the ratio of the absorbance with NPs to that without NPs (control).

3.2.7 Esterase-triggered release of Dox from Dox-NPs

An aqueous mixture consisting of an esterase stock solution (0.24 mL, 2.6 mg/mL) and a Dox-NP dispersion (0.9 mL, 5.1 mg/mL) in PBS was transferred into dialysis tubing (MWCO = 12,000 g/mol) and immersed in PBS (40 mL). The UV spectrum of Dox in outer water was recorded at indicated time intervals using a UV/Vis spectrometer. For quantitative analysis, Dox (94.8 µg, equivalent to Dox encapsulated in 0.9 mL Dox-NPs) was dissolved in PBS to record its UV/Vis spectrum.

3.2.8 Degradation of Dox upon oxidation

Dox (0.15 mg) was dissolved in 1% v/v (or 323 mM) hydrogen peroxide solution in water (5 mL). Aliquots taken periodically were analyzed by UV/vis spectroscopy to follow the absorbance at 498 nm.

3.2.9 Oxidation-responsive release of NR from aqueous NR-loaded NPs

First, aqueous NR-loaded NPs were prepared as follows; an aqueous stabilizer solution (B20/PEG = 0.05 w/w, 1.1 mg/mL, 10.5 mL) was mixed with an organic solution consisting of NR (0.9 mg) and DPE (11 mg) in THF (2.4 mL). The resulting mixture was homogenized for 5 min and stirred for 24 hrs to remove THF, followed by filtration using 0.85 μm PES filter (Pall Corporation) to remove free NR. Then, aliquots of NR-loaded NPs were mixed with hydrogen peroxide (1% and 5% v/v) while stirring at 37 ºC. Their fluorescence spectra (λ_{ex} = 480 nm) were recorded periodically to follow FL intensity at 620 nm.

3.2.10 Cell culture

HeLa cervical cancer cells were cultured in DMEM (Dulbecco's modified Eagle's medium) containing 10% FBS (fetal bovine serum) and 1% antibiotics (50 units/mL penicillin and 50 units/mL streptomycin) at 37 °C in a humidified atmosphere containing 5% CO_2. A549 cells were cultured in F12K media with same supplemental additives as previously mentioned; 10% FBS and 1% antibiotics.

3.2.11 Live cell imaging

HeLa cells were plated at densities of 1×10^5 cells/well in a 4-well glass-bottom plate (MatTek Corporation) and incubated in media (0.5 mL) at 37 ºC for 18 h. The cells were stained with Hoechst 33342 dye for 15 min. Then, the cells were washed with PBS three times to remove the dye. Phenol red free DMEM medium (0.5 mL) was added to the cells for imaging. Appropriate amounts of free Dox or Dox-NPs were added to attain a final Dox concentration of 2.5 μg/mL. Imaging was started 10 min post-incubation for 2 hours; images were captured every 10 minutes. Cells were placed in a chamber (Live Cell Imaging) at 37 ºC with 5% CO_2 and imaged using an epifluorescence microscope with a 40x/0.95NA objective. Dox and Hoescht 33342 were excited at 405 nm and at 555 nm, respectively. In another set, HeLa cells were incubated with Dox-NPs

(encapsulated Dox = 2.5 µg/mL) and free Dox for 12 hrs to examine the intracellular release of Dox from Dox-NPs; images were captured after 12 hrs of incubation with the same microscope setting.

3.2.12 Flow cytometry

HeLa cells were plated at densities of 5×10^5 cells/well in 6-well dishes and kept at 37 °C. After 24 h, cells were treated with Dox-NPs (48.6 µL, encapsulated Dox = 2.5 µg/mL) for either 30 min or 12 h. After, the cells were washed with DMEM and treated with trypsin. The cells were suspended in DMEM (500 µL) for flow cytometry measurements using a FACSCanto II flow cytometer (BD Biosciences) and FACSDiva software (BD Biosciences).

3.2.13 Multi-cellular tumor spheroids

Multi-cellular tumor spheroids (MCTS) were generated from HeLa and A549 cells in 96-well plates (BioLite, Thermo Scientific). Wells were coated with 1.5% agarose (Biotechnology Grade, BioShop), then seeded with 500-1000 cells in 150 µl of growth medium, which were left to aggregate with gravity at 37 °C and 5% CO_2. MCTS were grown for 6 to 10 days, and were monitored daily using an Inverted Invertoskop 40 C light microscope. Once MCTS formation was confirmed, they were transferred into 24-well plates coated with agarose in 2 mL of growth medium. MCTS were incubated with Dox-NPs (encapsulated Dox = 1.6 µg/mL), free Dox (1.6 µg/mL) or DPE-NPs (270 µg/mL; control) for 4 days to compare Dox penetration. Images of the spheroids were acquired using the epifluorescence microscope with 4x objective; Dox was excited at 488 nm. Quantitative analysis of the entire surface area of each spheroid was measured and normalized to their initial values at time = 0, thereby giving the fluorescence intensity relative to the first values.

3.2.14 Cellular uptake of Dox-NPs

HeLa cells were plated on 25 mm round coverslips (No. 1.5) at 40-50% confluency and kept at 37 ºC with 5% CO_2 using a heated chamber (Tokai Hit). Cells were pre-treated for 1 hr with (i) 100 µM Genistein (GEN) to block caveolae-mediated endocytosis, (ii) 5 µM Chlorpromazine Hydrochloride (CPZ) to block clathrin-dependent receptor-mediated endocytosis, or (iii) 100 µM Genistein and 5 µM Chlorpromazine Hydrochloride in combination to block both

pathways simultaneously. Cell nuclei were stained with Hoechst 33342 dye prior to imaging. The round coverslips were then placed in a 35 mm Chamlide magnetic chamber (Quorum).

Cells were imaged for 1 hr before and after treatment with a final concentration of encapsulated Dox = 2.5 µg/mL. Live imaging was performed on CLSM using 60x/1.4NA oil immersion objective. Dox and Hoescht 33342 were excited at 405 nm and at 488 nm, respectively. The settings were kept the same for control cells and each treatment. Z-stacks of 0.5 µm were taken every 5 minutes.

3.3 Results and Discussion

3.3.1 Preparation of DPE and DPE-based NP colloids

Figure B.1a illustrates our approach utilizing a base-catalyzed thiol-ene addition to synthesize a dual enzyme and oxidation-responsive polyester (DPE) containing both sulfide and ester linkages on the backbone. This step-growth polyaddition was designed with a stoichiometric balance of thiol to methacrylate group as a 1/1 mole ratio of DSH to EGDMA in the presence of triethylamine a base in DMSO, ensuring the synthesis of relatively high molecular weight DPEs. They were then purified with precipitation from cold methanol to remove unreacted monomers and catalysts. ^{1}H-NMR analysis in Figure B.1b confirms the structure of the DPE; however, the determination of the number of repeating units by end-group analysis was not strightforward. Its molecular weight as the number average molecular weight (M_n) was determined to be 17 kg/mol with molecular weight distribution as broad as Mw/Mn = 1.5, by GPC (Figure B.1c).

DPE is hydrophobic, and thus needs external stabilizers to form colloidally-stable NPs in aqueous solution. To prepare aqueous NPs, combined stabilizers consisting of PEG and B20 were empolyed. PEG is biocompatible and FDA-approved for clinincal use; has low cytotoxicity; provides excellent sheath effect; and prevents nonspecific protein adsorption.[158, 159] However, PEG used here has relatively high molecular weight with MW = 6,000 g/mol and thus has low ability to reduce the surface tension of water due its tendency to hydrophilicity.[160, 161] Although PEG can be used to prepare small and stable NPs by microfluidic process due to rapid mixing, PEG does not act as an effective stabilizer to form NPs in the desired size range by using solvent evaporation method. To circumvent this problem, a mixed stabilizer system was used by adding PEG and B20.

B20 has a relatively small molecular weight surface-active agent consisting of the short chains of hydrophilic PEG (MW = 800 g/mol) and a hydrophobic stearyl group.[162] The addition of B20 to the PEG stabilizing system allowed for the synthesis of a colloidally-stable DPE-NP dispersion. Figure 1a shows a DLS diagram of the formed colloids in the presence of PEG/B20 stabilizers under the conditions of DPE = 0.9 mg/mL, (PEG+B20)/DPE = 1/1, and B20/PEG = 5% (by weight) on toal stabilizers. The formed NPs had a diameter = 99 ± 1 nm (by volume) with size distribution as narrow as PDI = 0.11. TEM analysis indicates the NPs have a diameter = 116 ± 12 nm in dehydrated states (Figure 3.1b).
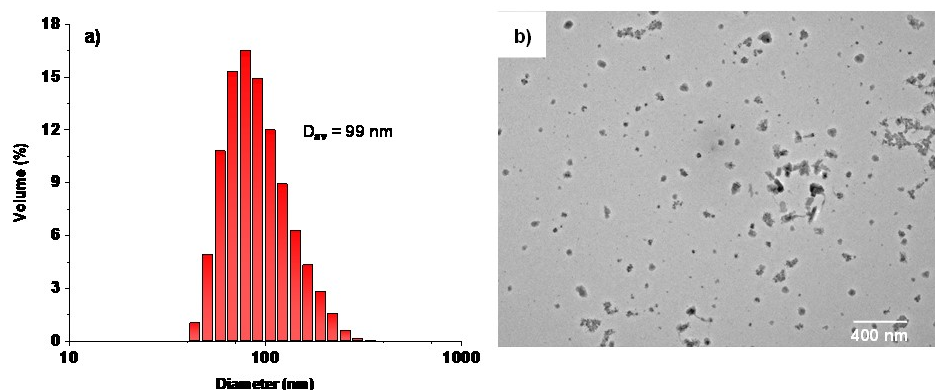
Figure 3. 1. DLS diagram (n = 3) (a) and TEM image (n = 30) (b) of aqueous DPE NP colloids with an aid of mixed PEG/B20 stabilizers.

3.3.2 Enzyme and oxidation-responsive disassembly

The formed DPE-NPs contain both sulfide and ester linkages in their hydrophobic cores. The ester linkages can be cleaved in the presence of esterase (an enzyme that reacts with ester bonds), causing destabilization of the NPs. Further, the sulfide linkages can be oxidized to the corresponding sulfoxide or sulfone groups in response to an oxidizing agent such as hydrogen peroxide. This oxidation process could change the hydrophobic/hydrophilic balance of PE chains, causing distabilization of the NPs.

To examine their enzyme-responsive disassembly, aqueous NPs were mixed with 10 U esterase (Figure 3.2a). After 7 hrs of incubation with enzyme, both DLS diagram and TEM image show the multimodal distribution of NP sizes, including large aggregates. In comparison, a control experiment was conducted in parallel with an aqueous solution of esterase only (without NPs). No

significant change in size distribtion of esterase was observed over 1 day (Figure B.2). This result suggests that changes in the size distribution of colloids is attributed to their destabilization in response to the enzymatic reaction, possibly due to the cleavage of ester linkages in response to esterase.

Oxidation-responsive disassembly was followed with 1% hydrogen peroxide. As seen in Figure 3.2b, both DLS and TEM images show that the NPs decreased in size with the diameter ≈59 ± 2 nm after 48 hrs of incubation (Figure 3.2b). Similar result of decrease in NP sizes in response to hydrogen peroxide has been reported.[163] Such a change in size distribution could be due to the oxidation-response of sulfide linakges to the corresponding sulfoxides and sulfones, as described in the report where 1H-NMR was used to quantively analyze the oxidative degradation of poly(carbonate-thioether) in the presence of hydrogen peroxide.[164]
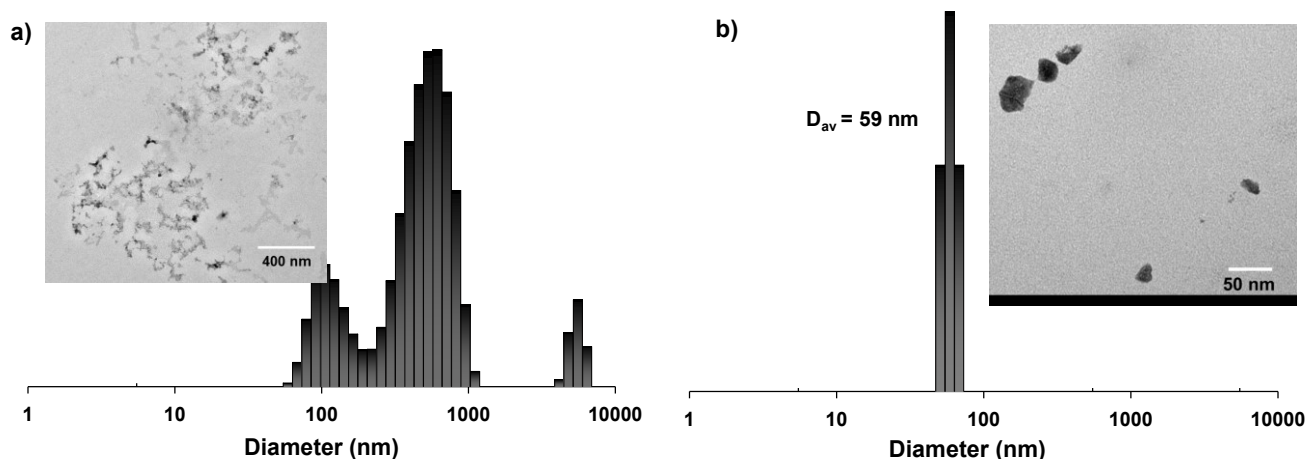
Figure 3. 2. DLS diagrams (by volume %) and TEM images of aqueous DPE-NPs in the presence of 10 U esterase incubated for 7 hrs (a) and 1 % hydrogen peroxide incubated for 43 hrs (b) at 0.1 mg/mL and pH = 7.2.

3.3.3 Preparation of Dox-loaded NPs

To assess the use of DPE-NPs as tumor-targeting intracellular drug delivery nanocarriers, Dox was encapsulated in the NPs. A mixture consisting of an organic solution of DPE and Dox with an aqueous solution of stabilizers was placed in dialysis tubing (MWCO = 12,000 g/mol) and

dialyzed against water for 6 hrs. This procedure allows for the removal of excess Dox and Et$_3$N, yielding colloidally-stable aqueous Dox-NPs at a concentration of 2.0 mg/mL. The capacity and efficiency of loading Dox in NPs was analyzed. The extinction coefficient of Dox in a mixture of water/THF at 1/4 v/v was determined to be 8,700 M^{-1} cm^{-1} (see Figure B.4 for overlaid UV spectra of Dox and linear progression of absorbance at λ_{max} = 498 nm over various concentrations). An aliquot of aqueous Dox-NPs was dissolved in a mixture of water/THF = 1/4 v/v and their UV spectrum were recorded (Figure 3.3a). Using the Beer-Lambert equation with the predetermined extinction coefficient of Dox in water/THF = 1/4 v/v, the loading level of Dox was 3.6% (weight of the Dox/weight of polyester) and encapsulation efficiency was 64% (weight of encapsulated Dox/weight of initially added Dox). DLS analysis showed that the diameter of Dox-loaded NPs was 144 ± 1 nm, which was larger than that of the empty NPs. Further, Dox-NPs had a monomodal distribution with no evidence of significant aggregation (Figure 3.3b).
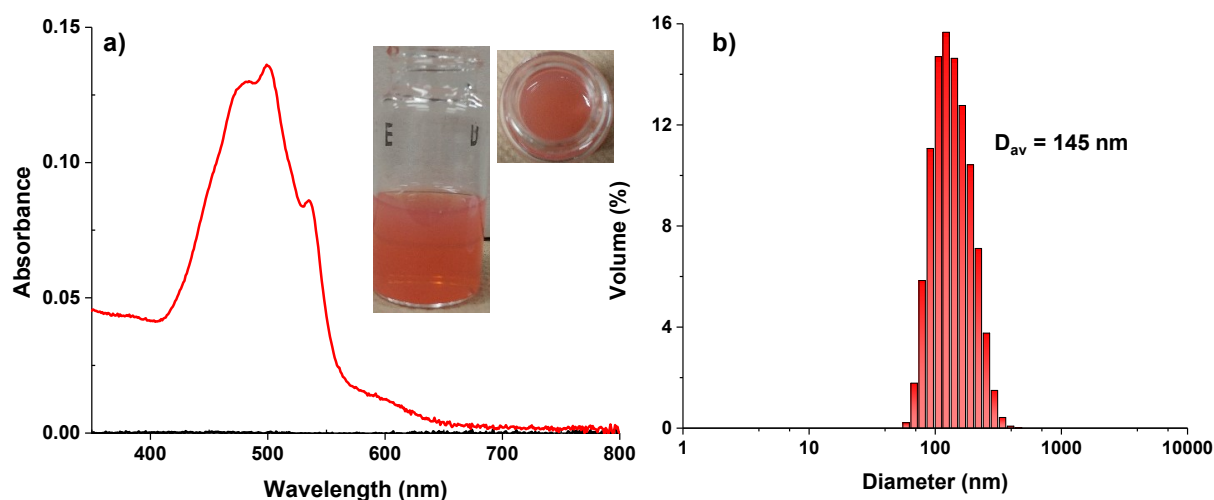
Figure 3. 3. UV/Vis spectrum (a) and DLS diagram (b) of aqueous Dox-NPs at 2.0 mg/mL.

3.3.4 Colloidal stability of Dox-NPs

The shelf-life colloidal stability of aqueous colloids was first evaluated using DLS. Their diameter was unchanged with no precipitation at room temperature over 330 days suggesting excellent colloidal stability (Figure B.5a). Next, the non-specific interaction of Dox-NPs with serum (plasma) proteins was examined. Serum proteins can form a "protein corona" around NPs,

which results in their rapid elimination from blood circulation and is highly undesirable.[165, 166] Two of the more abundant proteins in blood were examined: BSA (35 – 52 g/L) and human IgG (8 – 16 g/L). Aliquots of Dox-NPs were incubated with BSA (40 g/L) and IgG (8 g/L) in PBS at pH = 7.2 for 48 hrs. They were centrifuged to remove aggregates formed by undesired interactions between NPs and proteins, then the supernatants were analyzed using BCA assays to quantify the interaction of NPs with proteins. As Figure B.5b shows, both BSA and IgG proteins in the supernatants were determined to be >90%. This result suggests that there was no significant interaction of NPs with these common serum proteins, and thus the NPs should have excellent colloidal stability in circulation.

3.3.5 Enhanced release of encapsulated Dox and model drug

The Dox-NPs were examined for their ability to release in response to enzyme and oxidation. First, enzyme-responsive enhanced release of Dox from Dox-NPs was examined using UV/Vis spectroscopy. An aliquot of Dox-NPs was placed in dialysis tubing (MWCO = 12 kDa) and submerged in PBS containing 10 U or 20 U esterase. Samples were taken periodically to record UV spectra over time (Figure B.6). Then, the UV absorbance at λ_{max} = 498 nm was followed to investigate %Dox release. As seen in Figure 3.4, <20% Dox was released from Dox-NPs in the absence of esterase. In the presence of esterase, the backbone ester linkages should be targeted, causing destabilization (or disintegration) of Dox-NPs to enhance the release of Dox. The released Dox molecules should diffuse through the dialysis tubing into the outer water and thus UV absorbance of Dox in outer water increases. Compared with other supramolecular nanostructures (peptide amphiphile-drug conjugate),[167] where the change in esterase concentration does not have any effect, Dox release occurred in the presence of 10 U esterase, and was faster in the presence of 20 U esterase. For example, %Dox reached to as high as 85% with 20 U esterase, compared to 60% with 10 U esterase.
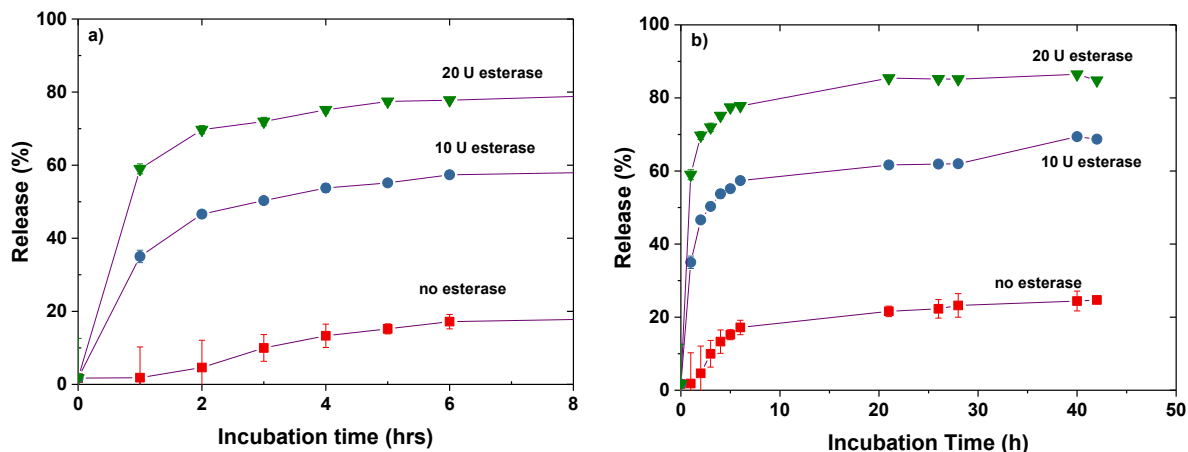
Figure 3. 4. Release profile in short-term (a) and long-term (b) time scale of Dox from Dox-NPs in the absence and presence of 10 U and 20 U esterase at pH = 7.2. Each sample was measured three times.

The oxidation-responsive release of Dox from Dox-NPs in response to hydrogen peroxide was determined. However, due to the instability of Dox in hydrogen peroxide (1% v/v), the experimental approach had to be modified. As seen in our control experiment where Dox was incubated with hydrogen peroxide, the absorbance of Dox decreased gradually over the incubation time (Figure B.7). A hydrophobic model for anti-cancer drugs is Nile Red (NR), which is stable for at least 170 h in hydrogen peroxide (5% v/v).[67] Thus, NR-loaded NPs were used as an alternative approach to monitor oxidation-responsive release in the presence of hydrogen peroxide using fluorsecence spectroscopy. This method can determine changes in the fluorescence intensity of NR in different conditions, which would change due to its low solubility in water. NR fluorescence is intense when encapsulsted in hydrophobic cores. However, the intensity significantly decreases when NR molecules are released and exposed to water as a consequence of the destabilization of NR-loaded NPs.[168, 169]

Here, the solvent evaporation method was used to prepare aqueous NR-loaded NPs (NR-NPs) with a diameter = 153 nm (Figure B.8). Aliquots were incubated with 1% and 5% hydrogen peroxide and their emission spectra were followed over time (Figure B.9). In the absence of hydrogen peroxide, the fluorescence intensity of NR-NPs at 620 nm remained unchanged, suggesting that NR was not released or photobleached (Figure 3.5a). In the presence of hydrogen peroxide, the fluorescence intensity decreased with kinetics that correlated with changes in the

concentration of hydrogen peroxide (Figure 3.5b). For example, the intensity rapidly decreased to 5% within 8 hrs in 5% hydrogen peroxide. Interestingly, there was an increase in intensity in 1% hydrogen peroxide (Figure 3.5b). This unusual phenomenon could be attributed to self-quenching of NR molecules confined in small-sized NR-loaded NPs. Upon destabilization of NR-loaded NPs in response to hydrogen peroxide, NP cores could swell, resulting in a decrease in self-quenching of NR molecules. After longer incubation, the fluorescence intensity decreased, likely due to further destabilization of NPs.[170, 171] In another analysis, the emission wavelength of maximum fluorescence intensity ($\lambda_{em,max}$) was monitored. As seen in Figure 3.5c, the $\lambda_{em,max}$ increased from 620 nm to 640 nm (max) over the incubation time. This increase in wavelength is similar to the decrease in intensity. Given that the $\lambda_{em,max}$ of NR is red-shifted when the polarity of the medium increases, this increase could arise due to the release of NR molecules from NPs upon oxidative degradation which was also supported by the TEM image (Figure 3.5d). These results show that NR was rapidily released from encapsulated NR in 5% hydrogen peroxide, and was more slowly released in a 1% solution.

Together, these results show the enhanced release of encapsulated drugs (Dox and NR) from DPE-NPs in response to both enzymatic activity and oxidation.
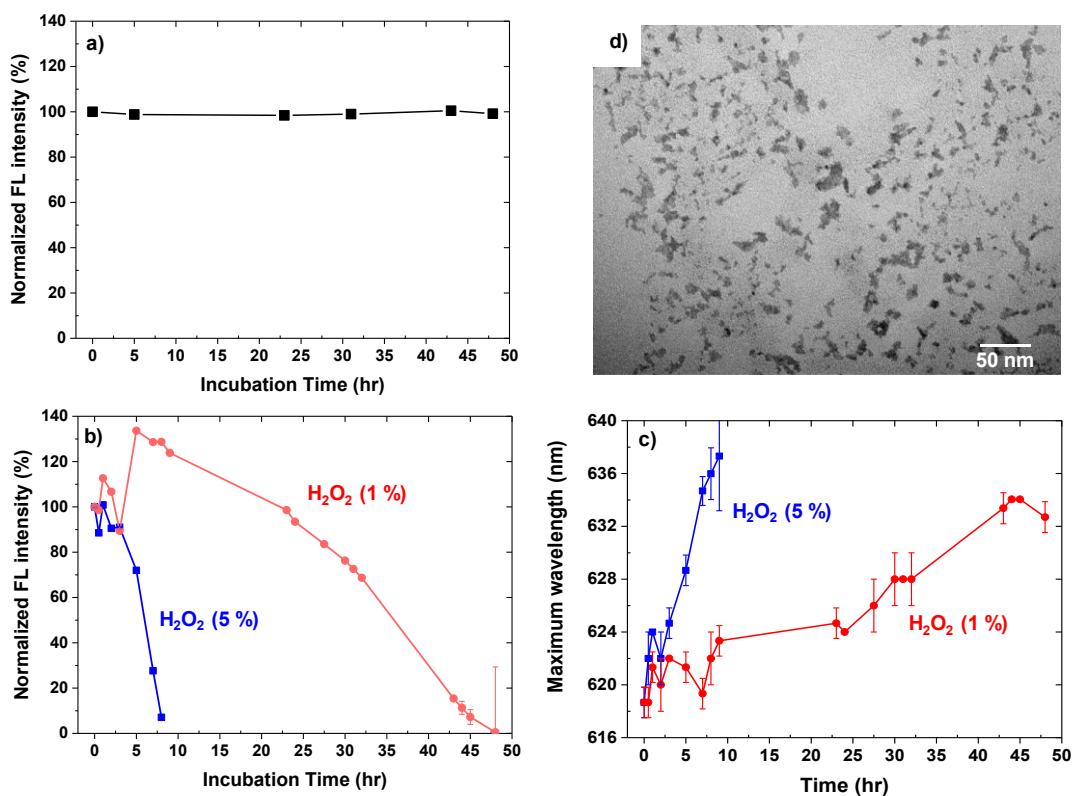
Figure 3. 5. Normalized fluorescence (FL) intensity of NR at $\lambda_{em} = 620$ nm in the mixture of aqueous NR-loaded NPs without (a) and with (b) hydrogen peroxide of 1% and 5%; emission wavelength of maximum FL intensity of NR in the mixture of aqueous NR-loaded NPs with hydrogen peroxide of 1% and 5% (c); and TEM image of NR-loaded NPs incubated with 1% hydrogen peroxide (d). Each sample was measured three times (n = 1).

3.3.6 Activity and intracellular uptake in HeLa cells

The cytotoxicity of DPE-NPs was evaluated on HeLa cervical cancer cells. Dox-loaded NPs were compared with empty NPs using a MTT colorimetric assay. As seen in Figure 3.6a, HeLa cell viability was >85% in the presence of empty NPs up to 500 µg/mL, suggesting non-toxicity of empty NPs to HeLa cells. When incubated with NPs loaded with Dox = 1.7 µg/mL (equivalent to 100 µg/mL of Dox-NPs), the viability of HeLa cells decreased to 44% (Figure 3.6b). The decreased viability suggests that the proliferation of HeLa cells was inhibited by the Dox-NPs. When HeLa cells were treated with the same concentration of free Dox, cell viability significantly decreased to <10%, suggesting that free Dox more effectively blocks HeLa cell proliferation over 48 hours, or two doubling times, compared with Dox-NPs.
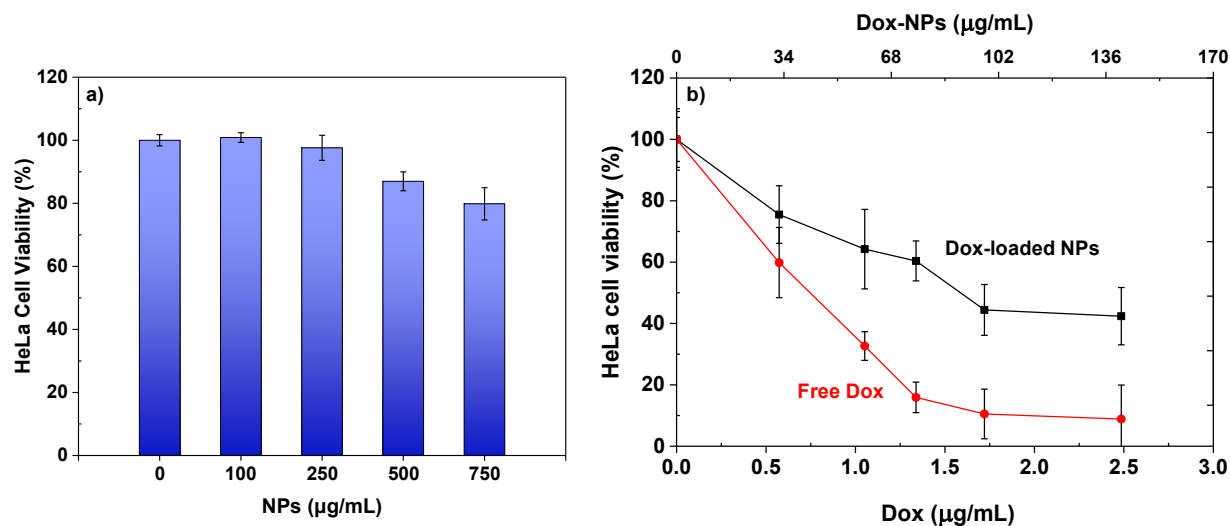
Figure 3. 6. Viability of HeLa cells incubated with different amounts of empty NPs (a) and Dox-NPs, compared with free Dox, (b) for 48 hrs determined by an MTT assay. Data are presented as the average ± standard deviation (n = 6).

Next, the intracellular localization of Dox-NPs was explored using fluorescence microscopy. Figure 3.7a shows fluorescence images of HeLa cells 10 min (t = 0) and 2 hrs after incubation with free Dox or Dox-NPs. The nuclei were stained with Hoechst 33342, shown in blue, and Dox fluorescence is shown in red.

Dox fluorescence increased with time in cells treated with free Dox or Dox-NPs. However, Dox was seen in the nuclei in cells treated with free Dox, while Dox was in the perinuclear region rich in endomembrane networks in cells treated with Dox-NPs. Therefore, the NPs likely enter cells via endocytosis and traffic to the endomembrane system, where their release may be more highly controlled vs. free Dox molecules. Followed by the accumulation in the perinuclear region, Dox accumulated in the nuclei after 12 hrs of incubation. This is ascribed to the intracellular release of Dox from Dox-NPs (Figure B.10).

The intracellular accumulation of Dox was also monitored using flow cytometry. HeLa cells were analysed using flow cytometry after 30 min and 12 hrs of incubation with free Dox or Dox-NPs. As shown in Figure 3.7b, the histogram for free Dox was shifted to higher fluorescence intensity, compared with Dox-NPs after 30 min of incubation. After 12 hrs, the histogram for Dox-NPs shifted to higher fluorescence intensity compared with free Dox (Figure 3.7c). These changes

are more obvious in Figure 3.7d-e. While there was only a slight increase in intensity for free Dox between 30 min and 12 h of incubation, there was a significant increase in intensity for Dox-NPs. This result suggests that the internalization of free Dox occurs very rapidly, but reaches a threshold with no further internalization. In contrast, the internalization of Dox-NPs gradually increases over time with a greater threshold.
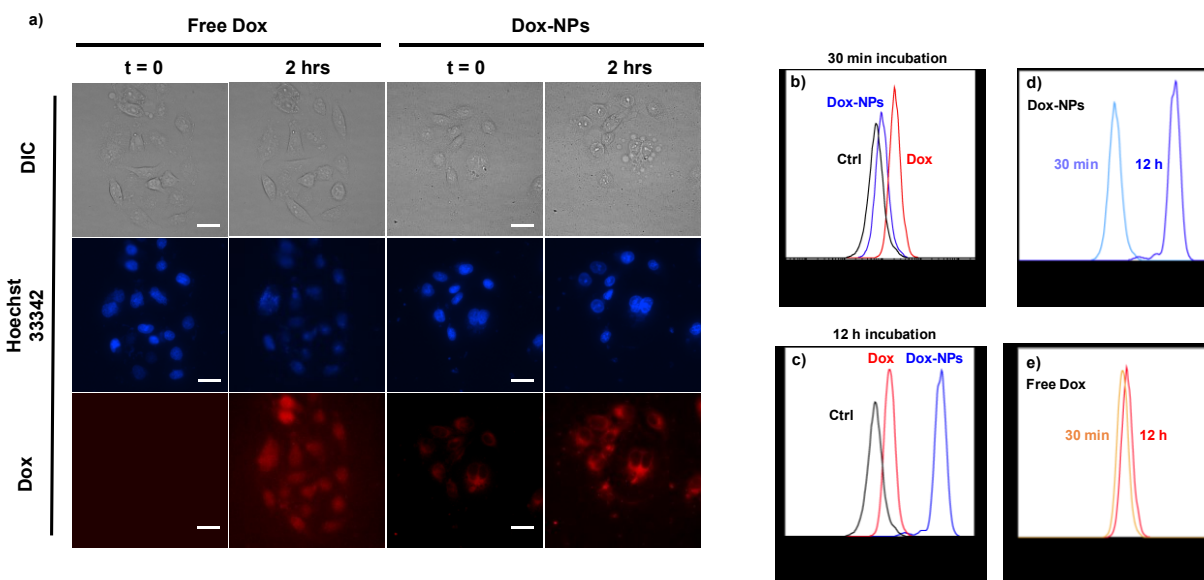
Figure 3. 7. Time-lapse fluorescence microscopy images of HeLa cells incubated with Dox-NPs (encapsulated Dox = 1.6 µg/mL), compared with free Dox (2.5 µg/mL), for 2 hrs (a) as well as their histograms from flow cytometry after 30 min (b) and 12 hrs (c) of incubation and their comparison of free Dox-NPs (d) and Dox (e) over incubation time. Note that the images in red color (Dox) were processed differently for free Dox and Dox-NPs due to low signal from free Dox and the high signal from Dox-NPs. For all experiments, the amount of Dox-NPs was designed to have the encapsulated Dox whose concentration was kept to be 2.5 µg/mL. (Scale bar = 30 µm).

3.3.7 Uptake by cells in multicellular tumor spheroids

Multicellular tumor spheroids (hereafter referred to as spheroids) grown from cultured cells *in vitro* have properties that mimic solid tumors *in vivo,* and thus serve as a model to predict the ability of drug-loaded NPs to penetrate tumors.[172] Here, HeLa cells were induced to form spheroids and incubated with Dox-NPs or free Dox at 1.6 µg/mL, or empty DPE NPs as a control for 4 days. The bright field and fluorescence images of HeLa spheroids in Figure 3.8a show the difference in

fluorescence intensity between Dox-NPs and free Dox. Further quantitative analysis in Figure 3.8b-c indicates that Dox-NPs show a sharp increase in fluorescence within 6 hrs; and upon further incubation, the signal steadily increased. After 4 days of incubation, spheroids with Dox-NPs had intensities that were five times greater than spheroids with free Dox. These results suggest that Dox-NPs are superior in their ability to penetrate HeLa spheroids compared with free Dox. Thus, the controlled uptake and increased threshold of Dox-NPs shown in Figure 3.8 could contribute to an overall increased efficacy of uptake at the multicellular level. To determine if Dox-NPs can also efficiently penetrate spheroids made from other cell types, a similar experiment was performed using spheroids made from A549 lung cancer cells (Figure S11). The uptake of Dox-NPs in A549 spheroids was greater than free Dox, suggesting that the NPs enhance uptake with multiple cancers.
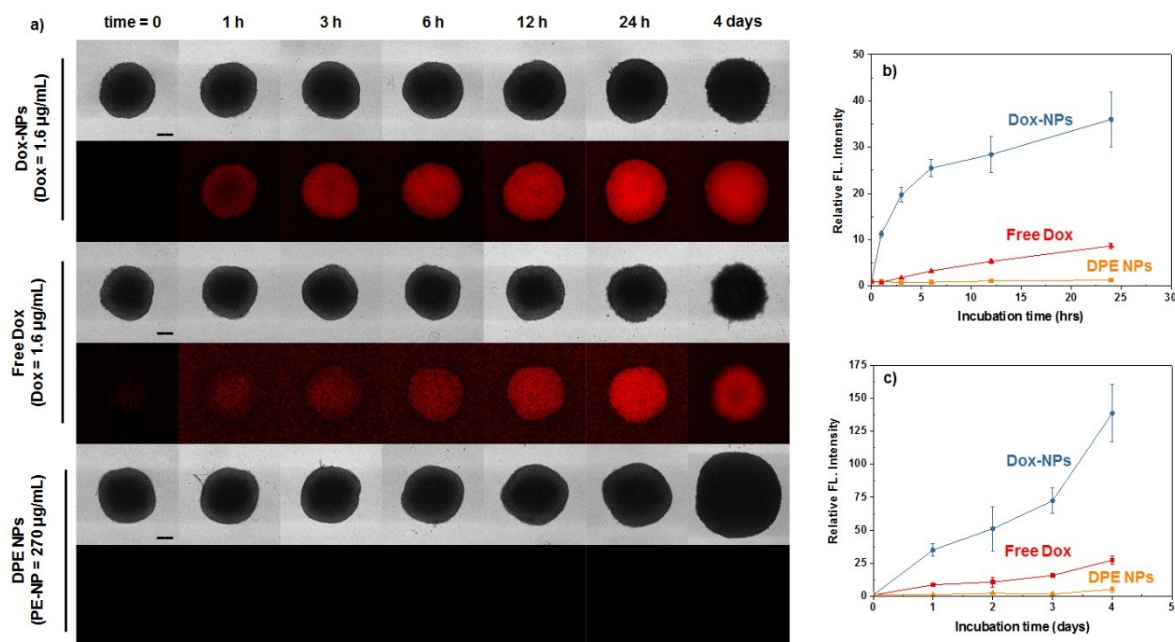
Figure 3. 8. Florescence microscope images of HeLa spheroids incubated for 4 days with Dox NPs (encapsulated Dox = 1.6 µg/mL), free Dox (1.6 µg/mL), and empty DPE-NPs (270 µg/mL) as a control (a). Quantitative analysis of florescence intensity of the spheroids after short term (24 hrs) (b) and long term (4 days) treatments (c). Each value was normalized by their initial value. *Note that the images were processed differently for free Dox and Dox-NPs due to low signal from free Dox and high signal from Dox-NPs. (n = 3, scale bar = 200 µm).

3.3.8 Endocytic uptake of Dox-NPs in HeLa cells

Polymer-based or inorganic NPs can be internalized through several pathways such as clathrin- or caveolae-mediated endocytosis, and macropinocytosis.[173-175] As shown in Figure 3.9, Dox-NPs were visualized in the endomembrane system, supporting that they were taken into cells via one of these mechanisms. To gain insight into the mechanism of entry for the DPE NPs, HeLa cells were incubated with Dox-NPs after being treated without (control) or with chlorpromazine, genistein or a combination of both inhibitors. It has been reported that chlorpromazine inhibits clathrin-mediated endocytosis,[176] while genistein inhibits caveolae-mediated endocytosis.[177] Thus, blocking the pathway that mediates the uptake of Dox-NPs should result in no fluorescence signal inside cells. Figure 9a shows the fluorescence images of HeLa cells treated with Dox-NPs for 1 hr. The red color represents the fluorescence Dox signal, while blue shows the nuclei. Figure 9b shows the quantitative analysis of Dox fluorescence intensity for each treatment normalized to maximum intensity for control (no inhibitors) over 1 hr. While control cells reached a maximum of 100% of normalized intensity after 1 hour, this signal was reduced to 50% after treatment with chlorpromazine and remained at 0% after genistein treatment, or when treated with both inhibitors. These results suggest that caveolae-mediated endocytosis is the dominant pathway for the internalization of Dox-NPs into HeLa cells. Furthermore, the results implicate the reason why Dox-NPs exhibit relatively less cytotoxicity, compared with free Dox, although they had greater cellular uptake based on flow cytometry results. Clathrin-mediated endocytosis and macropinocytosis carry NPs to lysosomes, which are acidic pH (4.5-5.5) and have degradative enzymes. Under these conditions, the NPs could be degraded, resulting in enhanced release of encapsulated Dox. On the other hand, caveolae-mediated endocytosis carries caveolar vesicles to caveosomes; thus the release of Dox is delayed through this endocytosis mechanism.[174, 178] However, the controlled release of Dox from NPs could be more beneficial over longer periods time in the context of tumors *in vivo*, as the capacity for their uptake is higher, this could result in a more tightly controlled release of Dox vs. rapid accumulation of free Dox at lower levels.
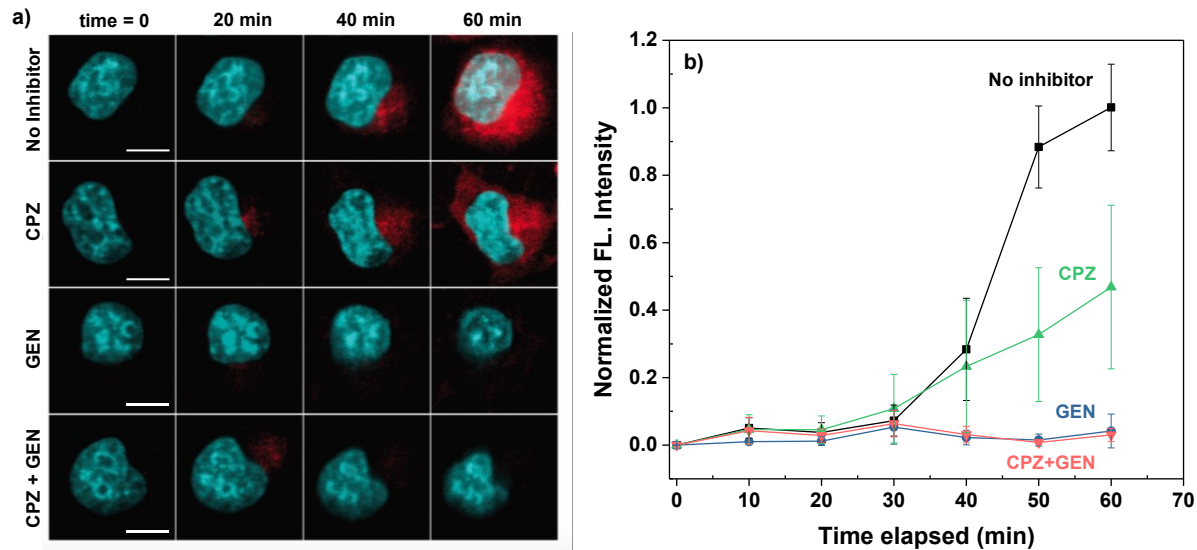
Figure 3. 9. FL images of single cell incubated with Dox-NPs in the absence (control) and presence of chlorpromazine (CPZ, inhibiting clathrin-mediated endocytosis), or genistein (GEN, inhibiting caveolae-mediated endocytosis), or both inhibitors (a) and quantitative analysis of FL intensity of Dox in the perinuclear region normalized with maximum FL intensity of control system (no inhibitors) over 1 hr (b) (scale bar = 10 µm).

3.4 Conclusion

Dual enzyme and oxidation-responsive DPEs with ester and sulfide linkages on their backbones was synthesized by a thiol-ene polyaddition reaction. DPEs were fabricated into aqueous DPE-NP colloids with a diameter = 99 nm, which were relatively non-toxic to HeLa cells up to 750 µg/mL. They were stable and exhibited prolonged colloidal stability when kept for long periods of time on the shelf, or in the presence of serum proteins to mimic physiological conditions. The NPs disassembled successfully in the presence of esterase and hydrogen peroxide, upon cleavages of the ester linkages and oxidation of the sulfide linkages, respectively, as confirmed by DLS analysis. Such dual stimuli-responsive degradation enabled the enhanced and controlled release of encapsulated Dox (clinical anticancer drug) and NR (fluorescent dye as a model hydrophobic drug) from NPs. The results showed that Dox-NPs effectively inhibited the proliferation of HeLa cells, supporting their ability to release Dox in cells. Excitingly, data from HeLa or A549 cells grown in 2D or 3D spheroids showed that Dox-NPs were internalized with higher thresholds compared to free Dox. Further, Dox-NPs appeared to enter cells predominantly by caveolae-mediated endocytosis, which would protect them from degradation in the lysosomes

and permit more controlled release. These results suggest that aqueous NPs are excellent candidates as intracellular nanocarriers for the efficient delivery of anti-cancer therapeutics to inhibit solid tumors.

Chapter 4
Conclusion and Future work

Stimuli-responsive drug delivery is a promising platform for targeted therapy. Among all pathology-associated triggers, ROS and esterase are of great interest because the dual responses can be beneficial for clinical translation. As a biological catalyst, esterase can cleave ester linkages of the esterase-responsive polymers producing small molecules. These small molecules can be excreted from the body by renal filtration rendering biocompatibility even after the delivery of the drug. However, the responsive components are embedded in the core of the nanocarriers to prevent premature release of the drug. Therefore, the cleavages of ester linkages can be delayed due to the size of esterase; the esterase penetrates slowly into the core part of the nanocarriers.[40, 179] On the other hand, ROS, such as H_2O_2, can easily reach the core part of the nanocarriers since they are small molecules. Therefore, they may act synergistically to initiate the release of therapeutic agents and reduce toxicity *in vivo*.

Facile and efficient thiol-ene click type reaction was utilized to synthesize hydrophobic polyester having oxidation-responsive sulfides and esterase-responsive esters. Chapter 2 explores the feasibilities to tune the size of DPE-based NPs using microfluidic method. Choice of appropriate stabilizer is required to produce ideal nanocarriers for cancer therapy. PEG and PL02, for instance, have been used as model stabilizers to study DPE-NPs. The NP sizes were successfully controlled from 50 - 150 nm by changing the formulation and microfluidic parameters. Destabilization of the DPE-NPs in the presence of esterase and H_2O_2 indicated the cleavage of ester linkages and oxidation of sulfide linkages. Results from *in vitro* experiments show that the PEG improved cytotoxicity and cellular uptake. The use of DPE-NPs prepared by using PEG can be further assessed as intracellular nanocarriers.

Chapter 3 describes the assessment of dual enzyme and oxidation-responsive polyester formulation as intracellular nanocarriers using Dox. Dox was incorporated into DPE-NPs stabilized with the PEG and Brij S20. The mixed stabilizer system allows for the preparation of smaller and more uniform DPE-NPs. Dox-loaded DPE-NPs (Dox-NPs) had excellent colloidal stability and exhibited an enhanced release of Dox upon introduction of esterase and H_2O_2. Furthermore, enhanced antitumor activity of the Dox-NPs in HeLa cells was confirmed by MTT

assay. The results from flow cytometry, CLSM and fluorescence microscopy demonstrated that the Dox-NPs possess desired properties as intracellular nanocarriers for cancer therapy with an excellent cellular uptake capability.

Overall, stimuli-responsive platform in conjunction with polymeric surfactant enabled the development of a nanoparticulate formulation for cancer therapy. Although the current design showed promising results, a few suggestions that could lead to an improvement. First, microfluidic instrument can be used to encapsulate Dox. Controlling the mixing rate can influence drug loading; the variation of microfluidic parameters can increase drug loading capacity and encapsulation efficiency. Second, branched polyesters consisting of esters and sulfides can be synthesized and characterized. Branched polyesters are relatively more hydrophobic than the linear polyester of similar molecular weight. This feature may improve encapsulation efficiency of hydrophobic drugs. It would be also interesting to compare the release kinetics since physical properties of the hydrophobic block, such as glass transition temperature (T_g), can affect the release rate.[180] Third, *in vivo* will be required to evaluate the antitumor activity of Dox-NPs for pre-clinical studies.

References

1.   Reuben, D. B.; Mor, V., Nausea and vomiting in terminal cancer patients. *Archives of Internal Medicine* **1986,** 146, 2021-2023.

2.   Corrie, P. G., Cytotoxic chemotherapy: clinical aspects. *Medicine* **2008,** 36, 24-28.

3.   Sun, T.; Zhang, Y. S.; Pang, B.; Hyun, D. C.; Yang, M.; Xia, Y., Engineered nanoparticles for drug delivery in cancer therapy. *Angewandte Chemie International Edition* **2014,** 53, 12320-12364.

4.   Cheng, J.; Teply, B. A.; Sherifi, I.; Sung, J.; Luther, G.; Gu, F. X.; Levy-Nissenbaum, E.; Radovic-Moreno, A. F.; Langer, R.; Farokhzad, O. C., Formulation of functionalized PLGA–PEG nanoparticles for in vivo targeted drug delivery. *Biomaterials* **2007,** 28, 869-876.

5.   Torchilin, V., Targeted polymeric micelles for delivery of poorly soluble drugs. *Cellular and Molecular Life Sciences* **2004,** 61, 2549-2559.

6.   Peer, D.; Karp, J. M.; Hong, S.; Farokhzad, O. C.; Margalit, R.; Langer, R., Nanocarriers as an emerging platform for cancer therapy. *Nature Nanotechnology* **2007,** 2, 751.

7.   Maeda, H.; Wu, J.; Sawa, T.; Matsumura, Y.; Hori, K., Tumor vascular permeability and the EPR effect in macromolecular therapeutics: a review. *Journal of Controlled Release* **2000,** 65, 271-284.

8.   Kazunori, K.; Masayuki, Y.; Teruo, O.; Yasuhisa, S., Block copolymer micelles as vehicles for drug delivery. *Journal of Controlled Release* **1993,** 24, 119-132.

9.   Kwon, G.; Suwa, S.; Yokoyama, M.; Okano, T.; Sakurai, Y.; Kataoka, K., Enhanced tumor accumulation and prolonged circulation times of micelle-forming poly (ethylene oxide-aspartate) block copolymer-adriamycin conjugates. *Journal of Controlled Release* **1994,** 29, 17-23.

10.   Shi, B.; Fang, C.; You, M. X.; Zhang, Y.; Fu, S.; Pei, Y., Stealth MePEG-PCL micelles: effects of polymer composition on micelle physicochemical characteristics, in vitro drug release, in vivo pharmacokinetics in rats and biodistribution in S 180 tumor bearing mice. *Colloid and Polymer Science* **2005,** 283, 954-967.

11.   Huynh, N. T.; Roger, E.; Lautram, N.; Benoît, J.-P.; Passirani, C., The rise and rise of stealth nanocarriers for cancer therapy: passive versus active targeting. *Nanomedicine* **2010,** 5, 1415-1433.

12.   Tenzer, S.; Docter, D.; Rosfa, S.; Wlodarski, A.; Kuharev, J. r.; Rekik, A.; Knauer, S. K.; Bantz, C.; Nawroth, T.; Bier, C., Nanoparticle size is a critical physicochemical determinant of the human blood plasma corona: a comprehensive quantitative proteomic analysis. *ACS Nano* **2011,** 5, 7155-7167.

13.   Nagayasu, A.; Uchiyama, K.; Kiwada, H., The size of liposomes: a factor which affects their targeting efficiency to tumors and therapeutic activity of liposomal antitumor drugs. *Advanced Drug Delivery Reviews* **1999,** 40, 75-87.

14.   Leroux, J.-C.; Allémann, E.; De Jaeghere, F.; Doelker, E.; Gurny, R., Biodegradable nanoparticles—from sustained release formulations to improved site specific drug delivery. *Journal of Controlled Release* **1996,** 39, 339-350.

15.   Nair, L. S.; Laurencin, C. T., Biodegradable polymers as biomaterials. *Progress in Polymer Science* **2007,** 32, 762-798.

16.   Dechy-Cabaret, O.; Martin-Vaca, B.; Bourissou, D., Controlled ring-opening polymerization of lactide and glycolide. *Chemical Reviews* **2004,** 104, 6147-6176.

17.   Li, S.; Girard, A.; Garreau, H.; Vert, M., Enzymatic degradation of polylactide stereocopolymers with predominant D-lactyl contents. *Polymer Degradation and Stability* **2000,** 71, 61-67.

18.   Athanasiou, K. A.; Niederauer, G. G.; Agrawal, C. M., Sterilization, toxicity, biocompatibility and clinical applications of polylactic acid/polyglycolic acid copolymers. *Biomaterials* **1996,** 17, 93-102.

19.   Shuai, X.; Ai, H.; Nasongkla, N.; Kim, S.; Gao, J., Micellar carriers based on block copolymers of poly (ε-caprolactone) and poly (ethylene glycol) for doxorubicin delivery. *Journal of Controlled Release* **2004,** 98, 415-426.

20.   Mura, S.; Nicolas, J.; Couvreur, P., Stimuli-responsive nanocarriers for drug delivery. *Nature Materials* **2013,** 12, 991.

21.   Stuart, M. A. C.; Huck, W. T.; Genzer, J.; Müller, M.; Ober, C.; Stamm, M.; Sukhorukov, G. B.; Szleifer, I.; Tsukruk, V. V.; Urban, M., Emerging applications of stimuli-responsive polymer materials. *Nature Materials* **2010,** 9, 101.

22.   Ganta, S.; Devalapally, H.; Shahiwala, A.; Amiji, M., A review of stimuli-responsive nanocarriers for drug and gene delivery. *Journal of Controlled Release* **2008,** 126, 187-204.

23.   Jazani, A. M.; Oh, J. K., Dual Location, Dual Acidic pH/Reduction-Responsive Degradable Block Copolymer: Synthesis and Investigation of Ketal Linkage Instability under ATRP Conditions. *Macromolecules* **2017,** 50, 9427-9436.

24.   An, S. Y.; Hong, S. H.; Tang, C.; Oh, J. K., Rosin-based block copolymer intracellular delivery nanocarriers with reduction-responsive sheddable coronas for cancer therapy. *Polymer Chemistry* **2016,** 7, 4751-4760.

25.   Xu, X.; Saw, P. E.; Tao, W.; Li, Y.; Ji, X.; Bhasin, S.; Liu, Y.; Ayyash, D.; Rasmussen, J.; Huo, M.; Shi, J.; Farokhzad, O. C., ROS-Responsive Polyprodrug Nanoparticles for Triggered Drug Delivery and Effective Cancer Therapy. *Advanced Materials* **2017,** 29, 1700141.

26.   Fouladi, F.; Steffen, K. J.; Mallik, S., Enzyme-Responsive Liposomes for the Delivery of Anticancer Drugs. *Bioconjugate Chemistry* **2017,** 28, 857-868.

27.   Wang, H.; Ke, F.; Mararenko, A.; Wei, Z.; Banerjee, P.; Zhou, S., Responsive polymer–fluorescent carbon nanoparticle hybrid nanogels for optical temperature sensing, near-infrared light-responsive drug release, and tumor cell imaging. *Nanoscale* **2014,** 6, 7443-7452.

28.   Sardon, H.; Tan, J. P. K.; Chan, J. M. W.; Mantione, D.; Mecerreyes, D.; Hedrick, J. L.; Yang, Y. Y., Thermoresponsive Random Poly(ether urethanes) with Tailorable LCSTs for Anticancer Drug Delivery. *Macromolecular Rapid Communications* **2015,** 36, 1761-1767.

29.   Hayashi, K.; Nakamura, M.; Miki, H.; Ozaki, S.; Abe, M.; Matsumoto, T.; Sakamoto, W.; Yogo, T.; Ishimura, K., Magnetically Responsive Smart Nanoparticles for Cancer Treatment with

a Combination of Magnetic Hyperthermia and Remote-Control Drug Release. *Theranostics* **2014,** 4, 834-844.

30. Lu, Y.; Sun, W.; Gu, Z., Stimuli-responsive nanomaterials for therapeutic protein delivery. *Journal of Controlled Release* **2014,** 194, 1-19.

31. Fleige, E.; Quadir, M. A.; Haag, R., Stimuli-responsive polymeric nanocarriers for the controlled transport of active compounds: concepts and applications. *Advanced Drug Delivery Reviews* **2012,** 64, 866-884.

32. Needham, L. A.; Davidson, A. H.; Bawden, L. J.; Belfield, A.; Bone, E. A.; Brotherton, D. H.; Bryant, S.; Charlton, M. H.; Clark, V. L.; Davies, S. J.; Donald, A.; Day, F. A.; Krige, D.; Legris, V.; McDermott, J.; McGovern, Y.; Owen, J.; Patel, S. R.; Pintat, S.; Testar, R. J.; Wells, G. M. A.; Moffat, D.; Drummond, A. H., Drug Targeting to Monocytes and Macrophages Using Esterase-Sensitive Chemical Motifs. *Journal of Pharmacology and Experimental Therapeutics* **2011,** 339, 132-142.

33. Fernando, I. R.; Ferris, D. P.; Frasconi, M.; Malin, D.; Strekalova, E.; Yilmaz, M. D.; Ambrogio, M. W.; Algaradah, M. M.; Hong, M. P.; Chen, X.; Nassar, M. S.; Botros, Y. Y.; Cryns, V. L.; Stoddart, J. F., Esterase- and pH-responsive poly(β-amino ester)-capped mesoporous silica nanoparticles for drug delivery. *Nanoscale* **2015,** 7, 7178-7183.

34. Turk, V.; Kos, J.; Turk, B., Cysteine cathepsins (proteases)—on the main stage of cancer? *Cancer Cell* **2004,** 5, 409-410.

35. Roy, R.; Yang, J.; Moses, M. A., Matrix metalloproteinases as novel biomarker s and potential therapeutic targets in human cancer. *Journal of Clinical Oncology* **2009,** 27, 5287-5297.

36. Sun, K.; Chang, Y.; Zhou, B.; Wang, X.; Liu, L., Gold nanoparticles-based electrochemical method for the detection of protein kinase with a peptide-like inhibitor as the bioreceptor. *International Journal of Nanomedicine* **2017,** 12, 1905.

37. Van Tomme, S. R.; Storm, G.; Hennink, W. E., In situ gelling hydrogels for pharmaceutical and biomedical applications. *International Journal of Pharmaceutics* **2008,** 355, 1-18.

38. Xia, X.; Yang, M.; Oetjen, L. K.; Zhang, Y.; Li, Q.; Chen, J.; Xia, Y., An enzyme-sensitive probe for photoacoustic imaging and fluorescence detection of protease activity. *Nanoscale* **2011,** 3, 950-953.

39. Hu, J.; Zhang, G.; Liu, S., Enzyme-responsive polymeric assemblies, nanoparticles and hydrogels. *Chemical Society Reviews* **2012,** 41, 5933-5949.

40. Amir, R. J.; Zhong, S.; Pochan, D. J.; Hawker, C. J., Enzymatically triggered self-assembly of block copolymers. *Journal of the American Chemical Society* **2009,** 131, 13949-13951.

41. Harnoy, A. J.; Rosenbaum, I.; Tirosh, E.; Ebenstein, Y.; Shaharabani, R.; Beck, R.; Amir, R. J., Enzyme-responsive amphiphilic PEG-dendron hybrids and their assembly into smart micellar nanocarriers. *Journal of the American Chemical Society* **2014,** 136, 7531-7534.

42. Rosenbaum, I.; Harnoy, A. J.; Tirosh, E.; Buzhor, M.; Segal, M.; Frid, L.; Shaharabani, R.; Avinery, R.; Beck, R.; Amir, R. J., Encapsulation and covalent binding of molecular payload in enzymatically activated micellar nanocarriers. *Journal of the American Chemical Society* **2015,** 137, 2276-2284.

43.   Harris, T. J.; von Maltzahn, G.; Lord, M. E.; Park, J. H.; Agrawal, A.; Min, D. H.; Sailor, M. J.; Bhatia, S. N., Protease-Triggered Unveiling of Bioactive Nanoparticles. *Small* **2008,** 4, 1307-1312.

44.   Chien, M. P.; Thompson, M. P.; Barback, C. V.; Ku, T. H.; Hall, D. J.; Gianneschi, N. C., Enzyme-Directed Assembly of a Nanoparticle Probe in Tumor Tissue. *Advanced Materials* **2013,** 25, 3599-3604.

45.   Jiang, T.; Olson, E. S.; Nguyen, Q. T.; Roy, M.; Jennings, P. A.; Tsien, R. Y., Tumor imaging by means of proteolytic activation of cell-penetrating peptides. *Proceedings of the National Academy of Sciences* **2004,** 101, 17867-17872.

46.   Huang, Y.; Jiang, Y.; Wang, H.; Wang, J.; Shin, M. C.; Byun, Y.; He, H.; Liang, Y.; Yang, V. C., Curb challenges of the "Trojan Horse" approach: smart strategies in achieving effective yet safe cell-penetrating peptide-based drug delivery. *Advanced Drug Delivery Reviews* **2013,** 65, 1299-1315.

47.   Dorresteijn, R.; Billecke, N.; Schwendy, M.; Pütz, S.; Bonn, M.; Parekh, S. H.; Klapper, M.; Müllen, K., Polylactide-block-Polypeptide-block-Polylactide Copolymer Nanoparticles with Tunable Cleavage and Controlled Drug Release. *Advanced Functional Materials* **2014,** 24, 4026-4033.

48.   Kherif, S.; Lafuma, C.; Dehaupas, M.; Lachkar, S.; Fournier, J.-G.; Verdière-Sahuqué, M.; Fardeau, M.; Alameddine, H. S., Expression of matrix metalloproteinases 2 and 9 in regenerating skeletal muscle: A study in experimentally injured andmdxmuscles. *Developmental Biology* **1999,** 205, 158-170.

49.   Callmann, C. E.; Barback, C. V.; Thompson, M. P.; Hall, D. J.; Mattrey, R. F.; Gianneschi, N. C., Therapeutic Enzyme-Responsive Nanoparticles for Targeted Delivery and Accumulation in Tumors. *Advanced Materials* **2015,** 27, 4611-4615.

50.   Szpaderska, A. M.; Frankfater, A., An intracellular form of cathepsin B contributes to invasiveness in cancer. *Cancer Research* **2001,** 61, 3493-3500.

51.   Rempel, S. A.; Rosenblum, M. L.; Mikkelsen, T.; Yan, P.-S.; Ellis, K. D.; Golembieski, W. A.; Sameni, M.; Rozhin, J.; Ziegler, G.; Sloane, B. F., Cathepsin B expression and localization in glioma progression and invasion. *Cancer Research* **1994,** 54, 6027-6031.

52.   Campo, E.; Munoz, J.; Miquel, R.; Palacín, A.; Cardesa, A.; Sloane, B. F.; Emmert-Buck, M. R., Cathepsin B expression in colorectal carcinomas correlates with tumor progression and shortened patient survival. *The American Journal of Pathology* **1994,** 145, 301.

53.   Li, N.; Li, N.; Yi, Q.; Luo, K.; Guo, C.; Pan, D.; Gu, Z., Amphiphilic peptide dendritic copolymer-doxorubicin nanoscale conjugate self-assembled to enzyme-responsive anti-cancer agent. *Biomaterials* **2014,** 35, 9529-9545.

54.   Zhang, C.; Pan, D.; Luo, K.; She, W.; Guo, C.; Yang, Y.; Gu, Z., Peptide Dendrimer–Doxorubicin Conjugate-Based Nanoparticles as an Enzyme-Responsive Drug Delivery System for Cancer Therapy. *Advanced Healthcare Materials* **2014,** 3, 1299-1308.

55.   She, W.; Li, N.; Luo, K.; Guo, C.; Wang, G.; Geng, Y.; Gu, Z., Dendronized heparin−doxorubicin conjugate based nanoparticle as pH-responsive drug delivery system for cancer therapy. *Biomaterials* **2013,** 34, 2252-2264.

56.   Lammers, T.; Subr, V.; Ulbrich, K.; Peschke, P.; Huber, P. E.; Hennink, W. E.; Storm, G., Simultaneous delivery of doxorubicin and gemcitabine to tumors in vivo using prototypic polymeric drug carriers. *Biomaterials* **2009,** 30, 3466-3475.

57.   Owen, C. A.; Campbell, E. J., The cell biology of leukocyte-mediated proteolysis. *Journal of Leukocyte Biology* **1999,** 65, 137-150.

58.   Aimetti, A. A.; Tibbitt, M. W.; Anseth, K. S., Human neutrophil elastase responsive delivery from poly (ethylene glycol) hydrogels. *Biomacromolecules* **2009,** 10, 1484-1489.

59.   Meers, P., Enzyme-activated targeting of liposomes. *Advanced Drug Delivery Reviews* **2001,** 53, 265-272.

60.   Habraken, G. J.; Peeters, M.; Thornton, P. D.; Koning, C. E.; Heise, A., Selective enzymatic degradation of self-assembled particles from amphiphilic block copolymers obtained by the combination of N-carboxyanhydride and nitroxide-mediated polymerization. *Biomacromolecules* **2011,** 12, 3761-3769.

61.   Devasagayam, T.; Tilak, J.; Boloor, K.; Sane, K. S.; Ghaskadbi, S. S.; Lele, R., Free radicals and antioxidants in human health: current status and future prospects. *Japi* **2004,** 52, 4.

62.   Toyokuni, S.; Okamoto, K.; Yodoi, J.; Hiai, H., Persistent oxidative stress in cancer. *FEBS letters* **1995,** 358, 1-3.

63.   Behrend, L.; Henderson, G.; Zwacka, R., Reactive oxygen species in oncogenic transformation. In Portland Press Limited: 2003.

64.   Trachootham, D.; Alexandre, J.; Huang, P., Targeting cancer cells by ROS-mediated mechanisms: a radical therapeutic approach? *Nature Reviews Drug Discovery* **2009,** 8, 579-591.

65.   Kawanishi, S.; Hiraku, Y.; Pinlaor, S.; Ma, N., Oxidative and nitrative DNA damage in animals and patients with inflammatory diseases in relation to inflammation-related carcinogenesis. *Biological Chemistry* **2006,** 387.

66.   Vo, C. D.; Kilcher, G.; Tirelli, N., Polymers and sulfur: what are organic polysulfides good for? Preparative strategies and biological applications. *Macromolecular Rapid Communications* **2009,** 30, 299-315.

67.   Gupta, M. K.; Meyer, T. A.; Nelson, C. E.; Duvall, C. L., Poly (PS-b-DMA) micelles for reactive oxygen species triggered drug release. *Journal of Controlled Release* **2012,** 162, 591-598.

68.   Herzberger, J.; Fischer, K.; Leibig, D.; Bros, M.; Thiermann, R.; Frey, H., Oxidation-responsive and "clickable" poly (ethylene glycol) via copolymerization of 2-(methylthio) ethyl glycidyl ether. *Journal of the American Chemical Society* **2016,** 138, 9212-9223.

69.   Haba, K.; Popkov, M.; Shamis, M.; Lerner, R. A.; Barbas, C. F.; Shabat, D., Single-Triggered Trimeric Prodrugs. *Angewandte Chemie International Edition* **2005,** 44, 716-720.

70.   Major Jourden, J. L.; Cohen, S. M., Hydrogen peroxide activated matrix metalloproteinase inhibitors: a prodrug approach. *Angewandte Chemie International Edition* **2010,** 49, 6795-6797.

71.   Sella, E.; Lubelski, A.; Klafter, J.; Shabat, D., Two-component dendritic chain reactions: Experiment and theory. *Journal of the American Chemical Society* **2010,** 132, 3945-3952.

72.   de Gracia Lux, C.; Joshi-Barr, S.; Nguyen, T.; Mahmoud, E.; Schopf, E.; Fomina, N.; Almutairi, A., Biocompatible polymeric nanoparticles degrade and release cargo in response to biologically relevant levels of hydrogen peroxide. *Journal of the American Chemical Society* **2012,** 134, 15758-15764.

73.   Nishiyama, N.; Kataoka, K., Nanostructured devices based on block copolymer assemblies for drug delivery: designing structures for enhanced drug function. *Advances in Polymer Science* **2006,** 193, 67-101.

74.   Mailander, V.; Landfester, K., Interaction of nanoparticles with cells. *Biomacromolecules* **2009,** 10, 2379-400.

75.   Harada, A.; Kataoka, K., Supramolecular assemblies of block copolymers in aqueous media as nanocontainers relevant to biological applications. *Progress in Polymer Science* **2006,** 31, 949-982.

76.   Khandare, J.; Minko, T., Polymer-drug conjugates: Progress in polymeric prodrugs. *Progress in Polymer Science* **2006,** 31, 359-397.

77.   Liu, S.; Maheshwari, R.; Kiick, K. L., Polymer-Based Therapeutics. *Macromolecules* **2009,** 42, 3-13.

78.   Du, J.-Z.; Du, X.-J.; Mao, C.-Q.; Wang, J., Tailor-Made Dual pH-Sensitive Polymer-Doxorubicin Nanoparticles for Efficient Anticancer Drug Delivery. *Journal of the American Chemical Society* **2011,** 133, 17560-17563.

79.   Tomalia, D. A., Birth of a new macromolecular architecture: dendrimers as quantized building blocks for nanoscale synthetic polymer chemistry. *Progress in Polymer Science* **2005,** 30, 294-324.

80.   Oh, J. K.; Lee, D. I.; Park, J. M., Biopolymer-based microgels/nanogels for drug delivery applications. *Progress in Polymer Science* **2009,** 34, 1261-1282.

81.   Oh, J. K.; Drumright, R.; Siegwart, D. J.; Matyjaszewski, K., The development of microgels/nanogels for drug delivery applications. *Progress in Polymer Science* **2008,** 33, 448-477.

82.   Hamidi, M.; Azadi, A.; Rafiei, P., Hydrogel nanoparticles in drug delivery. *Advanced Drug Delivery Reviews* **2008,** 60, 1638-1649.

83.   Raemdonck, K.; Demeester, J.; De Smedt, S., Advanced nanogel engineering for drug delivery. *Soft Matter* **2009,** 5, 707-715.

84.   Liu, Z.; Jiao, Y.; Wang, Y.; Zhou, C.; Zhang, Z., Polysaccharides-based nanoparticles as drug delivery systems. *Advanced Drug Delivery Reviews* **2008,** 60, 1650-1662.

85.   Blanazs, A.; Armes, S. P.; Ryan, A. J., Self-assembled block copolymer aggregates: from micelles to vesicles and their biological applications. *Macromolecular Rapid Communications* **2009,** 30, 267-277.

86.   Mikhail, A. S.; Allen, C., Block copolymer micelles for delivery of cancer therapy: Transport at the whole body, tissue and cellular levels. *Journal of Controlled Release* **2009,** 138, 214-223.

87.   Xiong, X.-B.; Falamarzian, A.; Garg, S. M.; Lavasanifar, A., Engineering of amphiphilic block copolymers for polymeric micellar drug and gene delivery. *Journal of Controlled Release* **2011,** 155, 248-261.

88.   Soliman, G. M.; Sharma, A.; Maysinger, D.; Kakkar, A., Dendrimers and miktoarm polymers based multivalent nanocarriers for efficient and targeted drug delivery. *Chemical Communications* **2011,** 47, 9572-9587.

89.   Ende, A. E. v. d.; Kravitz, E. J.; Harth, E., Approach to formation of multifunctional polyester particles in controlled nanoscopic dimensions. *Journal of the American Chemical Society* **2008,** 130, 8706-8713.

90.   Jacobson, G. B.; Shinde, R.; Contag, C. H.; Zare, R. N., Sustained release of drugs dispersed in polymer nanoparticles. *Angewandte Chemie International Edition* **2008,** 47, 7880-7882.

91.   Bertrand, N.; Wu, J.; Xu, X.; Kamaly, N.; Farokhzad, O. C., Cancer nanotechnology: The impact of passive and active targeting in the era of modern cancer biology. *Advanced Drug Delivery Reviews* **2014,** 66, 2-25.

92.   Owens III, D.; Peppas, N., Opsonization, biodistribution, and pharmacokinetics of polymeric nanoparticles. *International Journal of Pharmaceutics* **2006,** 307, 93-102.

93.   Lee, H.; Hoang, B.; Fonge, H.; Reilly, R. M.; Allen, C., In Vivo Distribution of Polymeric Nanoparticles at the Whole-Body, Tumor, and Cellular Levels. *Pharmaceutical Research* **2010,** 27, 2343-2355.

94.   Cabral, H.; Matsumoto, Y.; Mizuno, K.; Chen, Q.; Murakami, M.; Kimura, M.; Terada, Y.; Kano, M. R.; Miyazono, K.; Uesaka, M.; Nishiyama, N.; Kataoka, K., Accumulation of sub-100 nm polymeric micelles in poorly permeable tumours depends on size. *Nature Nanotechnology* **2011,** 6, 815-23.

95.   Liu, D.; Zhang, H.; Fontana, F.; Hirvonen, J. T.; Santos, H. A., Microfluidic-assisted fabrication of carriers for controlled drug delivery. *Lab on a Chip* **2017,** 17, 1856-1883.

96.   Ma, J.; Lee, S. M.-Y.; Yi, C.; Li, C.-W., Controllable synthesis of functional nanoparticles by microfluidic platforms for biomedical applications - a review. *Lab on a Chip* **2017,** 17, 209-226.

97.   Ran, R.; Sun, Q.; Baby, T.; Wibowo, D.; Middelberg, A. P. J.; Zhao, C.-X., Multiphase microfluidic synthesis of micro- and nanostructures for pharmaceutical applications. *Chemical Engineering Science* **2017,** 169, 78-96.

98.   Yoon, H. Y.; Koo, H.; Choi, K. Y.; Chan Kwon, I.; Choi, K.; Park, J. H.; Kim, K., Photo-crosslinked hyaluronic acid nanoparticles with improved stability for in vivo tumor-targeted drug delivery. *Biomaterials* **2013,** 34, 5273-5280.

99.   Zhigaltsev, I. V.; Belliveau, N.; Hafez, I.; Leung, A. K. K.; Huft, J.; Hansen, C.; Cullis, P. R., Bottom-Up Design and Synthesis of Limit Size Lipid Nanoparticle Systems with Aqueous and Triglyceride Cores Using Millisecond Microfluidic Mixing. *Langmuir* **2012,** 28, 3633-3640.

100.   Karnik, R.; Gu, F.; Basto, P.; Cannizzaro, C.; Dean, L.; Kyei-Manu, W.; Langer, R.; Farokhzad, O. C., Microfluidic Platform for Controlled Synthesis of Polymeric Nanoparticles. *Nano Letters* **2008,** 8, 2906-2912.

101.   Herranz-Blanco, B.; Liu, D.; Maekilae, E.; Shahbazi, M.-A.; Ginestar, E.; Zhang, H.; Aseyev, V.; Balasubramanian, V.; Salonen, J.; Hirvonen, J.; Santos, H. A., On-chip self-assembly of a smart hybrid nanocomposite for antitumoral applications. *Advanced Functional Materials* **2015,** 25, 1488-1497.

102.   Wilson, D. R.; Mosenia, A.; Suprenant, M. P.; Upadhya, R.; Routkevitch, D.; Meyer, R. A.; Quinones-Hinojosa, A.; Green, J. J., Continuous microfluidic assembly of biodegradable poly(beta-amino ester)/DNA nanoparticles for enhanced gene delivery. *Journal of Biomedical Materials Research, Part A* **2017,** 105, 1813-1825.

103.   Bolu, B. S.; Golba, B.; Boke, N.; Sanyal, A.; Sanyal, R., Designing Dendron–Polymer Conjugate Based Targeted Drug Delivery Platforms with a "Mix-and-Match" Modularity. *Bioconjugate Chemistry* **2017,** 28, 2962-2975.

104.   Leung, A. K. K.; Hafez, I. M.; Baoukina, S.; Belliveau, N. M.; Zhigaltsev, I. V.; Afshinmanesh, E.; Tieleman, D. P.; Hansen, C. L.; Hope, M. J.; Cullis, P. R., Lipid Nanoparticles Containing siRNA Synthesized by Microfluidic Mixing Exhibit an Electron-Dense Nanostructured Core. *Journal of Physical Chemistry C* **2012,** 116, 18440-18450.

105.   Valencia, P. M.; Pridgen, E. M.; Perea, B.; Gadde, S.; Sweeney, C.; Kantoff, P. W.; Bander, N. H.; Lippard, S. J.; Langer, R.; Karnik, R.; Farokhzad, O. C., Synergistic cytotoxicity of irinotecan and cisplatin in dual-drug targeted polymeric nanoparticles. *Nanomedicine* **2013,** 8, 687-698.

106.   Dimov, N.; Kastner, E.; Hussain, M.; Perrie, Y.; Szita, N., Formation and purification of tailored liposomes for drug delivery using a module-based micro continuous-flow system. *Scientific Reports* **2017,** 7.

107.   Balbino, T. A.; Serafin, J. M.; Malfatti-Gasperini, A. A.; de Oliveira, C. L.; Cavalcanti, L. P.; de Jesus, M. B.; de La Torre, L. G., Microfluidic assembly of pDNA/Cationic liposome lipoplexes with high pDNA loading for gene delivery. *Langmuir* **2016,** 32, 1799-1807.

108.   Sakurai, D.; Molino Cornejo, J. J.; Daiguji, H.; Takemura, F., Hollow polylactic acid microcapsules fabricated by gas/oil/water and bubble template methods. *Journal of Materials Chemistry A* **2013,** 1, 14562-14568.

109.   Park, M.-K.; Jun, S.; Kim, I.; Jin, S.-M.; Kim, J.-G.; Shin, T. J.; Lee, E., Stepwise Drug-Release Behavior of Onion-Like Vesicles Generated from Emulsification-Induced Assembly of Semicrystalline Polymer Amphiphiles. *Advanced Functional Materials* **2015,** 25, 4570-4579.

110.   Jiang, M.-Y.; Ju, X.-J.; Deng, K.; Fan, X.-X.; He, X.-H.; Wu, F.; He, F.; Liu, Z.; Wang, W.; Xie, R.; Chu, L.-Y., The microfluidic synthesis of composite hollow microfibers for K+-responsive controlled release based on a host–guest system. *Journal of Materials Chemistry B* **2016,** 4, 3925-3935.

111.   Gaitzsch, J.; Huang, X.; Voit, B., Engineering Functional Polymer Capsules toward Smart Nanoreactors. *Chemical Reviews* **2015,** 116, 1053-1093.

112.   Abbaspourrad, A.; Datta, S. S.; Weitz, D. A., Controlling Release From pH-Responsive Microcapsules. *Langmuir* **2013,** 29, 12697-12702.

113. Madrigal, J. L.; Stilhano, R. S.; Siltanen, C.; Tanaka, K.; Rezvani, S. N.; Morgan, R. P.; Revzin, A.; Han, S. W.; Silva, E. A., Microfluidic generation of alginate microgels for the controlled delivery of lentivectors. *Journal of Materials Chemistry B* **2016,** 4, 6989-6999.

114. Gaucher, G.; Marchessault, R. H.; Leroux, J.-C., Polyester-based micelles and nanoparticles for the parenteral delivery of taxanes. *Journal of Controlled Release* **2010,** 143, 2-12.

115. Pounder, R. J.; Dove, A. P., Towards poly(ester) nanoparticles: recent advances in the synthesis of functional poly(ester)s by ring-opening polymerization. *Polymer Chemistry* **2010,** 1, 260-271.

116. Klinger, D.; Landfester, K., Stimuli-responsive microgels for the loading and release of functional compounds: Fundamental concepts and applications. *Polymer* **2012,** 53, 5209-5231.

117. Rijcken, C. J. F.; Soga, O.; Hennink, W. E.; van Nostrum, C. F., Triggered destabilization of polymeric micelles and vesicles by changing polymers polarity: An attractive tool for drug delivery. *Journal of Controlled Release* **2007,** 120, 131-148.

118. Zhang, Q.; Ko, N. R.; Oh, J. K., Recent advances in stimuli-responsive degradable block copolymer micelles: synthesis and controlled drug delivery applications. *Chemical Communications* **2012,** 48, 7542-7552.

119. Jackson, A. W.; Fulton, D. A., Making polymeric nanoparticles stimuli-responsive with dynamic covalent bonds. *Polymer Chemistry* **2013,** 4, 31-45.

120. Wang, Y.; Xu, H.; Zhang, X., Tuning the Amphiphilicity of Building Blocks: Controlled Self-Assembly and Disassembly for Functional Supramolecular Materials. *Advanced Materials* **2009,** 21, 2849-2864.

121. Loomis, K.; McNeeley, K.; Bellamkonda, R. V., Nanoparticles with targeting, triggered release, and imaging functionality for cancer applications. *Soft Matter* **2011,** 7, 839-856.

122. Rikkou, M. D.; Patrickios, C. S., Polymers prepared using cleavable initiators: Synthesis, characterization and degradation. *Progress in Polymer Science* **2011,** 36, 1079-1097.

123. Alvarez-Lorenzo, C.; Concheiro, A., Smart drug delivery systems: from fundamentals to the clinic. *Chemical Communications* **2014,** 50, 7743-7765.

124. Harnoy, A. J.; Rosenbaum, I.; Tirosh, E.; Ebenstein, Y.; Shaharabani, R.; Beck, R.; Amir, R. J., Enzyme-Responsive Amphiphilic PEG-Dendron Hybrids and Their Assembly into Smart Micellar Nanocarriers. *J. Am. Chem. Soc.* **2014,** 136, 7531-7534.

125. Rosenbaum, I.; Harnoy, A. J.; Tirosh, E.; Buzhor, M.; Segal, M.; Frid, L.; Shaharabani, R.; Avinery, R.; Beck, R.; Amir, R. J., Encapsulation and Covalent Binding of Molecular Payload in Enzymatically Activated Micellar Nanocarriers. *J. Am. Chem. Soc.* **2015,** 137, 2276-2284.

126. Segal, M.; Avinery, R.; Buzhor, M.; Shaharabani, R.; Harnoy, A. J.; Tirosh, E.; Beck, R.; Amir, R. J., Molecular Precision and Enzymatic Degradation: From Readily to Undegradable Polymeric Micelles by Minor Structural Changes. *Journal of the American Chemical Society* **2017,** 139, 803-810.

127. Fu, X.; Ma, Y.; Shen, Y.; Fu, W.; Li, Z., Oxidation-Responsive OEGylated Poly-L-cysteine and Solution Properties Studies. *Biomacromolecules* **2014,** 15, 1055-1061.

128.	Xiong, M.-H.; Bao, Y.; Du, X.-J.; Tan, Z.-B.; Jiang, Q.; Wang, H.-X.; Zhu, Y.-H.; Wang, J., Differential Anticancer Drug Delivery with a Nanogel Sensitive to Bacteria-Accumulated Tumor Artificial Environment. *ACS Nano* **2013,** 7, 10636-10645.

129.	Sun, H.; Cheng, R.; Deng, C.; Meng, F.; Dias, A. A.; Hendriks, M.; Feijen, J.; Zhong, Z., Enzymatically and Reductively Degradable α-Amino Acid-Based Poly(ester amide)s: Synthesis, Cell Compatibility, and Intracellular Anticancer Drug Delivery. *Biomacromolecules* **2015,** 16, 597-605.

130.	Kashyap, S.; Singh, N.; Surnar, B.; Jayakannan, M., Enzyme and Thermal Dual Responsive Amphiphilic Polymer Core-Shell Nanoparticle for Doxorubicin Delivery to Cancer Cells. *Biomacromolecules* **2016,** 17, 384-398.

131.	Napoli, A.; Valentini, M.; Tirelli, N.; Müller, M.; Hubbell, J. A., Oxidation-responsive polymeric vesicles. *Nature Materials* **2004,** 3, 183.

132.	Greenspan, P.; Fowler, S. D., Spectrofluorometric studies of the lipid probe, nile red. *Journal of Lipid Research* **1985,** 26, 781-789.

133.	Matsumura, Y.; Kataoka, K., Preclinical and clinical studies of anticancer agent-incorporating polymer micelles. *Cancer Science* **2009,** 100, 572-579.

134.	Mikhail, A. S.; Allen, C., Block copolymer micelles for delivery of cancer therapy: Transport at the whole body, tissue and cellular levels. *J. Control. Release* **2009,** 138, 214-223.

135.	Bae, Y. H.; Park, K., Targeted drug delivery to tumors: Myths, reality and possibility. *Journal of Controlled Release* **2011,** 153, 198-205.

136.	Danhier, F.; Feron, O.; Préat, V., To exploit the tumor microenvironment: Passive and active tumor targeting of nanocarriers for anti-cancer drug delivery. *Journal of Controlled Release* **2010,** 148, 135-146.

137.	Brambilla, D.; Nicolas, J.; Le Droumaguet, B.; Andrieux, K.; Marsaud, V.; Couraud, P.-O.; Couvreur, P., Design of fluorescently tagged poly(alkyl cyanoacrylate) nanoparticles for human brain endothelial cell imaging. *Chemical Communications* **2010,** 46, 2602-2604.

138.	Taurin, S.; Nehoff, H.; Greish, K., Anticancer nanomedicine and tumor vascular permeability; Where is the missing link? *Journal of Controlled Release* **2012,** 164, 265-275.

139.	Zhang, L.; Li, Y.; Yu, J. C., Chemical modification of inorganic nanostructures for targeted and controlled drug delivery in cancer treatment. *Journal of Materials Chemistry B: Materials for Biology and Medicine* **2014,** 2, 452-470.

140.	Nichols, J. W.; Bae, Y. H., Odyssey of a cancer nanoparticle: From injection site to site of action. *Nano Today* **2012,** 7, 606-618.

141.	Wei, H.; Zhuo, R.-X.; Zhang, X.-Z., Design and development of polymeric micelles with cleavable links for intracellular drug delivery. *Progress in Polymer Science* **2013,** 38, 503-535.

142.	Ulijn, R. V., Enzyme-responsive materials: a new class of smart biomaterials. *Journal of Materials Chemistry* **2006,** 16, 2217-2225.

143.	Lee, M. H.; Yang, Z.; Lim, C. W.; Lee, Y. H.; Sun, D.; Kang, C.; Kim, J. S., Disulfide-Cleavage-Triggered Chemosensors and Their Biological Applications. *Chemical Reviews* **2013,** 113, 5071-5109.

144.	Deng, C.; Jiang, Y.; Cheng, R.; Meng, F.; Zhong, Z., Biodegradable polymeric micelles for targeted and controlled anticancer drug delivery: Promises, progress and prospects. *Nano Today* **2012,** 7, 467-480.

145.	Huo, M.; Yuan, J.; Tao, L.; Wei, Y., Redox-responsive polymers for drug delivery: from molecular design to applications. *Polymer Chemistry* **2014,** 5, 1519-1528.

146.	Binauld, S.; Stenzel, M. H., Acid-degradable polymers for drug delivery: a decade of innovation. *Chemical Communications* **2013,** 49, 2082-2102.

147.	Needham, L. A.; Davidson, A. H.; Bawden, L. J.; Belfield, A.; Bone, E. A.; Brotherton, D. H.; Bryant, S.; Charlton, M. H.; Clark, V. L.; Davies, S. J., Drug targeting to monocytes and macrophages using esterase-sensitive chemical motifs. *Journal of Pharmacology and Experimental Therapeutics* **2011,** 339, 132-142.

148.	Zhu, L.; Kate, P.; Torchilin, V. P., Matrix Metalloprotease 2-Responsive Multifunctional Liposomal Nanocarrier for Enhanced Tumor Targeting. *ACS Nano* **2012,** 6, 3491-3498.

149.	Dorresteijn, R.; Billecke, N.; Schwendy, M.; Puetz, S.; Bonn, M.; Parekh, S. H.; Klapper, M.; Muellen, K., Polylactide-block-polypeptide-block-polylactide copolymer nanoparticles with tunable cleavage and controlled drug release. *Advanced Functional Materials* **2014,** 24, 4026-4033.

150.	Gao, L.; Zheng, B.; Chen, W.; Schalley, C. A., Enzyme-responsive pillar[5]arene-based polymer-substituted amphiphiles: synthesis, self-assembly in water, and application in controlled drug release. *Chemical Communications* **2015,** 51, 14901-14904.

151.	Li, N.; Cai, H.; Jiang, L.; Hu, J.; Bains, A.; Hu, J.; Gong, Q.; Luo, K.; Gu, Z., Enzyme-Sensitive and Amphiphilic PEGylated Dendrimer-Paclitaxel Prodrug-Based Nanoparticles for Enhanced Stability and Anticancer Efficacy. *ACS Applied Materials & Interfaces* **2017,** 9, 6865-6877.

152.	Yin, W.; Li, J.; Ke, W.; Zha, Z.; Ge, Z., Integrated Nanoparticles To Synergistically Elevate Tumor Oxidative Stress and Suppress Antioxidative Capability for Amplified Oxidation Therapy. *ACS Applied Materials & Interfaces* **2017,** 9, 29538-29546.

153.	Levesque, S. G.; Shoichet, M. S., Synthesis of Enzyme-Degradable, Peptide-Cross-Linked Dextran Hydrogels. *Bioconjugate Chemistry* **2007,** 18, 874-885.

154.	Guo, J.; Zhuang, J.; Wang, F.; Raghupathi, K. R.; Thayumanavan, S., Protein and Enzyme Gated Supramolecular Disassembly. *Journal of the American Chemical Society* **2014,** 136, 2220-2223.

155.	Allen, B. L.; Johnson, J. D.; Walker, J. P., Encapsulation and Enzyme-Mediated Release of Molecular Cargo in Polysulfide Nanoparticles. *ACS Nano* **2011,** 5, 5263-5272.

156.	Wilson, D. S.; Dalmasso, G.; Wang, L.; Sitaraman, S. V.; Merlin, D.; Murthy, N., Orally delivered thioketal nanoparticles loaded with TNF-α–siRNA target inflammation and inhibit gene expression in the intestines. *Nature Materials* **2010,** 9, 923-928.

157.	Broaders, K. E.; Grandhe, S.; Fréchet, J. M., A biocompatible oxidation-triggered carrier polymer with potential in therapeutics. *Journal of the American Chemical Society* **2010,** 133, 756-758.

158.   Brannon-Peppas, L., Poly(ethylene glycol): Chemistry and biological applications, edited by J. M. Harris and S. Zalipsky. *J. Control. Release* **2000,** 66, 321.

159.   Knop, K.; Hoogenboom, R.; Fischer, D.; Schubert, U. S., Poly(ethylene glycol) in Drug Delivery: Pros and Cons as Well as Potential Alternatives. *Angewandte Chemie, International Edition* **2010,** 49, 6288-6308.

160.   Kim, M. W., Surface activity and property of polyethyleneoxide (PEO) in water. *Colloids and Surfaces, A: Physicochemical and Engineering Aspects* **1997,** 128, 145-154.

161.   Cao, B. H.; Kim, M. W., Molecular weight dependence of the surface tension of aqueous poly(ethylene oxide) solutions. *Faraday Discuss.* **1995,** 98, 245-52.

162.   Bera, A.; Ojha, K.; Mandal, A., Synergistic Effect of Mixed Surfactant Systems on Foam Behavior and Surface Tension. *Journal of Surfactants and Detergents* **2013,** 16, 621-630.

163.   Gupta, M. K.; Meyer, T. A.; Nelson, C. E.; Duvall, C. L., Poly(PS-b-DMA) micelles for reactive oxygen species triggered drug release. *Journal of Controlled Release* **2012,** 162, 591-598.

164.   Yan, B.; Zhang, Y.; Wei, C.; Xu, Y., Facile synthesis of ROS-responsive biodegradable main chain poly(carbonate-thioether) copolymers. *Polymer Chemistry* **2018,** 9, 904-911.

165.   Gao, Z.; Ma, T.; Zhao, E.; Docter, D.; Yang, W.; Stauber, R. H.; Gao, M., Small is Smarter: Nano MRI Contrast Agents - Advantages and Recent Achievements. *Small* **2016,** 12, 556-576.

166.   Walkey, C. D.; Olsen, J. B.; Guo, H.; Emili, A.; Chan, W. C. W., Nanoparticle Size and Surface Chemistry Determine Serum Protein Adsorption and Macrophage Uptake. *Journal of the American Chemical Society* **2012,** 134, 2139-2147.

167.   Conda-Sheridan, M.; Lee, S. S.; Preslar, A. T.; Stupp, S. I., Esterase-activated release of naproxen from supramolecular nanofibers. *Chemical Communications* **2014,** 50, 13757-13760.

168.   Aleksanian, S.; Khorsand, B.; Schmidt, R.; Oh, J. K., Rapidly thiol-responsive degradable block copolymer nanocarriers with facile bioconjugation. *Polymer Chemistry* **2012,** 3, 2138-2147.

169.   Chan, N.; Khorsand, B.; Aleksanian, S.; Oh, J. K., A dual location stimuli-responsive degradation strategy of block copolymer nanocarriers for accelerated release. *Chemical Communications* **2013,** 49, 7534-7536.

170.   Kurniasih, I. N.; Liang, H.; Mohr, P. C.; Khot, G.; Rabe, J. P.; Mohr, A., Nile Red Dye in Aqueous Surfactant and Micellar Solution. *Langmuir* **2015,** 31, 2639-2648.

171.   Bohnert, J. A.; Karamian, B.; Nikaido, H., Optimized Nile Red Efflux Assay of AcrAB-TolC Multidrug Efflux System Shows Competition between Substrates. *Antimicrobial Agents and Chemotherapy* **2010,** 54, 3770-3775.

172.   Phung, Y. T.; Barbone, D.; Broaddus, V. C.; Ho, M., Rapid generation of in vitro multicellular spheroids for the study of monoclonal antibody therapy. *Journal of Cancer* **2011,** 2, 507.

173.   Iversen, T.-G.; Skotland, T.; Sandvig, K., Endocytosis and intracellular transport of nanparticles: present knowledge and need for future studies. *Nano Today* **2011,** 6, 176-185.

174.   Yameen, B.; Choi, W. I.; Vilos, C.; Swami, A.; Shi, J.; Farokhzad, O. C., Insight into nanoparticle cellular uptake and intracellular targeting. *Journal of Controlled Release* **2014,** 190, 485-499.

175.   Seo, S.-J.; Chen, M.; Wang, H.; Kang, M. S.; Leong, K. W.; Kim, H.-W., Extra- and intracellular fate of nanocarriers under dynamic interactions with biology. *Nano Today* **2017,** 14, 84-99.

176.   Wang, L. H.; Rothberg, K. G.; Anderson, R. G. W., Mis-assembly of clathrin lattices on endosomes reveals a regulatory switch for coated pit formation. *Journal of Cell Biology* **1993,** 123, 1107-18.

177.   Parton, R. G.; Joggerst, B.; Simons, K., Regulated internalization of caveolae. *Journal of Cell Biology* **1994,** 127, 1199-216.

178.   Sahay, G.; Alakhova, D. Y.; Kabanov, A. V., Endocytosis of nanomedicines. *Journal of Controlled Release* **2010,** 145, 182-195.

179.   Rosenbaum, I.; Avinery, R.; Harnoy, A. J.; Slor, G.; Tirosh, E.; Hananel, U.; Beck, R.; Amir, R. J., Reversible dimerization of polymeric amphiphiles acts as a molecular switch of enzymatic degradability. *Biomacromolecules* **2017,** 18, 3457-3468.

180.   Karavelidis, V.; Giliopoulos, D.; Karavas, E.; Bikiaris, D., Nanoencapsulation of a water soluble drug in biocompatible polyesters. Effect of polyesters melting point and glass transition temperature on drug release behavior. *European Journal of Pharmaceutical Sciences* **2010,** 41, 636-643.

Appendix A

Figure A. 1. DLS diagram of aqueous HDPE-NPs prepared in the presence of PEG. NP concentration = 7 mg/mL (a) and 14 mg/mL (b). Microfluidic conditions: TFR = 12 mL/min, FRR = 1/3, and PEG/HDPE = 0.1/1 wt/wt.

NP = 7 mg/mL

Z_{ave} = 93 nm
PDI = 0.07

NP = 14 mg/mL

D_{av} = 181 nm
PDI = 0.27
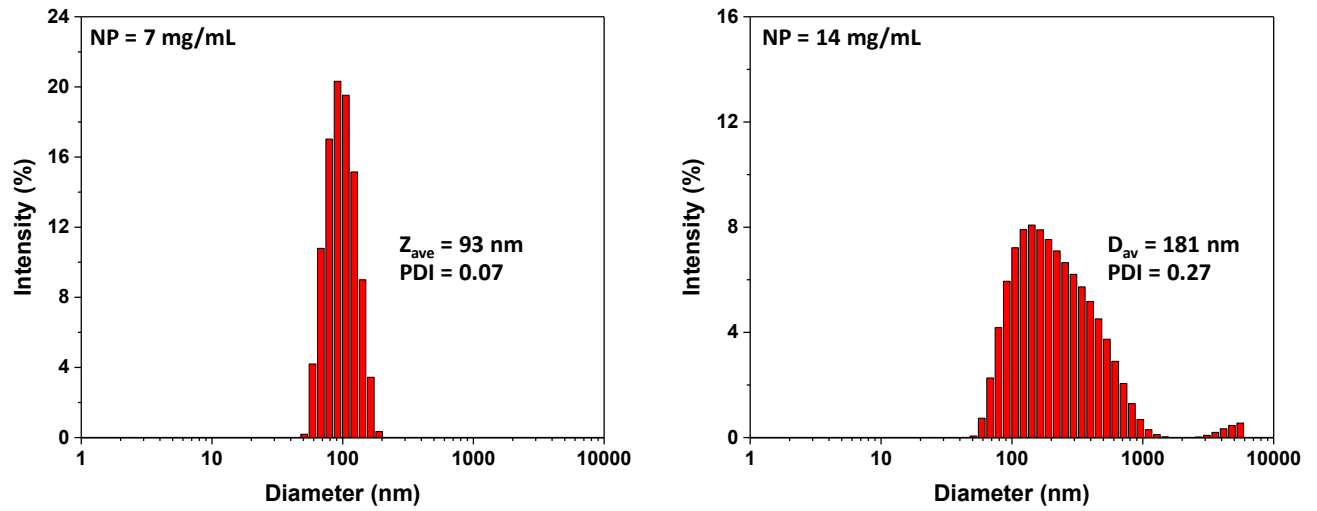
Figure A. 2. DLS diagram of aqueous HDPE-NPs prepared with no stabilizers. Microfluidic conditions: TFR = 12 mL/min, FRR = 1/3, and NP concentration = 3.4 g/mL.
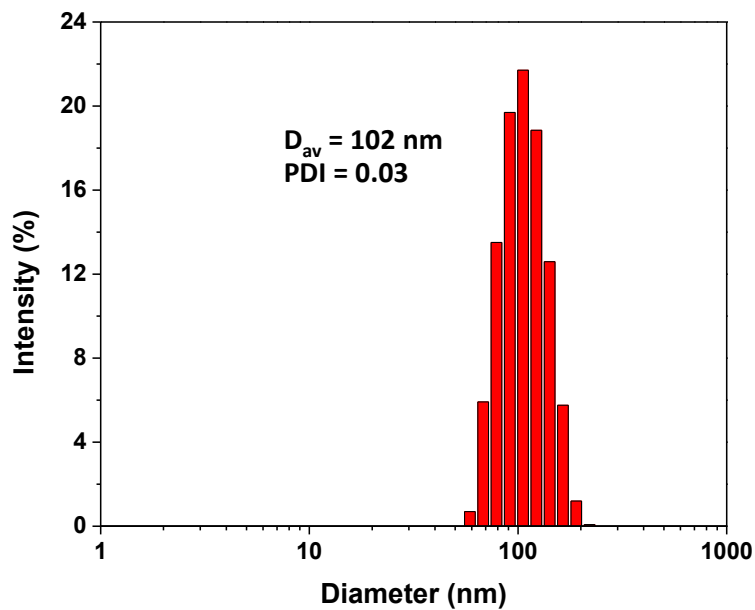

Figure A. 3. DLS diagram (a) and emission spectrum (b) of aqueous NR-loaded HDPE-NPs.
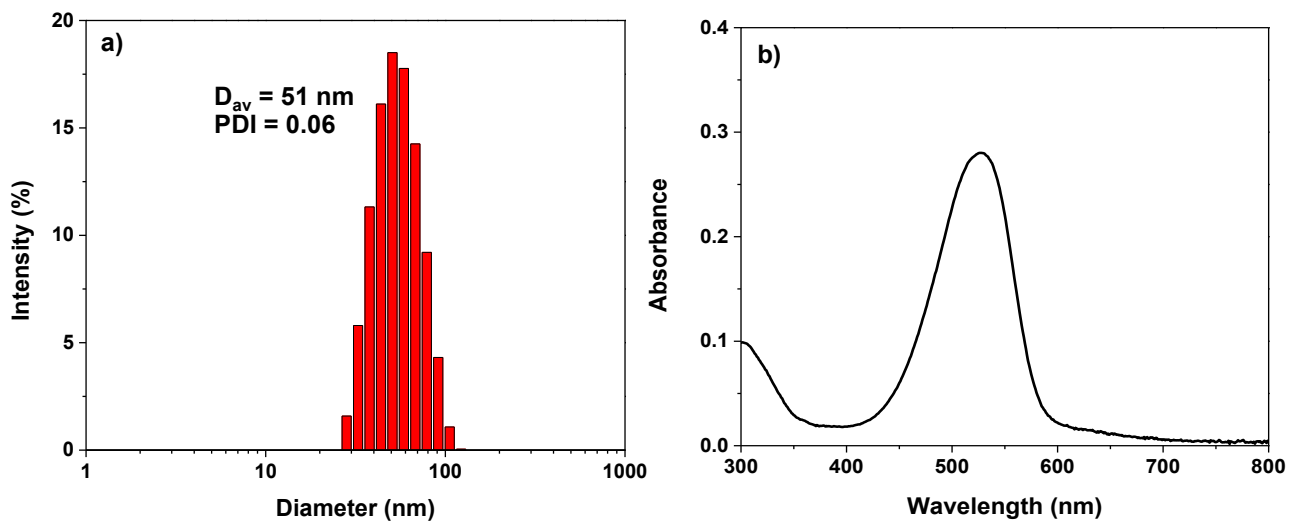
Figure A. 4. DLS diagram (a) and sizes and size distribution of HDPE-NPs stabilized by using PL02 (b). Microfluidic conditions: TFR = 12 mL/min, FRR = 1/1, PL02/HDPE = 0.1/1 (wt/wt), and NP concentration = 3.7 mg/mL.
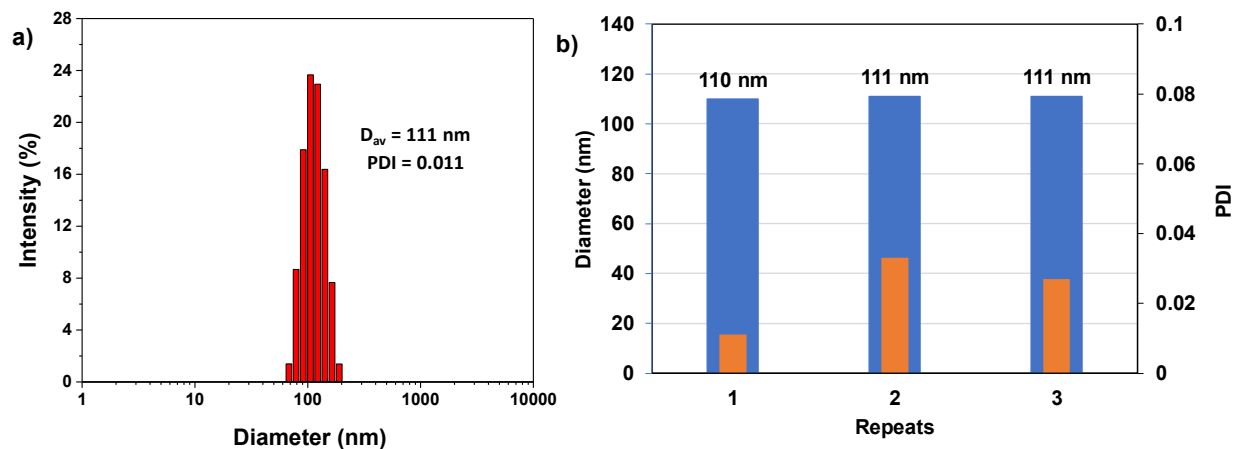
Appendix B

Figure B. 1. Synthesis (a), ^{1}H NMR spectrum (b), and GPC trace (c) of a dual enzyme and oxidation-responsive polyester (DPE) through a base-catalyzed thiol-ene polyaddition.
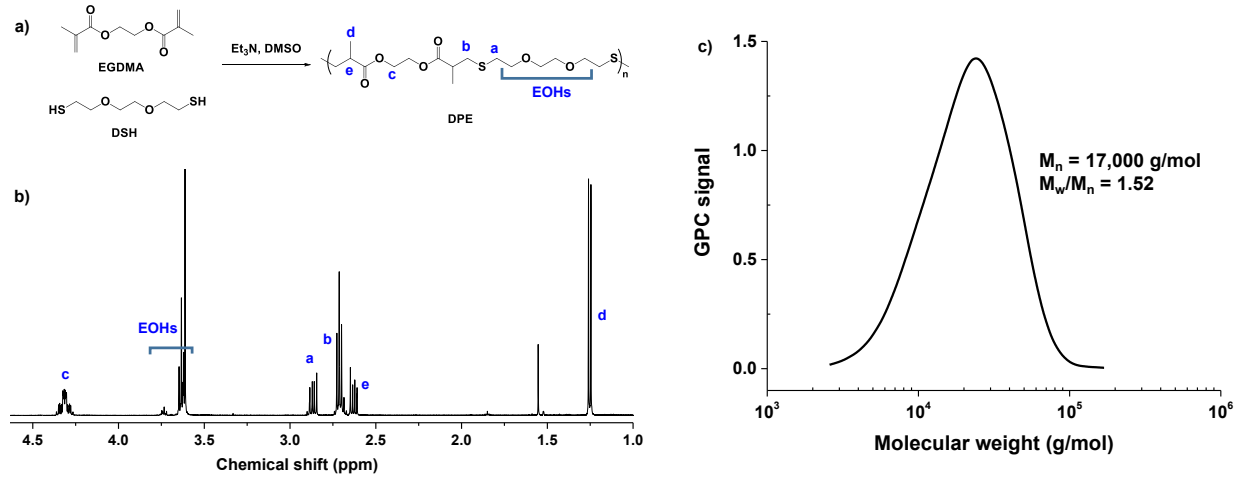
Figure B. 2. DLS diagrams (volume %) of esterase only (no NPs present) in PBS solution at pH = 7.2.
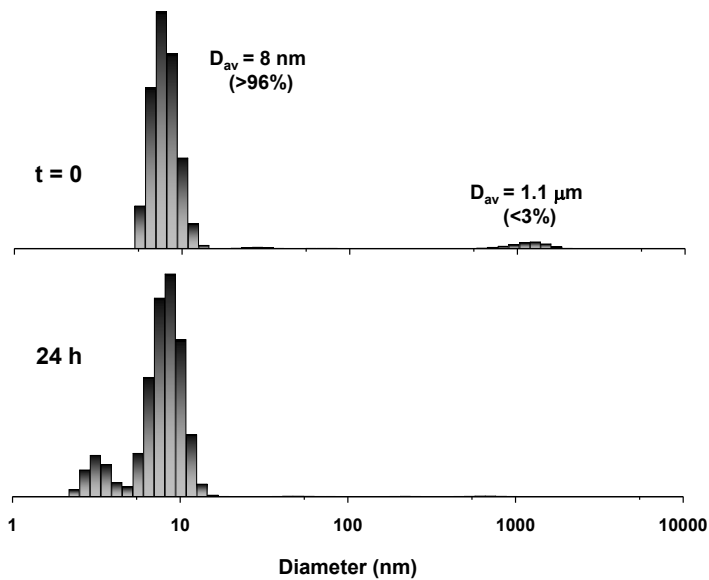
Figure B. 3. ^{1}H-NMR spectra of DPE-NPs before and after treatment with 1% hydrogen peroxide treated with GPC trace of DPE.
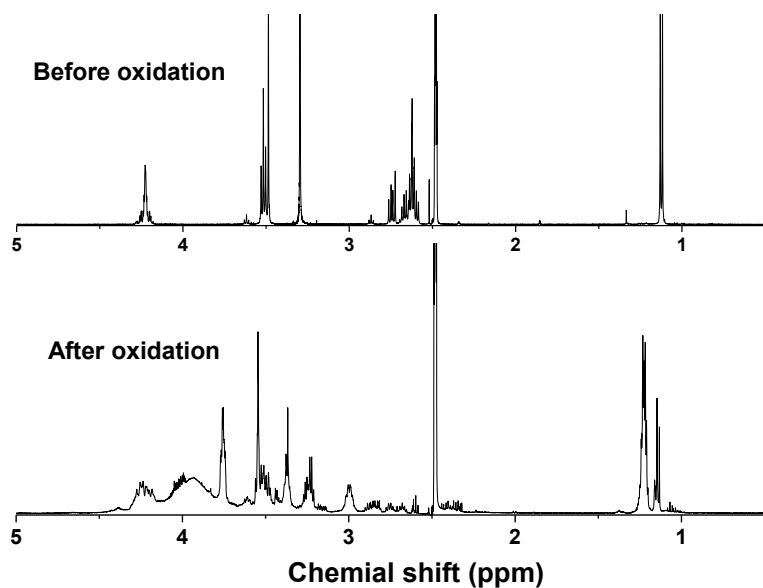
Figure B. 4. Overlaid UV/vis spectra of Dox (a) and plot of absorbance at 498 nm over Dox (b) in a mixture of water/THF at 1/4 v/v.
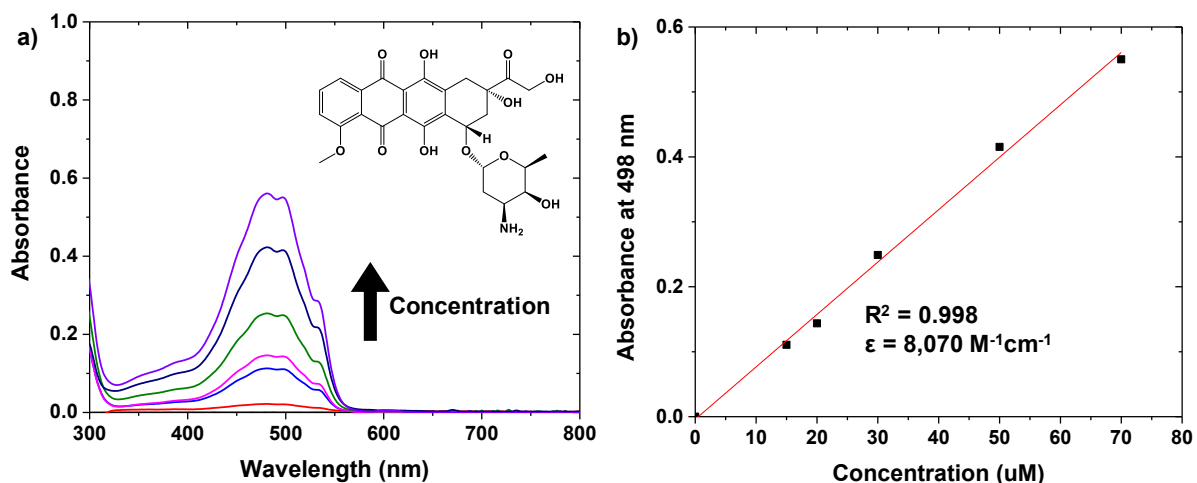
Figure B. 5. Colloidal stability of aqueous Dox-NPs on shelf (a) and in the presence of BSA (40 g/L) and IgG (8 g/L) (b). (n = 3)
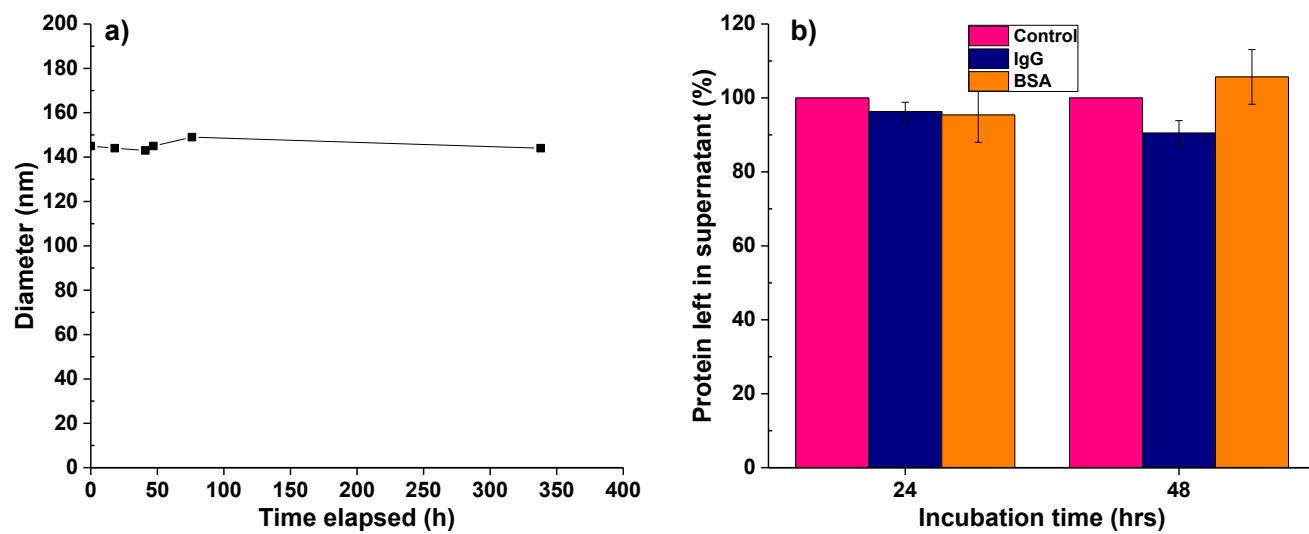
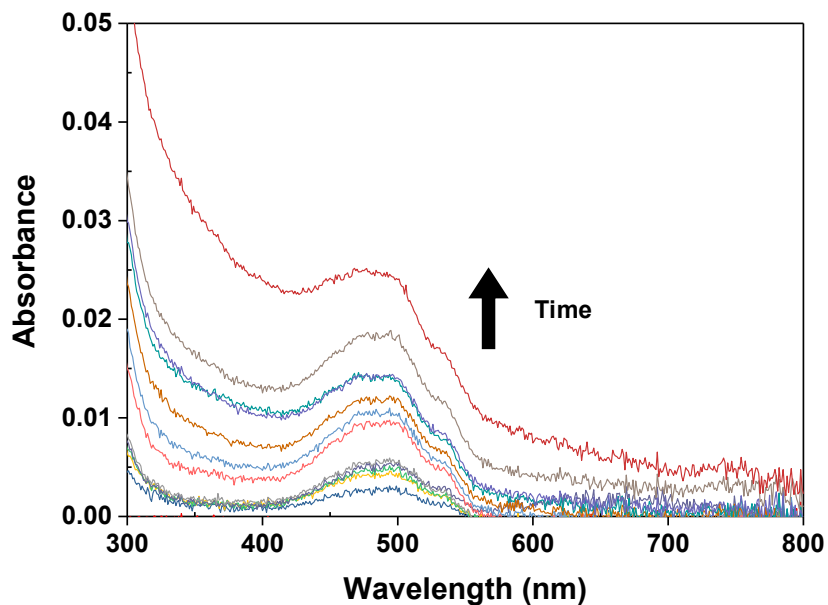**Figure B. 6.** Overlaid UV/vis spectra of Dox in outer water over time.

Figure B. 7. Overlaid UV/vis spectra (a) and evolution of absorbance at 498 nm (b) of free Dox incubated with 1% hydrogen peroxide in aqueous solution.
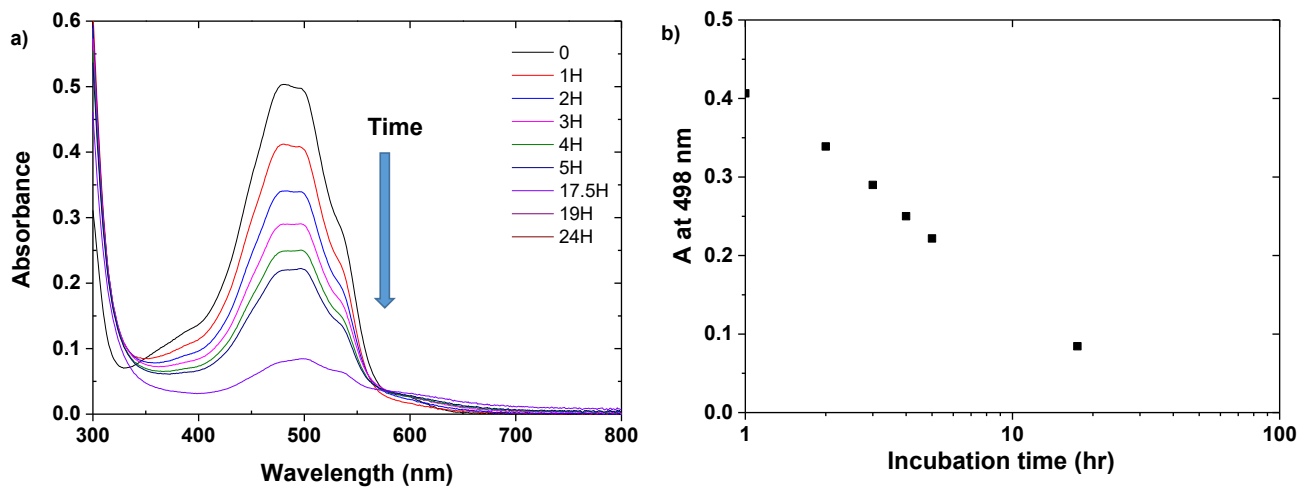
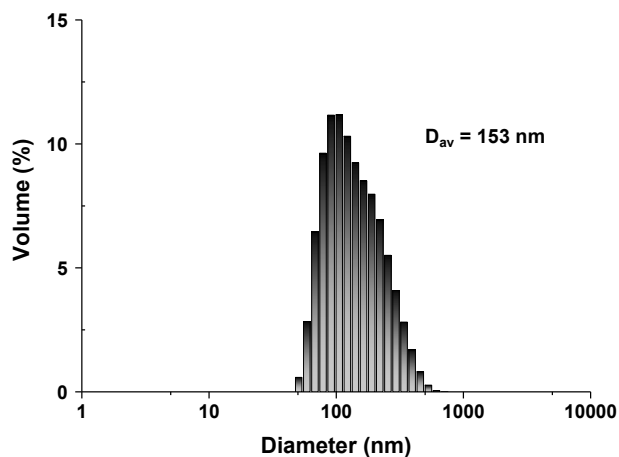**Figure B. 8.** DLS diagram of aqueous NR-loaded NPs at 2 mg/mL.

Figure B. 9. Overlaid emission spectra of aqueous NR-loaded NPs incubated without (a) and with hydrogen peroxide of 1% (b) and 5% (c) over time.
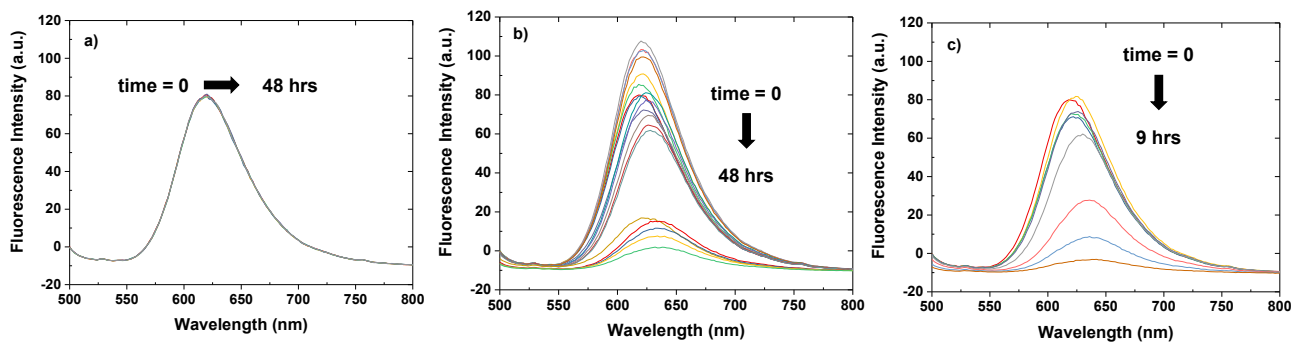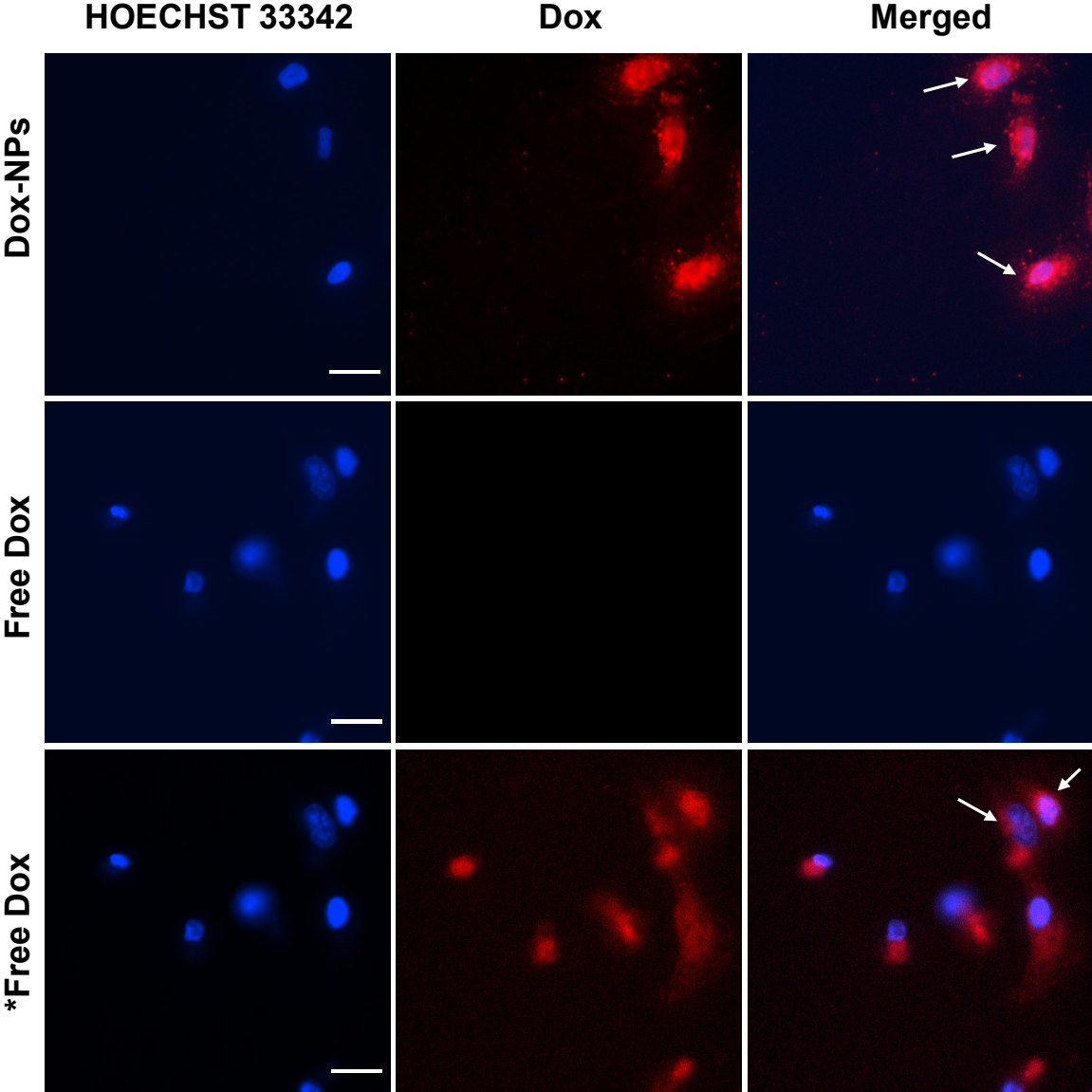
Figure B. 10. Epifluorescence microscopy images of HeLa cells incubated with Dox-NPs (2.5 µg/mL), compared with free Dox (2.5 µg/mL) for 12 hrs. Arrows indicate the localization of Dox-NPs and free Dox in HeLa cell nuclei. *Brightness and contrast were adjusted to show the internalization of the Free Dox. (scale bar = 30 µm)

Note: *Brightness and contrast were adjusted to show the internalization of Free Dox.

Figure B. 11. Florescence microscope images of A549 MCTS incubated for 4 days with Dox NPs (encapsulated Dox = 1.6 µg/mL) and free Dox (1.6 µg/mL). (n = 1, scale bar = 100 µm)